POLITECNICO DI TORINO

Master's degree in
Mechatronic Engineering

Modeling and simulation of a tethered remotely piloted aircraft system

Supervisors:
Prof. Fabrizio Dabbene
Prof. Giorgio Guglieri
Prof. Elisabetta Punta
Ph.D. Matteo Scanavino
Ph.D. Martina Mammarella

Candidate:
Emilio Dicembrini
242045

March 2020

Abstract

In the past years the use of Unmanned Aircraft Systems (UAS) has become widespread. In particular, multi-rotor vehicles have gained momentum and today they are able to support or even substitute traditional air vehicles in both civil and military applications. Battery lifetime is one of the main limitations when considering rotary wing UAS operations. Multi-rotor platforms usually suffer limited payload capabilities and flight time. For the applications where endurance is the driving requirement a promising solution to increase the energy available onboard is to power the Unmanned Aircraft Vehicle (UAV) with a cable from ground.

In this thesis, we propose a mathematical model able to describe the dynamic behaviour of a tethered UAS. The Finite Elements Method (FEM) and Lagrange's Equation of motion are used to evaluate the dynamic behaviors of the system. The cable consists of n segments linked end to end by spherical joints. Each element is modelled as weightless rod with lumped mass to its end. In order to implement a variable cable length, the length of the first segment is a function of time. An additional virtual element, with the same UAV inertia proprieties, is added to simulate the unmanned vehicle. Thrust and torque generated by the propellers are computed using the Blade Element Theory. The propulsion system is modelled separately from the Lagrangian cable/UAV model. Moreover, aerodynamic forces due to the wind are introduced as external disturbances acting on the cable and UAV. Compared to other works, a variable cable length in the three dimensional space is implemented as well as wind effects on overall system are included.

This thesis is part of a wider project on modelling and control of tethered UAV promoted by CNR-IEIIT - Torino Italy. In the same project, a preliminary study on electrical power architecture of a tethered UAV was developed by Eugenio Mercatali[1]. While in this previous work a feasibility study concerning the propulsion system of the tethered UAV was developed, the following thesis focuses on the overall system dynamics. Based on other literature researches, in this work the cable dynamic behaviour is modelled using the Finite Element Method (FEM). The Lagrange's equations are derived and discussed to describe both the fixed and the variable cable length cases. The mathematical model is implemented in Matlab/Simulink. UAV's attitude and altitude Proportional, Integrative, Derivative (PID) controllers were added to the system to perform the simulations. The controllers' gains were tuned by him in order to stabilize the system.

Simulation results corroborate that the proposed approach is able to accurately describe how the cable and UAS work in different operational conditions, such as take-off and hovering in both still air and wind scenario. The main limitation of the model is given by the representation of the cable segment orientations based on the Euler's angles. Gimbal lock occurs when the cable is placed on the ground or the UAS propeller plane is perpendicular to the ground.

Future works include decoupling the dynamics of the UAS from the cable making it even more versatile. A detailed mathematical model for the UAV will be introduced, in addition to the implementation of a position controller for the aerial vehicle. Moreover, a simplified winch model will be proposed to control the tension and unwinding velocity of the cable as a function of the UAS operations.

An article based on this work was submitted to the "2020 International Conference on Unmanned Aircraft Systems" (ICUAS 2020).

[1]E. Mercatali, "Tethered UAV Feasibility study for the propulsion ofa tethered UAV," Politecnico di Torino, 2018.

Contents

List of Figures

1 Introduction

1.1 Motivations

In the past years the use of Unmanned Aircraft Systems (UAS) has become widespread. In particular, multi-rotor vehicles have gained momentum and today they are able to support or even substitute traditional air vehicles in both civil and military applications [1]. The reason can be summarized in three aspects: Vertical Take-Off and Landing (VTOL) capability, simplified propulsion system and reduced flight control complexity. The technology level reached by autopilot control boards, as well as sensor miniaturization and cost reduction have enabled a lot of applications in which Unmanned Aerial Vehicles (UAVs) can get involved. Considering commercial operations, precision farming, photogrammetry as well as delivery are typical examples in which unmanned systems provide benefits thanks to their flexibility and low cost. Many research activities ([2]–[5]) exploit UAS platforms for monitoring purposes such as air pollution tracking, traffic management or water river analysis.

Battery lifetime is one of the main limitations when considering rotary wing UAS operations. Moreover, despite fixed wing architecture, multi-rotor vehicles are affected by a lower aerodynamic efficiency, resulting in limited flight time or payload capabilities. Different solutions have been proposed in literature to overcome this challenge. As reported by [6], solar cells and hydrogen fuel cells are possible alternatives to replace LiPo batteries. Solar cells are preferred for fixed wing UAV due to their wide wing surface [7]; on the other hand, the total weight of a hydrogen fuel cell system (7 kg) would reasonable for UAS with a maximum take off in the range from 10 kg to 35 kg vehicles [8]. The complexity of a hydrogen fuel cell propulsion system (thank, fuel, cooling and management) would not be suitable for small scale vehicles.

A promising solution to increase the energy available onboard UAVs is to power the vehicle with a cable from ground. Tethered UAS can exploit a virtually unlimited flight time. Moreover, a secure and stable data transmission is possible as no radio link is required. On the other hand, the main disadvantage is related to the limited flight range. However, for monitoring or surveillance or internet coverage extension applications where endurance is the driving requirement, tethered UAS have great potential. This is further enhanced by industrial platforms commercially available in the market:

Aquila 100 by Eagle Sky Light or Orion by Elistair are just a few examples.

1.2 Objective

The main objective of this work is the preliminary modelling and simulation of a tethered UAS to investigate the cable and vehicle dynamics.

This thesis is part of a wider project on modelling and controll of tethered UAV promoted by CNR-IEIIT - Torino Italy. In the same project, a preliminary study on electrical power architecture of a tethered UAV was developed by Eugenio Mercatali [9]. While in this previous work a feasibility study concerning the propulsion system of the tethered UAV was developed, the following thesis focus on the overall system dynamics. Starting from the existing industrial platforms based on the target vehicle mass ($25kg$). He identified commercially available components for the system. His results about the mechanical and electrical characteristics of the propulsion system are used to model the UAS. An article based on this work was submitted to the "2020 International Conference on Unmanned Aircraft Systems" (ICUAS 2020).

In literature, several works concerning the dynamic modelling and simulation of tethered underwater robots are available. Choo and Casarella in [10] present different approaches to describe tethered underwater systems. They identify the Finite Element Method (FEM) as the most versatile. It can be used to simulate whatever unsteady cable's motion. The elements of the cable can be modelled as a rigid or extensible thin rod lumped mass. Newton's law ([11]) or Lagrange's Equation ([12], [13]) are the primary way to derive the dynamic equations. Another method is based on the fundamental equations of structural mechanics. The tension along the cable is given as function of the longitudinal strain ([14]–[17]). In this case, the Hooke's law is commonly leveraged. This can be used to represent unsteady cable motion; however, due to the complexity of the problem this simplification is not always suitable and other constitutive law must be adopted. Sometimes, the Linearization Method can be exploited to simulate small deviations from an equilibrium state ([18], [19]). However, this solution does not coincide with the purpose of the present work. Finally, it is possible to describe the cable neglecting its mass. In this approach, the degree of freedom are the cable's stretch and its orientation as reported in [20], [21]. In this case, the cable is modelled as a single elastic element between the vehicle and the attachment point. In this thesis we propose a mathematical model able to simulate the dynamic behaviour of the cable and the tethered UAS. Compared to other works where the cable has a fixed length, we provide a solution to describe the cable unwinding. Based on the work in [12], [13], [22], our model is able to simulate the complete dynamic system (cable and UAV) in a three dimensional space. Moreover, we introduce the effect of wind force in both UAS and cable. Simulations results are discussed to evaluate the overall system behaviour in wind and still air conditions.

The overall system modelling is presented in Section 2 where the focus is given to the Finite Element Method, the reference systems as well as variable cable length and UAV model. The cable is divided in rigid segments with finite length. Each element is modelled as weightless rod with lumped mass to his end. A local reference frame that describes the orientation of the elements is defined using the Euler angles. This approach is inspired by [13]. Different Euler angles from the just cited work are used, such that the matrix singularity is located out the UAS operational conditions. Moreover, a variable length cable is implemented. The UAV is modelled as virtual cable element having geometrical and mechanical characteristics of the target vehicle (section 2.3). The propulsion system is implemented separately from the Lagrangian cable/UAV model. It is designed by Mercatali in [9]. Some simplifications are adopted in order to speed up the simulations: the electrical and electronic dynamics are neglected since its time constant is much lower than the mechanical one. The propellers thrust are calculated through the Blade Element Theory (BET). Moreover, the aerodynamic forces acting on the cable and UAS are presented to the reader in section 2.4. Section 3 provides details on the derivations of the Lagrange's Equations. In order to make it more readable, the Lagrange's equations are first derived in section 3.2 for the fixed cable length. In a later step, section 3.3, they are extended to the variable length case. The length of the first segment is a function of time. When it reaches a maximum value a new element is added. Vice versa when the cable is winded up the first element will be eliminated at the moment his length reaches an arbitrary small value. The section 3 includes assumptions and related simplifications to the described model. In particular, the torsion kinetic energy is neglected for the cable elements. As a consequence, the complexity of the system is reduced cancelling n degrees of freedom. Section 4 re-elaborates the Lagrange equations to a matrix form suitable for a numerical implementation. Moreover, a schematic block diagram describing the simulation flow is reported. Simulation results are discussed in Section 5 with different operational conditions of the UAS. Take-off and hovering in still air and wind conditions are simulated to corroborate the proposed model. Conclusions and future works are reported in Section 6.

2 System Model

2.1 Cable Model

Several method are reported to model flexible cable from Choo and Cassarella [10]. The Finite Element Method (FEM) is considered the most versatile. It can be used to simulate whatever unsteady cable's motion. The cable is divided in segments. It is considered as a system of n rigid segments in sequence. They are linked all together trough a spherical joint called nodes. Only forces can be exchanged by spherical joint between contiguous elements. Each of them in literature is modelled in different ways for example: simple pendulum, spring-mass, thin-rod, curved beam, viscoelastic spring. In this study it's used the simple pendulum model made up by a weightless rigid rod and mass lumped on the far end of the involved segment, as Figure 2.1.

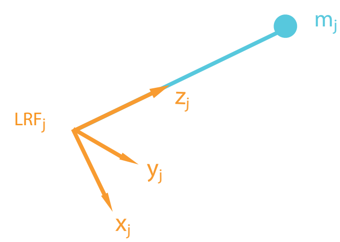

Figure 2.1: Cable element as weightless rigid rod and mass lumped.

This approach is chosen because has a reduced computational costs compared to the other mentioned method. Since the stiffness of the modelled cable is necessary high, the error introduced, respect a spring-mass model, by neglecting the effect of the strain is acceptable. Smaller element's dimension allows more accurate simulation results. The validity of this method to model the system is proved by [12], [13] by which this work is inspired.
The cable is considered as a system of n rigid bodies connected end to end, with the first element bound to the ground. Figure 2.2 shows schematically a cable subdivision in three elements. A rigid body on space has 6 Degrees Of Freedom (DOFs), three locate it in space and three define its orientation. Observe that the $(j+1)^{th}$ element is connected to the j^{th} lumped mass m_j. Each rigid element DOFs are reduced by 3 transitional DOFs. As a consequence the overall system's DOFs are $3(n+1)$.

In order to model a variable cable length, [22], the length of the first segment is a function of time, $l_1 = l_1(t)$. When it reaches a maximum value

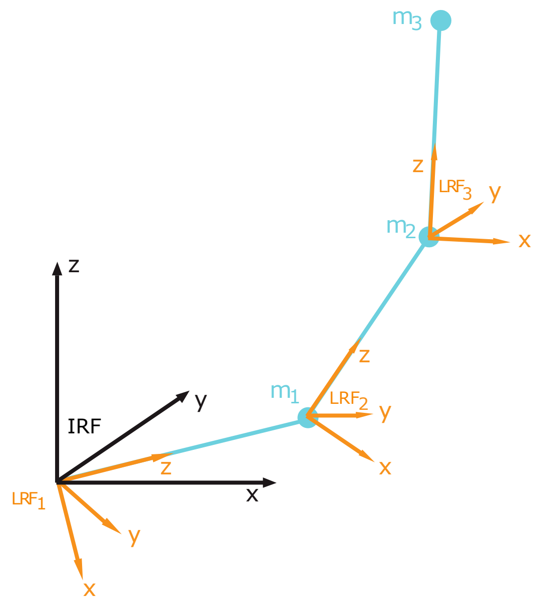

Figure 2.2: Cable divided in three finite elements joint end to end.

a new element is added. Vice versa when the cable is winded up the first element's length reduces up to an arbitrary small value it will be eliminated.

2.2 Reference system

The orientation of rigid body that compose the cable is represented with Euler angles. An inertial Cartesian Reference Frame (RF) label XYZ is centered on the attaching point of the cable to the ground. A local reference frame xyz with arbitrary origin is obtained with three successive rotations (Figure 2.3), starting from the inertial reference frame orientation. Each fundamental rotation can be around one of the three axes of the halfway rotated reference frame. The choice of the sequence of rotation and consequently of the Euler angles must be accurate in fact it can fall into gimbal look. For each possible combination of rotation sequence in some configuration of the Euler angles the rotational matrix, which represents mathematically the rotation, become singular. Geometrically this happen when two Euler angles coincide, and they can't be separated.
The simplest way to overcome this problem is avoiding the gimbal lock. This is done choosing a sequence of rotations so that it is localized as far as pos-

sible from the operational work conditions. The first rotation is above the inertial RF's X axis of an angle ϕ to achieve the rotated reference frame $x'y'z'$. This intermediate reference system is rotated by an angle θ around the y' axis obtain the RF $x''y''z''$. Finally the local RF xyz is achieved rotating above the z'' axis by an angle ψ the previous RF (Figure 2.3). Gimbal lock occurs when $\theta = \pm\frac{\pi}{2}$ [23]. This condition corresponds to the z axis of the local reference frame parallel to the XY plane. In other words, the cable is placed on the ground or the UAS propeller plane is perpendicular to ground.

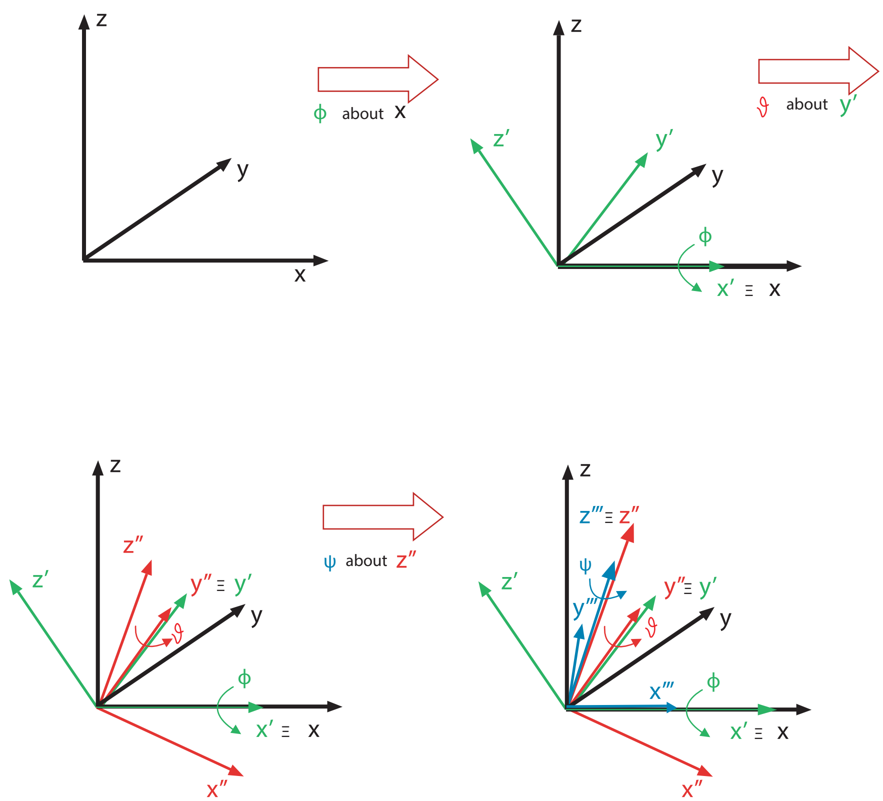

Figure 2.3: Euler angles and reference system rotation.

The rotational matrices are:

$$R_\phi = \begin{pmatrix} 1 & 0 & 0 \\ 0 & \mathrm{c}_\phi & \mathrm{s}_\phi \\ 0 & -\mathrm{s}_\phi & \mathrm{c}_\phi \end{pmatrix} \tag{1}$$

$$R_\theta = \begin{pmatrix} \mathrm{c}_\vartheta & 0 & \mathrm{s}_\vartheta \\ 0 & 1 & 0 \\ -\mathrm{s}_\vartheta & 0 & \mathrm{c}_\vartheta \end{pmatrix} \tag{2}$$

$$R_\psi = \begin{pmatrix} \mathrm{c}_\psi & \mathrm{s}_\psi & 0 \\ -\mathrm{s}_\psi & \mathrm{c}_\psi & 0 \\ 0 & 0 & 1 \end{pmatrix} \tag{3}$$

Multiplying this three matrix $R_{\phi\theta\psi} = R_\phi R_\theta R_\psi$ we obtain the rotational matrix that transforms from the inertial RF to the j^{th} local RF.

$$R_{\phi\theta\psi} = \begin{pmatrix} \mathrm{c}_\psi \,\mathrm{c}_\vartheta & \left(\mathrm{s}_\psi \,\mathrm{c}_\phi - \mathrm{c}_\psi \,\mathrm{s}_\vartheta \,\mathrm{s}_\phi\right) & \left(\mathrm{s}_\psi \,\mathrm{s}_\phi + \mathrm{c}_\psi \,\mathrm{s}_\vartheta \,\mathrm{c}_\phi\right) \\ -\mathrm{s}_\psi \,\mathrm{c}_\vartheta & \left(\mathrm{c}_\psi \,\mathrm{c}_\phi + \mathrm{s}_\psi \,\mathrm{s}_\vartheta \,\mathrm{s}_\phi\right) & \left(\mathrm{c}_\psi \,\mathrm{s}_\phi - \mathrm{s}_\psi \,\mathrm{s}_\vartheta \,\mathrm{c}_\phi\right) \\ -\mathrm{s}_\vartheta & -\mathrm{c}_\vartheta \,\mathrm{s}_\phi & \mathrm{c}_\vartheta \,\mathrm{c}_\phi \end{pmatrix} \tag{4}$$

Moreover, the inverse of this matrix transforms from the j^{th} local RF to the inertial RF.

$$R_{\phi\theta\psi}^{-1} = \begin{pmatrix} \mathrm{c}_\phi \,\mathrm{c}_\vartheta & -\mathrm{c}_\vartheta \,\mathrm{s}_\psi & -\mathrm{s}_\vartheta \\ \left(\mathrm{s}_\psi \,\mathrm{c}_\phi - \mathrm{c}_\psi \,\mathrm{s}_\vartheta \,\mathrm{s}_\phi\right) & \left(\mathrm{c}_\psi \,\mathrm{c}_\phi + \mathrm{s}_\psi \,\mathrm{s}_\vartheta \,\mathrm{s}_\phi\right) & -\mathrm{c}_\vartheta \,\mathrm{s}_\phi \\ \left(\mathrm{s}_\psi \,\mathrm{s}_\phi + \mathrm{c}_\psi \,\mathrm{s}_\vartheta \,\mathrm{c}_\phi\right) & \left(\mathrm{c}_\psi \,\mathrm{s}_\phi - \mathrm{s}_\psi \,\mathrm{s}_\vartheta \,\mathrm{c}_\phi\right) & \mathrm{c}_\vartheta \,\mathrm{s}_\phi \end{pmatrix} \tag{5}$$

Observe that the origin of the $(j+1)^{th}$ RF is centered on the j^{th} lumped mass m_j. The coordinate on inertial RF k^{th} segment's lumped mass can be expressed like a sum:

$$\begin{pmatrix} X_k \\ Y_k \\ Z_k \end{pmatrix} = \sum_{j=1}^{k} R_{\phi_\mathrm{j}\,\vartheta_\mathrm{j}\,\psi_\mathrm{j}}^{-1} \begin{pmatrix} x_j \\ y_j \\ z_j \end{pmatrix} \tag{6}$$

In the j^{th} local RF the m_j is located in $(0, 0, l_j)$, where l_j is the length of the j^{th} cable segment. Substituting in (6), results:

$$\begin{pmatrix} X_k \\ Y_k \\ Z_k \end{pmatrix} = \sum_{j=1}^{k} R_{\phi_j\,\vartheta_\mathrm{j}\,\psi_\mathrm{j}}^{-1} \begin{pmatrix} 0 \\ 0 \\ l_j \end{pmatrix} \tag{7}$$

At this point, one of the reasons leading us to choose this Euler angles becomes clear. The matrix-vector product insides the sum symbol on (7) results:

$$
\begin{cases}
X_k = \sum_{j=1}^{k} -l_j \, \mathrm{s}_{\vartheta_\mathrm{j}} \\
Y_k = \sum_{j=1}^{k} -l_j \, \mathrm{s}_{\phi_\mathrm{j}} \, \mathrm{c}_{\vartheta_\mathrm{j}} \\
Z_k = -\sum_{j=1}^{k} l_j \, \mathrm{c}_{\phi_\mathrm{j}} \, \mathrm{c}_{\vartheta_\mathrm{j}}
\end{cases} \tag{8}
$$

We can observe that each node position does not depend on the angle ψ.

2.3 UAV Model

The UAV and the cable are coupled trough a spherical joint. The UAV dynamics model must be solved simultaneously with the cable. Like suggested by [13] it is modeled as a virtual segment of the cable label $n+1^{th}$ connected to the last element of the cable. The length of this virtual segment is equal to the distance between the center of mass of UAV and the connection point with the last cable element. In order to proper model the UAV his inertia proprieties are applied to the virtual segment, including mass and inertia moments (section 2.3.1). The thrust generated by the UAS propellers system (section 2.3.2) are introduced in the model as external forces acting along the z axis of the UAS local RF.

2.3.1 UAV's parameters estimation

The UAV inertial moments are estimated assuming the generic setup of the drone shown in Figure 2.4. The quad copter is simplified in geometric shapes ([24]) such as boxes, cylinder and cross-beam. The body label $Mainbox$ contains the flight computer and electronics. The battery pack has an emergency function and it supply the UAV should the power transmission from the ground station fail. It is sized by Mercatali in [9] in order to guarantee the vehicle landing from a quote of $100m$. The choice fell on a Kokam SLPB78205130H with a total weight of $5.53kg$. The propulsion system is composed by two T-MOTOR products: the motor U15II KV 100 and the propeller FA36,2x11,8". They are simplified respectively as cylinder and solid disk. The cross structure supporting the motors is made of circular thin rods. Finally, the pay load is supposed to be attach under the main box. No information about the main box weight is given and it is supposed equal to $2kg$. Assuming also the cross frame made of carbon fiber tubular beam of thickness equal to $3mm$ and density $2000kg/m^3$, it weight amounts about to $1.7kg$. The pay load with a target UAV take-off weight of $25kg$ is about $7.6kg$. The estimated geometrical and inertia characteristics of the vehicle are reported in appendix A.

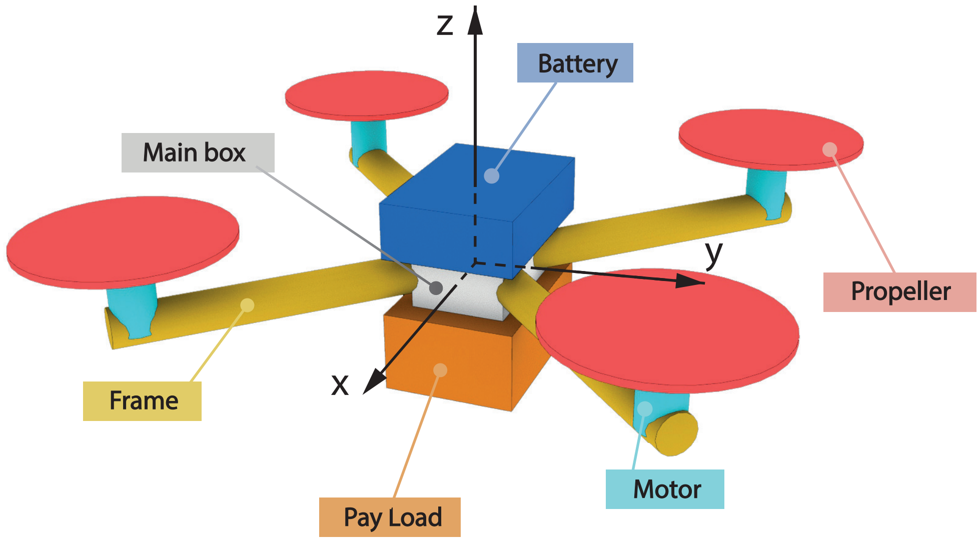

Figure 2.4: UAV setup as elementary bodies.

The high symmetry of the vehicle relative to the axis x and y involves that center of mass is located along the z axis in Figure 2.4 and that even the inertia tensor is reduced to diagonal matrix.

$$I^{body} = \begin{pmatrix} I_{xx} & 0 & 0 \\ 0 & I_{yy} & 0 \\ 0 & 0 & I_{zz} \end{pmatrix} \tag{9}$$

The drawn reference frame in Figure 2.4 is arbitrary centered in the UAV's main bodies. It is useful to calculate the position of the center of mass. Calling m_i the mass of the i^{th} body and s_i his coordinates the center of mass is situated in

$$z_{CM} = \frac{\sum_{i=1}^{N} m_i s_i}{\sum_{i=1}^{N} m_i}$$

where N is the number of elementary bodies. The UAV body RF is obtained by translating the previous RF along the z axis of a quantity equal to z_{CM}. The total inertial moments respect body RF can be estimated as sum of those calculated for each elementary bodies reported in Table 2.1.

$$I_{xx} = \sum_{i=1}^{N} I_{x_i}$$
$$I_{yy} = \sum_{i=1}^{N} I_{y_i}$$
$$I_{zz} = \sum_{i=1}^{N} I_{z_i}$$

Modelling the UAV as a virtual segment its inertial moments must be transformed to the $n+1^{th}$ element local RF. Assuming that the connection point is located at the intersection of the symmetry axis (along z axis) of the UAV and shifted down of arbitrary quantity the $n+1^{th}$ local reference system has same orientation of the body RF. Remembering the Huygens Steiner theorem, results:

$$I^{n+1} = \begin{pmatrix} I_{xx} + m_{UAV} d_{UAV}^2 & 0 & 0 \\ 0 & I_{yy} + m_{UAV} d_{UAV}^2 & 0 \\ 0 & 0 & I_{zz} \end{pmatrix} \tag{10}$$

where d_{UAV} is the distance between the UAV's center of mass with the cable connection point.

In order to calculate the aerodynamics force acting on the UAV the cross sections between it and the planes perpendicular to each axis are estimated. As done for the inertial moments, they are calculated as the sum of each elementary bodies sections showed in Table 2.1. Observe that the cross area of the propellers is supposed to be zero in all planes. They aerodynamics effects have an impact on thrust generation, section 2.3.2.

$$A_x = \sum_{i=1}^{N} A_{x_i}, \quad A_y = \sum_{i=1}^{N} A_{y_i}, \quad A_z = \sum_{i=1}^{N} A_{z_i}$$

Part #	Geometry	Inertial moments $[kgm^2]$	Cross sections $[m^2]$
box	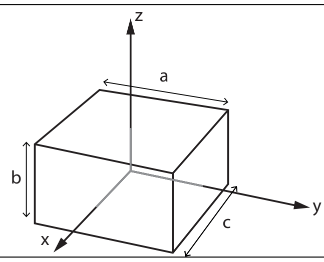	$I_{x_i} = \frac{m_i}{12}(b_i^2 + c_i^2) + m_i z_i^2$ $I_{y_i} = \frac{m_i}{12}(a_i^2 + b_i^2) + m_i z_i^2$ $I_{z_i} = \frac{m_i}{12}(a_i^2 + c_i^2)$	$A_{x_i} = a_i b_i$ $A_{y_i} = b_i c_i$ $A_{z_i} = a_i c_i$
motors	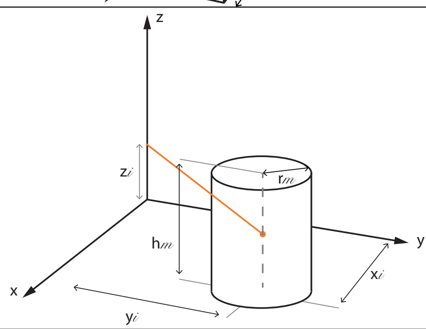	$I_{x_i} = m_i(\frac{r_m^2}{4} + \frac{h_m^2}{12} + z_i^2 + x_i^2)$ $I_{y_i} = m_i(\frac{r_m^2}{4} + \frac{h_m^2}{12} + z_i^2 + y_i^2)$ $I_{z_i} = m_i(\frac{r_m^2}{2} + z_i^2)$	$A_{x_i} = 2r_m h_m$ $A_{y_i} = 2r_m h_m$ $A_{z_i} = \pi r_m^2$
propellers	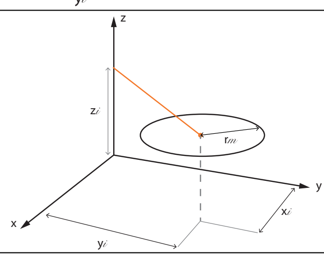	$I_{x_i} = m_i(\frac{r_p^2}{4} + z_i^2 + y_i^2)$ $I_{y_i} = m_i(\frac{r_p^2}{4} + z_i^2 + x_i^2)$ $I_{z_i} = m_i(\frac{r_p^2}{4} + z_i^2)$	$A_{x_i} = 0$ $A_{y_i} = 0$ $A_{z_i} = 0$
frame	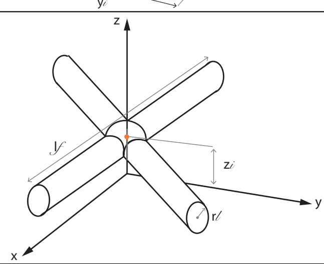	$I_{x_i} = \frac{2}{12} m_i (l_f^2 s_\alpha^2 + z_i^2)$ $I_{y_i} = \frac{2}{12} m_i (l_f^2 c_\alpha^2 + z_i^2)$ $I_{z_i} = \frac{2}{12} m_i l_f^2$	$A_{x_i} = l_f(2r_f)s_\alpha$ $A_{y_i} = l_f(2r_f)c_\alpha$ $A_{z_i} = 2l_f(2r_f)$

Table 2.1: Elementary bodies Inertial Moments respect the body RF and cross section area.

2.3.2 Propulsion System

This work adopts the propulsion system identified by Eugenio Mercatali [9] as part of the same project. He has researched commercially solutions for the propellers and motors appropriate for the target UAV. The choice fell on two T-MOTOR products: the motor U15II KV 100 and the propeller FA36,2x11,8". [9] develops a model and speed controller for system. The electrical component has a much smaller time constant than the mechanical. Consequently, it is neglected. The used model assumes that the current in the motor is equal to the commanded one. This is transformed in motor's torque M_M by a gain. The mechanical part is implemented as first order transfer function, Equation (11). A Proportional, Integrative (PI) speed controller is deployed with omega as feedback.

$$\frac{\omega_M(s)}{M_M - M_r(s)} = \frac{1}{Js + f} \tag{11}$$

where ω_M is the motor's angular speed, M_r is the reaction torque on motor's axis by the propeller, J is the rotational inertial moment at motor's axis, and f is viscous damping coefficient.

The propeller FA36,2x11,8" has a Selig1210 profile (Figure 2.5) with a pitch of 11.8".

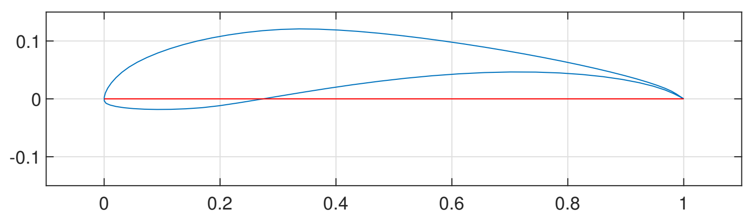

Figure 2.5: Selig1210 normalized cord profile.

The lift and drag coefficient (respectively C_l, C_d) graph is created using XFoil, [25]. They are truncated at the attack angles corresponding at the maximum and minimum value of C_l [26], Figure 2.6. Out of this range the profile is supposed in stall condition and both coefficient are set to zero.

The thrust generated by the chosen propeller and his reaction torque to the motor axis are obtained through the Blade Element Theory (BET) by [9]. This is extended considering a range of V_∞: velocity of the undisturbed axial flow that invest the propeller. These are reported in the above Figures 2.7, 2.8 varying the angular velocity of the motor and V_∞.

The thrust and reaction torque are inserted in a table with input motor's angular speed and the relative velocity between the wind and the UAV's velocity along the z axis in his local RF.

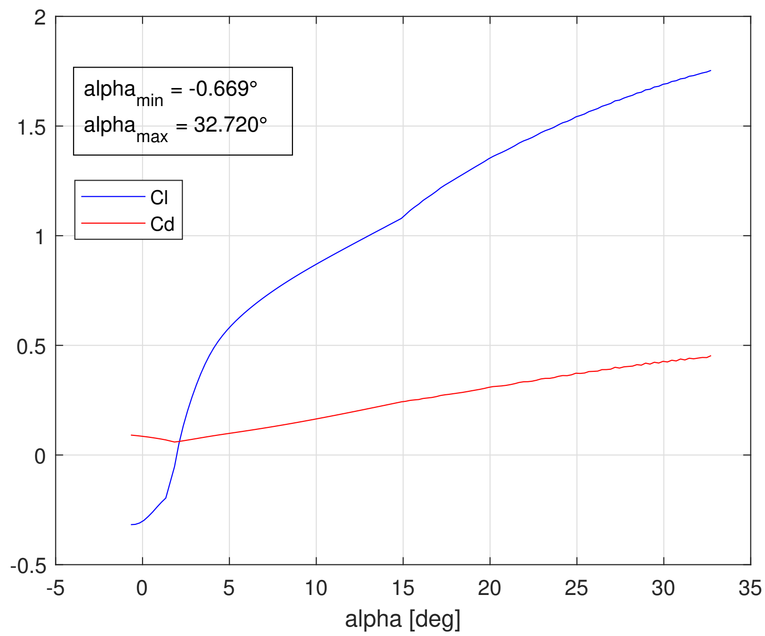

Figure 2.6: C_l, C_d respect the attack angle α.

Each motor causes a force moment around the UAV's body axis. Observe that they must rotate in opposite wise in pairs. In this way in undisturbed condition the overall UAV's $\mathrm{z_{body}}$ moment is null. Referring to Figure 2.9 they can be derived.

$$\begin{aligned}
T_{\mathrm{z_{body}}} &= T_I + T_{II} + T_{III} + T_{IV} \\
M_{\mathrm{x_{body}}} &= (T_I + T_{II} - T_{III} - T_{IV})b_x \\
M_{\mathrm{y_{body}}} &= (-T_I + T_{II} + T_{III} - T_{IV})b_y \\
M_{\mathrm{z_{body}}} &= M_{rI} - M_{rII} + M_{rIII} - M_{rIV}
\end{aligned} \tag{12}$$

where b_x, b_y are the distances of one motor respectively from x_{body} and y_{body} axis, $T_{\mathrm{z_{body}}}$ is the overall UAV's thrust, $T_I, T_{II}, T_{III}, T_{IV}$ are the single motors thrust and $M_{rI}, M_{rII}, M_{rIII}, M_{rIV}$ are the propeller reaction torques at the motors' axis.

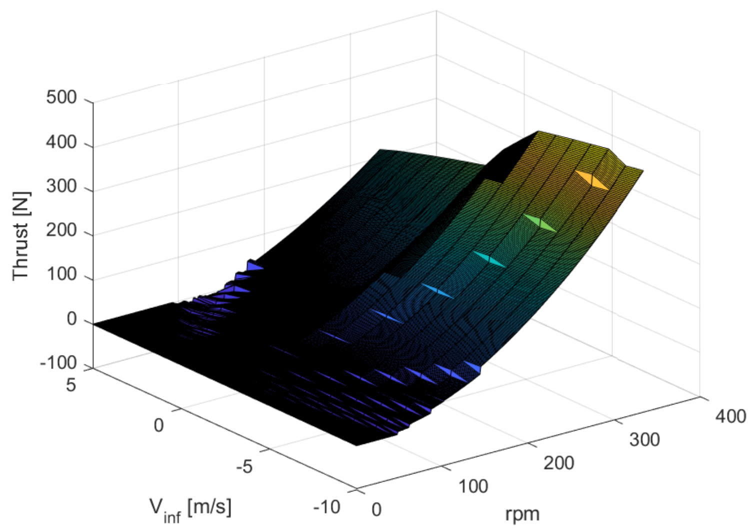

Figure 2.7: Propeller Thrust varying motor's speed and V_∞.

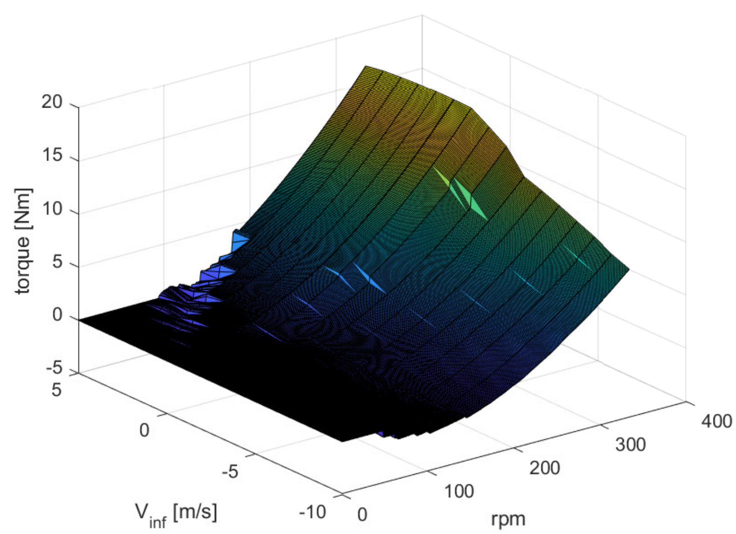

Figure 2.8: Reaction Torque at motor's axis varying motor's speed and V_∞.

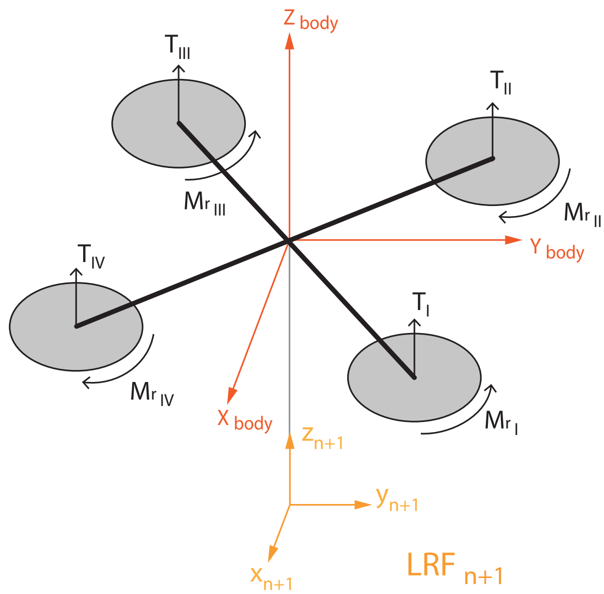

Figure 2.9: UAV thrust and moments.

2.3.3 Altitude and Attitude control

A altitude and attitude controllers are included in the model. A Proportional, Integrative, Derivative (PID) algorithm is used to keep stable the attitude and the desired altitude. The controller evaluates the reference thrusts that each propeller must generate. They are then converted in motors' speed knowing the propeller characteristic in Figure 2.7.

The altitude controller calculates the necessary thrust T_z^{ref} in the inertial RF comparing the actual UAV altitude and the reference one. The error thus generate is elaborated by the PID in an acceleration command. Once multiplied for the system's mass it is transformed in the body RF $T_{z_{\text{body}}}^{ref}$ trough the rotational matrix (4). Each motor must provide the same thrust in order to not disturb the vehicle attitude. Their magnitude is calculated for each propeller, recalling Equation (12), as

$$T^{altref} = T_I^{altref} = T_{II}^{altref} = T_{III}^{altref} = T_{IV}^{altref} = T_{z_{\text{body}}}^{ref}/4$$

Similarly, the attitude controller calculates a reference thrust for the motors. The error, equal to the difference between the reference attitude and the actual, is processed by the PID in angular accelerations about the three body axis. Multiplying it for the respective inertia moments the reference moments $M^{ref}_{\mathrm{x_{body}}}$, $M^{ref}_{\mathrm{y_{body}}}$, $M^{ref}_{\mathrm{z_{body}}}$ are obtained. They must be traduced in thrust references for each propeller. Taken the reference moments one at time in order to keep $T_{\mathrm{z_{body}}}$ and the other two moments constant the propellers reference must change symmetrically in accordance to the considered axis. A particular note must be done for $M_{\mathrm{z_{body}}}$. The reaction torque should be expressed as function of thrust. Comparing the toque and the thrust reported on section 2.3.2 varying the motor's speed for $V_\infty = 0.01m/s$ the curve in Figure 2.10 can be drawn. A first order fit is adopted.

$$M_{r*} = p_1 T_* + p2$$

where M_{r*}, T_* are respectively the reaction torque and the thrust of the $*$ motor.

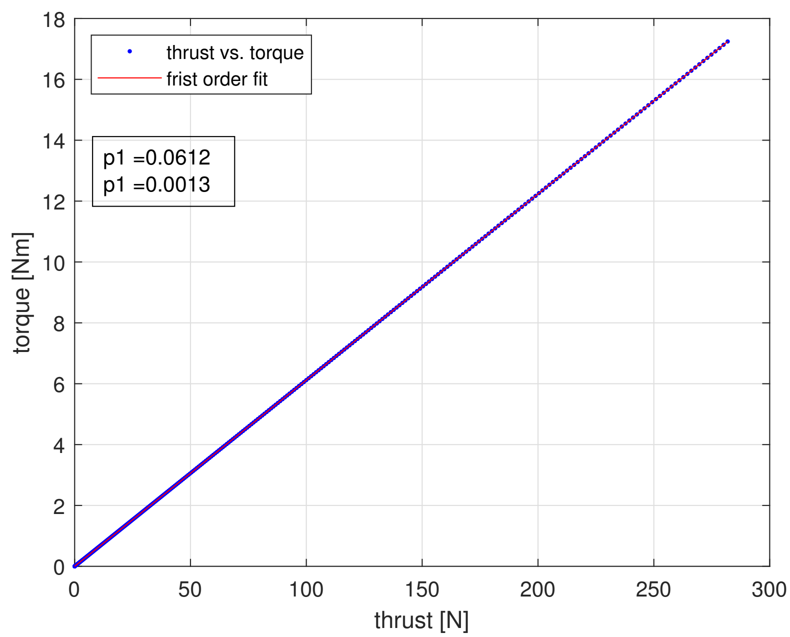

Figure 2.10: Torque as function of thrust at $V_\infty = 0.01m$.

Finally, applying the superposition principle, the reference thrust of the motors results:

$$\begin{pmatrix} T_I^{ref} \\ T_{II}^{ref} \\ T_{III}^{ref} \\ T_{IV}^{ref} \end{pmatrix} = \begin{pmatrix} 1 & 1 & -1 & 1 \\ 1 & 1 & 1 & -1 \\ 1 & -1 & 1 & 1 \\ 1 & -1 & -1 & -1 \end{pmatrix} \begin{pmatrix} T_{\mathrm{z_{body}}}^{ref}/4 \\ M_{\mathrm{x_{body}}}^{ref}/4b_x \\ M_{\mathrm{y_{body}}}^{ref}/4b_y \\ M_{\mathrm{z_{body}}}^{ref}/4p_1 \end{pmatrix} \tag{13}$$

2.4 Aerodynamics Forces

The aerodynamics forces are calculated by cross flow principle described by [27] in the same way proposed by [13]. Each cable element is considered as cylinder of diameter d and length equal to the segment length l_j. The aerodynamics forces are applied to the segment lumped mass m_j. Calling

$$\vec{V^w} = \begin{pmatrix} V_x^w \\ V_y^w \\ V_z^w \end{pmatrix}$$

the wind velocity in the inertial RF. The relative velocity $\vec{V}'_{jr}$ between the j^{th} cable segment and the wind in the j^{th} element's local RF is

$$\begin{aligned} \vec{V}'_{jr} &= R_{\phi_j\,\vartheta_\mathrm{j}\,\psi_\mathrm{j}} V_{jr} \\ \vec{V}_{jr} &= \vec{V^w} - \vec{V}_k \end{aligned} \qquad j = 1, \dots, n+1$$

where $\vec{V}_k$ is the velocity of j^{th} cable's element in the inertial RF. For the sake of simplicity, image a plane passing through the axis of the cable segment and $\vec{V}'_{jr}$. In this plane the three dimensional problem is reduced to a two dimensional problem. Let's define the direction $\|$ parallel to the cylinder's axis and $\perp$ the direction perpendicular to it (Figure 2.11).

$$\begin{cases} F_\| = L\,\mathrm{c}_\alpha + D\,\mathrm{s}_\alpha \\ F_\perp = L\,\mathrm{s}_\alpha - D\,\mathrm{c}_\alpha \end{cases} \qquad j = 1, \dots, n \tag{14}$$

where

$$\begin{cases} L = \frac{1}{2}\rho d l_j \left|\vec{V}'_{jr}\right|^2 \mathrm{C_l} \\ D = \frac{1}{2}\rho d l_j \left|\vec{V}'_{jr}\right|^2 \mathrm{C_d} \end{cases} \qquad j = 1, \dots, n \tag{15}$$

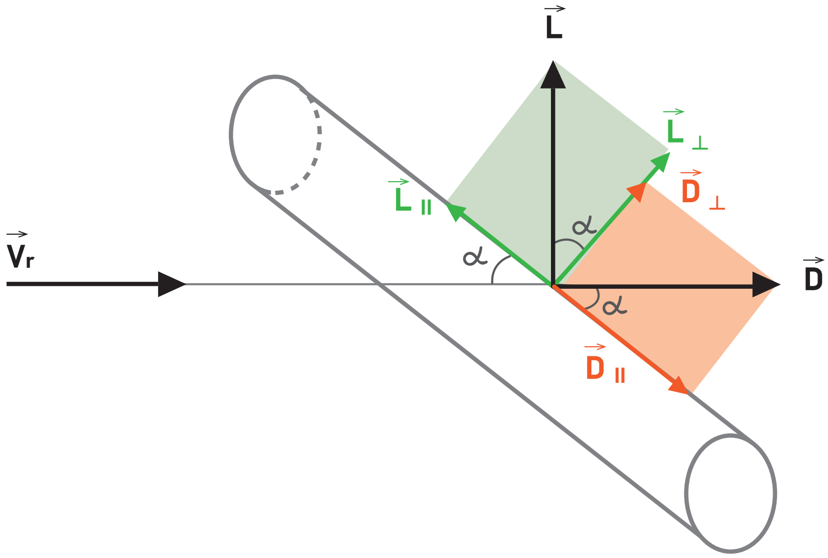

Figure 2.11: Cylindrical cable segment invested by the wind

where ρ is the air density

The $\mathrm{C_l}$ and $\mathrm{C_d}$ can be expressed according to [27]

$$\begin{aligned} \mathrm{C_l} &= \mathrm{C_{d0}}\,\mathrm{s}_\alpha{}^2\,\mathrm{c}_\alpha \\ \mathrm{C_d} &= \mathrm{C_{d0}}\,\mathrm{s}_\alpha{}^3 + \pi\,\mathrm{C_f} \end{aligned} \qquad j = 1, \ldots, n \tag{16}$$

where $\mathrm{C_{d0}}$ is the drag coefficient and $\mathrm{C_f}$ is the frictional coefficient.

Substituting the equations (15) and (16) in (14), results:

$$\begin{cases} F_\parallel = \frac{1}{2}\rho d l_j \left|\vec{V}'_{jr}\right| V_\parallel \pi\,\mathrm{C_f} \\ F_\perp = \frac{1}{2}\rho d l_j V_\perp \left(|V_\perp|\,\mathrm{C_{d0}} + \left|\vec{V}'_{jr}\right| \pi\,\mathrm{C_f}\right) \end{cases} \qquad j = 1, \ldots, n$$

where $V_\parallel = -\left|\vec{V}'_{jr}\right| \mathrm{c}_\alpha$ and $V_\perp = \left|\vec{V}'_{jr}\right| \mathrm{s}_\alpha$.

The aerodynamics forces are transformed into the cable element local RF observing that $V'_{jrx} = V_\perp c_\beta$, $V'_{jry} = V_\perp s_\beta$ and $V'_{jrz} = V_\parallel$, where β is the angle between the consider plane and the element's local RF x axis. Finally, in the

j^{th} local RF $\vec{F}'_j$ is

$$\begin{cases} F'_{jx} = F_{\perp} c_{\beta} = \frac{1}{2}\rho dl_j V'_{jrx} \left(|V_{\perp}| \, \mathrm{C_{d0}} + \left| \vec{V}'_{jr} \right| \pi \, \mathrm{C_f} \right) \\ F'_{jy} = F_{\perp} s_{\beta} = \frac{1}{2}\rho dl_j V'_{jry} \left(|V_{\perp}| \, \mathrm{C_{d0}} + \left| \vec{V}'_{jr} \right| \pi \, \mathrm{C_f} \right) \qquad j = 1, \ldots, n \\ F'_{jz} = F_{\parallel} = \frac{1}{2}\rho dl_j \left| \vec{V}'_{jr} \right| V'_{jrz} \pi \, \mathrm{C_f} \end{cases}$$

where $|V_{\perp}| = \sqrt{{V'_{jrx}}^2 + {V'_{jry}}^2}$ and $\left| \vec{V}'_{jr} \right| = \sqrt{{V'_{jrx}}^2 + {V'_{jry}}^2 + {V'_{jrz}}^2}$.

The aerodynamics forces acting on the virtual UAV segment cannot be calculated in the same way used for the cable's elements. For $j = n + 1$:

$$\begin{cases} F'_{n+1x} = \frac{1}{2}\rho A_x V'_{n+1rx} \left| V'_{n+1rx} \right| C_{dx} \\ F'_{n+1y} = \frac{1}{2}\rho A_y V'_{n+1ry} \left| V'_{n+1ry} \right| C_{dy} \\ F'_{n+1z} = \frac{1}{2}\rho A_z V'_{n+1rz} \left| V'_{n+1rz} \right| C_{dz} \end{cases}$$

where (A_x, A_y, A_z) are the cross section calculated in section 2.3.1 and (C_{dx}, C_{dy}, C_{dz}) are the drag coefficients derived by [28].

The forces thus calculated are in the element's local RF. They are rotated in the inertial RF with the rotational matrix 5, $\vec{F}_j = R^{-1}_{\phi_j \, \vartheta_\mathrm{j} \, \psi_\mathrm{j}} \vec{F}'_j$.

3 Lagrangian Model

The Lagrangian is defined

$$\mathcal{L} = E_{kinetic} - E_{potential} \tag{17}$$

The Lagrange's equation of a multi-body system can be written

$$\frac{d}{dt}\Big(\frac{\partial \mathcal{L}}{\partial \dot{q}_i}\Big) - \frac{\partial \mathcal{L}}{\partial q_i} = Q'_i \tag{18}$$

where q_i are the generalized coordinates and Q'_i are the applied forces. Substituting Equation (17) on Equation (18), assuming that the potential energy is independent from the velocity, results

$$\frac{d}{dt}\Big(\frac{\partial E_{kinetic}}{\partial \dot{q}_i}\Big) - \frac{\partial E_{kinetic}}{\partial q_i} = Q'_i - \frac{\partial E_{potential}}{\partial q_i} = Q_i \tag{19}$$

First of all, it is necessary to write the expression of kinetic energy. It can be decomposed into a sum of two terms: transnational and rotational kinetic energy.

$$E_{kinetic} = E_{trans} + E_{rot}$$

For simplicity of notation below we derive separately Lagrange's equations for these two components. Remembering that derivation is a linear function the superposition principle is applicable.

Recalling the system DOFs presented in section 2.1. The number of generalized coordinates must be equal to the DOFs of the multi-body system, therefore they are $3(n+1)$. The chosen generalized coordinates are the angles ϕ_{j},ϑ_{j},ψ_{j} for $j = 1, \ldots, n+1$. We reveal in advance that the transitional kinetic energy obtained in section 3.2.1 is independent from the Euler angles ψ_{j}. Moreover, in section 3.2.2, in particular in Equation (66), the torsion of the cable is neglected. Due to this simplification for the cable segment, except for the virtual one, the system energy is independent from the angle ψ_{j}. In other word the DOFs of the UAS are reduced by n fixing the angle $\psi_{\mathrm{j}} = 0$ for $j = 1, \ldots, n$. Finally the generalized coordinates are $2n + 3$: $2(n + 1)$ angles ϕ_{j},ϑ_{j}, a couple for each cable's elements that describe totally the Cartesian location of the cable nodes and the angle ψ_{n+1} that define the rotation of UAV along his z axis. Recalling that $\sin(0) = 0$ and $\cos(0) = 1$ the rotational matrix (4) (and his inverse (5)), for the cable's segments reduce to:

$$R_{0\,\phi_j\,\vartheta_j} = \begin{pmatrix} c_{\vartheta_j} & -s_{\vartheta_j}\,s_{\phi_j} & s_{\vartheta_j}\,c_{\phi_j} \\ 0 & c_{\phi_j} & s_{\phi_j} \\ -s_{\vartheta_j} & -c_{\vartheta_j}\,s_{\phi_j} & c_{\vartheta_j}\,c_{\phi_j} \end{pmatrix} \qquad j = 1, \dots, n \tag{20}$$

$$R^{-1}_{0\,\phi_j\,\vartheta_j} = \begin{pmatrix} c_{\phi_j}\,c_{\vartheta_j} & 0 & -s_{\vartheta_j} \\ -s_{\vartheta_j}\,s_{\phi_j} & c_{\phi_j} & -c_{\vartheta_j}\,s_{\phi_j} \\ s_{\vartheta_j}\,c_{\phi_j} & s_{\phi_j} & c_{\vartheta_j}\,s_{\phi_j} \end{pmatrix} \qquad j = 1, \dots, n \tag{21}$$

3.1 Generalized forces Q_{q_i}

The generalize forces associated with the system generalized coordinates can be calculated applying the virtual work principle. Referring to [29] the generalized forces Q'_{q_i} are:

$$\begin{aligned} Q'_{q_i} &= \sum_{k=1}^{n+1} \left\{ \vec{F}_e^k \cdot \frac{\partial \vec{r^k}}{\partial q_i} + M_{q_k} \frac{\partial q_k}{\partial q_i} \right\} = \\ &\sum_{k=1}^{n+1} \left\{ F_{x_k} \frac{\partial X_k}{\partial q_i} + F_{y_k} \frac{\partial Y_k}{\partial q_i} + F_{z_k} \frac{\partial Z_k}{\partial q_i} \right\} + M_{q_i} \qquad i = 1, \dots, 2n+3 \end{aligned} \tag{22}$$

where $\vec{F}_e^k$ and M_{q_k} are, respectively the external forces and moment acting on the k^{th} node and $\vec{r_k} = (X_k, Y_k, Z_k)$ is his Cartesian's position relative to the inertial RF.
Recalling the Equation (19)

$$Q_{q_i} = Q'_{q_i} - \frac{\partial E_{potential}}{\partial q_i} \tag{23}$$

The total potential energy of the multi-body system is, assuming that the XY-plane ($Z = 0$) corresponds to null level of potential energy:

$$E_{potential} = \sum_{k=1}^{n+1} m_k Z_k g \tag{24}$$

where m_k is the mass of the k^{th} cable segment and Z_k is his elevation related to the inertial RF. Observe that the potential energy is independent from the generalized coordinates time derivatives ($\dot{\phi}_i$, $\dot{\vartheta}_i$ and $\dot{\psi}_i$), for this reason it can be canceled inside the time derivative of Equation (18) obtaining the Equation (19). Since the partial deviate is a linear application, it results:

$$\frac{\partial E_{potential}}{\partial q_i} = \sum_{k=1}^{n+1} m_k g \frac{\partial Z_k}{\partial q_i} \tag{25}$$

Finally, substituting Equation (22) and Equation (25) in the Equation (23):

$$Q_{q_i} = \sum_{k=1}^{n+1} \Big\{ F_{x_k} \frac{\partial X_k}{\partial q_i} + F_{y_k} \frac{\partial Y_k}{\partial q_i} + \big(F_{z_k} - m_k g\big) \frac{\partial Z_k}{\partial q_i} \Big\} + M_{q_i} \qquad i = 1, \dots, 3(n+1) \tag{26}$$

The generalized forces Q_{q_i} should be calculated for all the $3(n+1)$ generalized coordinates q_i. They are evaluated separately for the three angle ϕ, θ and ψ, starting from the first one, remembering that the k^{th} cable element lumped mass position's expression is Equation (8).

$$\begin{cases} \frac{\partial X_k}{\partial \phi_\mathrm{i}} = 0 \\ \frac{\partial Y_k}{\partial \phi_\mathrm{i}} = -l_i \, \mathrm{c}_{\phi_\mathrm{i}} \, \mathrm{c}_{\vartheta_\mathrm{i}} \qquad k \geq i \quad i = 1, \dots, n+1 \\ \frac{\partial Z_k}{\partial \phi_\mathrm{i}} = -l_i \, \mathrm{s}_{\phi_\mathrm{i}} \, \mathrm{c}_{\vartheta_\mathrm{i}} \end{cases}$$

$$Q_{\phi_\mathrm{i}} = \sum_{k=i}^{n+1} \Big\{ F_{y_k}(-l_i \, \mathrm{c}_{\phi_\mathrm{i}} \, \mathrm{c}_{\vartheta_\mathrm{i}}) + (F_{z_k} - m_k g)(-l_i \, \mathrm{s}_{\phi_\mathrm{i}} \, \mathrm{c}_{\vartheta_\mathrm{i}}) \Big\} + M_{\phi_\mathrm{i}} \tag{27}$$

$$\begin{cases} \frac{\partial X_k}{\partial \vartheta_\mathrm{i}} = -l_i \, \mathrm{c}_{\vartheta_\mathrm{i}} \\ \frac{\partial Y_k}{\partial \vartheta_\mathrm{i}} = l_i \, \mathrm{s}_{\phi_\mathrm{i}} \, \mathrm{s}_{\vartheta_\mathrm{i}} \qquad k \geq i \quad i = 1, \dots, n+1 \\ \frac{\partial Z_k}{\partial \vartheta_\mathrm{i}} = -l_i \, \mathrm{c}_{\phi_\mathrm{i}} \, \mathrm{s}_{\vartheta_\mathrm{i}} \end{cases}$$

$$Q_{\vartheta_\mathrm{i}} = \sum_{k=i}^{n+1} \Big\{ F_{x_k}(-l_i \, \mathrm{c}_{\vartheta_\mathrm{i}}) + F_{y_k}(l_i \, \mathrm{s}_{\phi_\mathrm{i}} \, \mathrm{s}_{\vartheta_\mathrm{i}}) + (F_{z_k} - m_k g)(-l_i \, \mathrm{c}_{\phi_\mathrm{i}} \, \mathrm{s}_{\vartheta_\mathrm{i}}) \Big\} + M_{\vartheta_\mathrm{i}} \tag{28}$$

Since the cable's nodes position is independent from the angle ψ, the partial derivatives of the Cartesian position $\vec{r_k}$ are null. The only not null term for these generalized coordinates is the moment

$$Q_{\psi_\mathrm{i}} = M_{\psi_\mathrm{i}} \tag{29}$$

Observe that for the cable elements no moments are applied to the nodes, so $M_{\phi_\mathrm{i}} = M_{\vartheta_\mathrm{i}} = M_{\psi_\mathrm{i}} = 0$ for $i = 1, \ldots, n$. Q_{ψ_i} exists only for the UAV virtual segment, $i = n + 1$:

$$Q_{\psi_{n+1}} = M_{\psi_{n+1}} \tag{30}$$

Let's define the generalized moment for the UAV virtual segment

$$\mathbf{M}_{n+1} = \begin{pmatrix} M_{\phi_{n+1}} \\ M_{\theta_{n+1}} \\ M_{\psi_{n+1}} \end{pmatrix} \tag{31}$$

These generalized moments are different from those calculated in the section 2.3. The UAV moments $\mathbf{M}_{UAV} = (M_{\mathrm{x_{body}}}, M_{\mathrm{y_{body}}}, M_{\mathrm{z_{body}}})$ are the moments due to the differential thrust of the propellers relative to the body reference system. The generalized moments are the moments projected in the inertial RF. Recalling the rotation matrix (5) the generalized moments are: .

$$\mathbf{M}_{n+1} = R^{-1}_{\phi\theta\psi_{UAV}} \begin{pmatrix} M_{\mathrm{x_{body}}} \\ M_{\mathrm{y_{body}}} \\ M_{\mathrm{z_{body}}} \end{pmatrix} \tag{32}$$

3.2 Lagrange's equation with cable fixed length

3.2.1 Lagrange's equations of transitional kinetic energy

The transitional kinetic energy of a multi-body system can be written as sum of the kinetic energy of each system's element:

$$E_{trans} = \frac{1}{2} \sum_{k=1}^{n+1} m_k \left| \vec{V_k} \right|^2 \tag{33}$$

where $\vec{V_k}$ is the velocity vector of the k^{th} cable segment element with respect to the inertial reference frame. It is known that $\left| \vec{V_k} \right|^2$ can be expressed as:

$$\left|\vec{V}_k\right|^2 = \vec{V}_k^T \ \vec{V}_k = \dot{X}_k^2 + \dot{Y}_k^2 + \dot{Z}_k^2 \qquad (k = 1, \dots, n+1)$$

The formulation of the nodes' velocity in the inertial reference frame are obtained deriving respect the time their position, Equation (8):

$$\begin{cases} \dot{X}_k = \sum_{j=1}^{k} -l_j(\dot{\vartheta}_\mathrm{j}\, \mathrm{c}_{\vartheta_\mathrm{j}}) \\ \dot{Y}_k = \sum_{j=1}^{k} l_j(-\dot{\phi}_\mathrm{j}\, \mathrm{c}_{\phi_\mathrm{j}}\, \mathrm{c}_{\vartheta_\mathrm{j}} + \dot{\vartheta}_\mathrm{j}\, \mathrm{s}_{\phi_\mathrm{j}}\, \mathrm{s}_{\vartheta_\mathrm{j}}) \qquad k = 1, \dots, n+1 \\ \dot{Z}_k = \sum_{j=1}^{k} l_j(-\dot{\phi}_\mathrm{j}\, \mathrm{s}_{\phi_\mathrm{j}}\, \mathrm{c}_{\vartheta_\mathrm{j}} - \dot{\vartheta}_\mathrm{j}\, \mathrm{c}_{\phi_\mathrm{j}}\, \mathrm{s}_{\vartheta_\mathrm{j}}) \end{cases} \tag{34}$$

Recalling that $(\sum_{i=1}^{n} x_i)^2 = \sum_{i=1}^{n} \sum_{j=1}^{n} x_i x_j$, the square velocity, for $k = 1, \dots, n+1$ results:

$$\begin{cases} \dot{X}_k^2 = \sum_{i=1}^{k} \sum_{j=1}^{k} l_i l_j(\dot{\vartheta}_\mathrm{i}\, \mathrm{c}_{\vartheta_\mathrm{i}})(\dot{\vartheta}_\mathrm{j}\, \mathrm{c}_{\vartheta_\mathrm{j}}) \\ \dot{Y}_k^2 = \sum_{i=1}^{k} \sum_{j=1}^{k} l_i l_j(-\dot{\phi}_\mathrm{i}\, \mathrm{c}_{\phi_\mathrm{i}}\, \mathrm{c}_{\vartheta_\mathrm{i}} + \dot{\vartheta}_\mathrm{i}\, \mathrm{s}_{\phi_\mathrm{i}}\, \mathrm{s}_{\vartheta_\mathrm{i}})(-\dot{\phi}_\mathrm{j}\, \mathrm{c}_{\phi_\mathrm{j}}\, \mathrm{c}_{\vartheta_\mathrm{j}} + \dot{\vartheta}_\mathrm{j}\, \mathrm{s}_{\phi_\mathrm{j}}\, \mathrm{s}_{\vartheta_\mathrm{j}}) \\ \dot{Z}_k^2 = \sum_{i=1}^{k} \sum_{j=1}^{k} l_i l_j(-\dot{\phi}_\mathrm{i}\, \mathrm{s}_{\phi_\mathrm{i}}\, \mathrm{c}_{\vartheta_\mathrm{i}} - \dot{\vartheta}_\mathrm{i}\, \mathrm{c}_{\phi_\mathrm{i}}\, \mathrm{s}_{\vartheta_\mathrm{i}})(-\dot{\phi}_\mathrm{j}\, \mathrm{s}_{\phi_\mathrm{j}}\, \mathrm{c}_{\vartheta_\mathrm{j}} - \dot{\vartheta}_\mathrm{j}\, \mathrm{c}_{\phi_\mathrm{j}}\, \mathrm{s}_{\vartheta_\mathrm{j}}) \end{cases} \tag{35}$$

Assembling Equation (35) in the total square velocity

$$\left|\vec{V}_k\right|^2 = \sum_{i=1}^{k} \sum_{j=1}^{k} \Big\{ l_i l_j \big[\, \dot{\phi}_\mathrm{i}\, \dot{\phi}_\mathrm{j}\, \mathrm{c}_{\vartheta_\mathrm{i}}\, \mathrm{c}_{\vartheta_\mathrm{j}}\, \mathrm{c}_{\phi_\mathrm{ji}} + \dot{\vartheta}_\mathrm{i}\, \dot{\vartheta}_\mathrm{j} \left(\mathrm{s}_{\vartheta_\mathrm{i}}\, \mathrm{s}_{\vartheta_\mathrm{j}}\, \mathrm{c}_{\phi_\mathrm{ji}} + \mathrm{c}_{\vartheta_\mathrm{i}}\, \mathrm{c}_{\vartheta_\mathrm{j}} \right) + 2 \ \dot{\vartheta}_\mathrm{i}\, \dot{\phi}_\mathrm{j}\, \mathrm{s}_{\vartheta_\mathrm{i}}\, \mathrm{c}_{\vartheta_\mathrm{j}}\, \mathrm{s}_{\phi_\mathrm{ji}} \,\big] \Big\} \tag{36}$$

It is now possible to explicit the kinetic energy substituting Equation (36) in Equation (33). To make easier the successive step we isolate the velocity terms with i index.

$$E_{trans} = \frac{1}{2} \sum_{k=1}^{n+1} \sum_{i=1}^{k} \sum_{j=1}^{k} \Big\{ m_k l_i l_j \Big[\dot{\phi}_\mathrm{i} \left(\dot{\phi}_\mathrm{j}\, \mathrm{c}_{\vartheta_\mathrm{i}}\, \mathrm{c}_{\vartheta_\mathrm{j}}\, \mathrm{c}_{\phi_\mathrm{ji}} - \dot{\vartheta}_\mathrm{j}\, \mathrm{c}_{\vartheta_\mathrm{i}}\, \mathrm{s}_{\vartheta_\mathrm{j}}\, \mathrm{s}_{\phi_\mathrm{ji}} \right) + \dot{\vartheta}_\mathrm{i} \left(\dot{\phi}_\mathrm{j}\, \mathrm{s}_{\vartheta_\mathrm{i}}\, \mathrm{c}_{\vartheta_\mathrm{j}}\, \mathrm{s}_{\phi_\mathrm{ji}} + \dot{\vartheta}_\mathrm{j} \left(\mathrm{s}_{\vartheta_\mathrm{i}}\, \mathrm{s}_{\vartheta_\mathrm{j}}\, \mathrm{c}_{\phi_\mathrm{ji}} + \mathrm{c}_{\vartheta_\mathrm{i}}\, \mathrm{c}_{\vartheta_\mathrm{j}} \right) \right) \Big] \Big\} \tag{37}$$

Observe that Equation (37) is independent from ψ_{i}. Therefore no such Lagrange's equations are derived for these generalized coordinates.

In order to write the Lagrange's equations several derivations must be performed. To simplify the notation the indication about the index i is omitted. The above equation must be intended for i varying between $i = 1, \ldots, n+1$.

We derive the kinetic energy relative to the angle ϕ_{i} and his time derivative $\dot{\phi}_{\mathrm{i}}$.

$$\frac{\partial E_{trans}}{\partial\,\phi_{\mathrm{i}}} = \sum_{k=i}^{n+1}\sum_{j=1}^{k}\Big\{m_k l_i l_j\Big[\,\dot{\phi}_{\mathrm{i}}\Big(\,\dot{\phi}_{\mathrm{j}}\,\mathrm{c}_{\vartheta_{\mathrm{i}}}\,\mathrm{c}_{\vartheta_{\mathrm{j}}}\,\mathrm{s}_{\phi_{\mathrm{ji}}} + \dot{\vartheta}_{\mathrm{j}}\,\mathrm{c}_{\vartheta_{\mathrm{i}}}\,\mathrm{s}_{\vartheta_{\mathrm{j}}}\,\mathrm{c}_{\phi_{\mathrm{ji}}}\Big) + \dot{\vartheta}_{\mathrm{i}}\Big(-\,\dot{\phi}_{\mathrm{j}}\,\mathrm{s}_{\vartheta_{\mathrm{i}}}\,\mathrm{c}_{\vartheta_{\mathrm{j}}}\,\mathrm{c}_{\phi_{\mathrm{ji}}} + \dot{\vartheta}_{\mathrm{j}}\,\mathrm{s}_{\vartheta_{\mathrm{i}}}\,\mathrm{s}_{\vartheta_{\mathrm{j}}}\,\mathrm{s}_{\phi_{\mathrm{ji}}}\Big)\Big]\Big\} \tag{38}$$

$$\frac{\partial E_{trans}}{\partial\,\dot{\phi}_{\mathrm{i}}} = \sum_{k=i}^{n+1}\sum_{j=1}^{k}\Big\{m_k l_i l_j\big[\,\dot{\phi}_{\mathrm{j}}\,\mathrm{c}_{\vartheta_{\mathrm{i}}}\,\mathrm{c}_{\vartheta_{\mathrm{j}}}\,\mathrm{c}_{\phi_{\mathrm{ji}}} - \dot{\vartheta}_{\mathrm{j}}\,\mathrm{c}_{\vartheta_{\mathrm{i}}}\,\mathrm{s}_{\vartheta_{\mathrm{j}}}\,\mathrm{s}_{\phi_{\mathrm{ji}}}\,\big]\Big\} \tag{39}$$

Deriving the Equation (39) with respect to the time, results:

$$\begin{aligned}\frac{d}{dt}\Big(\frac{\partial E_{trans}}{\partial\,\dot{\phi}_{\mathrm{i}}}\Big) = \sum_{k=i}^{n+1}\sum_{j=1}^{k}\Big\{m_k l_i l_j\Big[\; & \ddot{\phi}_{\mathrm{j}}\big(\,\mathrm{c}_{\vartheta_{\mathrm{i}}}\,\mathrm{c}_{\vartheta_{\mathrm{j}}}\,\mathrm{c}_{\phi_{\mathrm{ji}}}\big) + \ddot{\vartheta}_{\mathrm{j}}\big(-\,\mathrm{c}_{\vartheta_{\mathrm{i}}}\,\mathrm{s}_{\vartheta_{\mathrm{j}}}\,\mathrm{s}_{\phi_{\mathrm{ji}}}\big)\\ & -\dot{\phi}_{\mathrm{j}}^{\,2}\big(\,\mathrm{c}_{\vartheta_{\mathrm{i}}}\,\mathrm{c}_{\vartheta_{\mathrm{j}}}\,\mathrm{s}_{\phi_{\mathrm{ji}}}\big) + \dot{\vartheta}_{\mathrm{j}}^{\,2}\big(-\,\mathrm{c}_{\vartheta_{\mathrm{i}}}\,\mathrm{c}_{\vartheta_{\mathrm{j}}}\,\mathrm{s}_{\phi_{\mathrm{ji}}}\big)\\ & +\dot{\phi}_{\mathrm{i}}\,\dot{\phi}_{\mathrm{j}}\big(\,\mathrm{c}_{\vartheta_{\mathrm{i}}}\,\mathrm{c}_{\vartheta_{\mathrm{j}}}\,\mathrm{s}_{\phi_{\mathrm{ji}}}\big) + \dot{\vartheta}_{\mathrm{i}}\,\dot{\vartheta}_{\mathrm{j}}\big(\,\mathrm{s}_{\vartheta_{\mathrm{i}}}\,\mathrm{s}_{\vartheta_{\mathrm{j}}}\,\mathrm{s}_{\phi_{\mathrm{ji}}}\big)\\ & +\dot{\phi}_{\mathrm{j}}\,\dot{\vartheta}_{\mathrm{j}}\big(-2\,\mathrm{c}_{\vartheta_{\mathrm{i}}}\,\mathrm{s}_{\vartheta_{\mathrm{j}}}\,\mathrm{c}_{\phi_{\mathrm{ji}}}\big) + \dot{\phi}_{\mathrm{i}}\,\dot{\vartheta}_{\mathrm{j}}\big(\,\mathrm{c}_{\vartheta_{\mathrm{i}}}\,\mathrm{s}_{\vartheta_{\mathrm{j}}}\,\mathrm{c}_{\phi_{\mathrm{ji}}}\big)\\ & +\dot{\phi}_{\mathrm{j}}\,\dot{\vartheta}_{\mathrm{i}}\big(-\,\mathrm{s}_{\vartheta_{\mathrm{i}}}\,\mathrm{c}_{\vartheta_{\mathrm{j}}}\,\mathrm{c}_{\phi_{\mathrm{ji}}}\big)\Big\}\end{aligned} \tag{40}$$

Assembling the derivatives just calculate Equation (38) and Equation (40) in the Lagrange's equation Equation (19) we obtain $n+1$ equations of the type:

$$
\begin{aligned}
\frac{d}{dt}\Big(\frac{\partial E_{trans}}{\partial\,\dot{\phi}_\mathrm{i}}\Big) - \frac{\partial E_{kinetic}}{\partial\,\phi_\mathrm{i}} = \sum_{k=i}^{n+1}\sum_{j=1}^{k}\Big\{ m_k l_i l_j \big[\\
\ddot{\phi}_\mathrm{j}\,\big(\,\mathrm{c}_{\vartheta_\mathrm{i}}\,\mathrm{c}_{\vartheta_\mathrm{j}}\,\mathrm{c}_{\phi_\mathrm{ji}}\,\big) + \ddot{\vartheta}_\mathrm{j}\,\big(-\,\mathrm{c}_{\vartheta_\mathrm{i}}\,\mathrm{s}_{\vartheta_\mathrm{j}}\,\mathrm{s}_{\phi_\mathrm{ji}}\,\big) \\
+\,\dot{\phi}_\mathrm{j}^{\,2}\,\big(-\,\mathrm{c}_{\vartheta_\mathrm{i}}\,\mathrm{c}_{\vartheta_\mathrm{j}}\,\mathrm{s}_{\phi_\mathrm{ji}}\,\big) + \dot{\vartheta}_\mathrm{j}^{\,2}\,\big(-\,\mathrm{c}_{\vartheta_\mathrm{i}}\,\mathrm{c}_{\vartheta_\mathrm{j}}\,\mathrm{s}_{\phi_\mathrm{ji}}\,\big) \\
+\,\dot{\phi}_\mathrm{j}\,\dot{\vartheta}_\mathrm{j}\,\big(-\,2\,\mathrm{c}_{\vartheta_\mathrm{i}}\,\mathrm{s}_{\vartheta_\mathrm{j}}\,\mathrm{c}_{\phi_\mathrm{ji}}\,\big)\big]\Big\} = Q_{\phi_\mathrm{i}}
\end{aligned} \tag{41}
$$

Following a similar path the Lagrange's equations referred to the generalized coordinates ϑ_i are evaluated.

$$
\begin{aligned}
\frac{\partial E_{trans}}{\partial\,\vartheta_\mathrm{i}} = \sum_{k=i}^{n+1}\sum_{j=1}^{k}\Big\{ m_k l_i l_j \Big[\,\dot{\phi}_\mathrm{i}\,\Big(-\,\dot{\phi}_\mathrm{j}\,\mathrm{s}_{\vartheta_\mathrm{i}}\,\mathrm{c}_{\vartheta_\mathrm{j}}\,\mathrm{c}_{\phi_\mathrm{ji}} + \dot{\vartheta}_\mathrm{j}\,\mathrm{s}_{\vartheta_\mathrm{i}}\,\mathrm{s}_{\vartheta_\mathrm{j}}\,\mathrm{s}_{\phi_\mathrm{ji}}\Big) \\
+\,\dot{\vartheta}_\mathrm{i}\,\Big(\,\dot{\phi}_\mathrm{j}\,\mathrm{c}_{\vartheta_\mathrm{i}}\,\mathrm{c}_{\vartheta_\mathrm{j}}\,\mathrm{s}_{\phi_\mathrm{ji}} + \dot{\vartheta}_\mathrm{j}\,\big(\,\mathrm{c}_{\vartheta_\mathrm{i}}\,\mathrm{s}_{\vartheta_\mathrm{j}}\,\mathrm{c}_{\phi_\mathrm{ji}} - \mathrm{s}_{\vartheta_\mathrm{i}}\,\mathrm{c}_{\vartheta_\mathrm{j}}\,\big)\Big)\Big]\Big\}
\end{aligned} \tag{42}
$$

$$
\begin{aligned}
\frac{\partial E_{trans}}{\partial\,\dot{\vartheta}_\mathrm{i}} = \sum_{k=i}^{n+1}\sum_{j=1}^{k}\Big\{ m_k l_i l_j \big[\,\dot{\phi}_\mathrm{j}\,\mathrm{s}_{\vartheta_\mathrm{i}}\,\mathrm{c}_{\vartheta_\mathrm{j}}\,\mathrm{s}_{\phi_\mathrm{ji}} \\
+\,\dot{\vartheta}_\mathrm{j}\,\big(\,\mathrm{s}_{\vartheta_\mathrm{i}}\,\mathrm{s}_{\vartheta_\mathrm{j}}\,\mathrm{c}_{\phi_\mathrm{ji}} + \mathrm{c}_{\vartheta_\mathrm{i}}\,\mathrm{c}_{\vartheta_\mathrm{j}}\,\big)\big]\Big\}
\end{aligned} \tag{43}
$$

Deriving the Equation (43) relative to the time, results:

$$
\begin{aligned}
\frac{d}{dt}\Big(\frac{\partial E_{trans}}{\partial\,\dot{\vartheta}_\mathrm{i}}\Big) = \sum_{k=i}^{n+1}\sum_{j=1}^{k}\Big\{ m_k l_i l_j \big[\\
\ddot{\phi}_\mathrm{j}\,\big(\,\mathrm{s}_{\vartheta_\mathrm{i}}\,\mathrm{c}_{\vartheta_\mathrm{j}}\,\mathrm{s}_{\phi_\mathrm{ji}}\,\big) + \ddot{\vartheta}_\mathrm{j}\,\big(\,\mathrm{s}_{\vartheta_\mathrm{i}}\,\mathrm{s}_{\vartheta_\mathrm{j}}\,\mathrm{c}_{\phi_\mathrm{ji}} + \mathrm{c}_{\vartheta_\mathrm{i}}\,\mathrm{c}_{\vartheta_\mathrm{j}}\,\big) \\
+\,\dot{\phi}_\mathrm{j}^{\,2}\,\big(\,\mathrm{s}_{\vartheta_\mathrm{i}}\,\mathrm{c}_{\vartheta_\mathrm{j}}\,\mathrm{c}_{\phi_\mathrm{ji}}\,\big) + \dot{\vartheta}_\mathrm{j}^{\,2}\,\big(\,\mathrm{s}_{\vartheta_\mathrm{i}}\,\mathrm{c}_{\vartheta_\mathrm{j}}\,\mathrm{c}_{\phi_\mathrm{ji}} - \mathrm{c}_{\vartheta_\mathrm{i}}\,\mathrm{s}_{\vartheta_\mathrm{j}}\,\big) \\
+\,\dot{\phi}_\mathrm{i}\,\dot{\phi}_\mathrm{j}\,\big(-\,\mathrm{s}_{\vartheta_\mathrm{i}}\,\mathrm{c}_{\vartheta_\mathrm{j}}\,\mathrm{c}_{\phi_\mathrm{ji}}\,\big) + \dot{\vartheta}_\mathrm{i}\,\dot{\vartheta}_\mathrm{j}\,\big(\,\mathrm{c}_{\vartheta_\mathrm{i}}\,\mathrm{s}_{\vartheta_\mathrm{j}}\,\mathrm{c}_{\phi_\mathrm{ji}} - \mathrm{s}_{\vartheta_\mathrm{i}}\,\mathrm{c}_{\vartheta_\mathrm{j}}\,\big) \\
+\,\dot{\phi}_\mathrm{j}\,\dot{\vartheta}_\mathrm{j}\,\big(-\,2\,\mathrm{s}_{\vartheta_\mathrm{i}}\,\mathrm{s}_{\vartheta_\mathrm{j}}\,\mathrm{s}_{\phi_\mathrm{ji}}\,\big) + \dot{\phi}_\mathrm{i}\,\dot{\vartheta}_\mathrm{j}\,\big(\,\mathrm{s}_{\vartheta_\mathrm{i}}\,\mathrm{s}_{\vartheta_\mathrm{j}}\,\mathrm{s}_{\phi_\mathrm{ji}}\,\big) \\
+\,\dot{\phi}_\mathrm{j}\,\dot{\vartheta}_\mathrm{i}\,\big(\,\mathrm{c}_{\vartheta_\mathrm{i}}\,\mathrm{c}_{\vartheta_\mathrm{j}}\,\mathrm{s}_{\phi_\mathrm{ji}}\,\big)\Big\}
\end{aligned} \tag{44}
$$

Assembling the derivatives just calculate Equation (42) and Equation (44) in the Lagrange's equation Equation (19) we obtain $n+1$ equations of the type:

$$\begin{aligned}\frac{d}{dt}\Big(\frac{\partial E_{trans}}{\partial\,\dot{\vartheta}_{\mathrm{i}}}\Big) - \frac{\partial E_{trans}}{\partial\,\vartheta_{\mathrm{i}}} = \sum_{k=i}^{n+1}\sum_{j=1}^{k}\Big\{ m_k l_i l_j \big[\\ \ddot{\phi}_{\mathrm{j}}\,\big(\,\mathrm{s}_{\vartheta_{\mathrm{i}}}\,\mathrm{c}_{\vartheta_{\mathrm{j}}}\,\mathrm{s}_{\phi_{\mathrm{ji}}}\,\big) + \ddot{\vartheta}_{\mathrm{j}}\,\big(\,\mathrm{s}_{\vartheta_{\mathrm{i}}}\,\mathrm{s}_{\vartheta_{\mathrm{j}}}\,\mathrm{c}_{\phi_{\mathrm{ji}}} + \mathrm{c}_{\vartheta_{\mathrm{i}}}\,\mathrm{c}_{\vartheta_{\mathrm{j}}}\,\big) \\ + \dot{\phi}_{\mathrm{j}}^{\,2}\,\big(\,\mathrm{s}_{\vartheta_{\mathrm{i}}}\,\mathrm{c}_{\vartheta_{\mathrm{j}}}\,\mathrm{c}_{\phi_{\mathrm{ji}}}\,\big) + \dot{\vartheta}_{\mathrm{j}}^{\,2}\,\big(\,\mathrm{s}_{\vartheta_{\mathrm{i}}}\,\mathrm{c}_{\vartheta_{\mathrm{j}}}\,\mathrm{c}_{\phi_{\mathrm{ji}}} - \mathrm{c}_{\vartheta_{\mathrm{i}}}\,\mathrm{s}_{\vartheta_{\mathrm{j}}}\,\big) \\ + \dot{\phi}_{\mathrm{j}}\,\dot{\vartheta}_{\mathrm{j}}\,\big(-2\,\mathrm{s}_{\vartheta_{\mathrm{i}}}\,\mathrm{s}_{\vartheta_{\mathrm{j}}}\,\mathrm{s}_{\phi_{\mathrm{ji}}}\,\big)\big]\Big\} = Q_{\vartheta_{\mathrm{i}}} \end{aligned} \tag{45}$$

Assembling in matrix form

The obtained $3(n+1)$ equation in this representation are arduous to read and it needs an easier writing to implement them in a computer simulation. For this reason, they are rewritten in a matrix form, Equation (46). As already written no Lagrange's equations are derived from the angles ψ_{i}. Therefore, the submatrices related to them are null.

$$\begin{aligned}\begin{pmatrix}\mathbf{A}_{11}^{trn} & \mathbf{A}_{12}^{trn} & \mathbf{0}\\ \mathbf{A}_{21}^{trn} & \mathbf{A}_{22}^{trn} & \mathbf{0}\\ \mathbf{0} & \mathbf{0} & \mathbf{0}\end{pmatrix}\begin{pmatrix}\ddot{\boldsymbol{\phi}}\\ \ddot{\boldsymbol{\theta}}\\ \ddot{\boldsymbol{\psi}}\end{pmatrix} + \begin{pmatrix}\mathbf{B}_{11}^{trn} & \mathbf{B}_{12}^{trn} & \mathbf{0}\\ \mathbf{B}_{21}^{trn} & \mathbf{B}_{22}^{trn} & \mathbf{0}\\ \mathbf{0} & \mathbf{0} & \mathbf{0}\end{pmatrix}\, diag\begin{pmatrix}\dot{\boldsymbol{\phi}}\\ \dot{\boldsymbol{\theta}}\\ \dot{\boldsymbol{\psi}}\end{pmatrix}\begin{pmatrix}\dot{\boldsymbol{\phi}}\\ \dot{\boldsymbol{\theta}}\\ \dot{\boldsymbol{\psi}}\end{pmatrix} \\ + \begin{pmatrix}\mathbf{C}_{11}^{trn} & \mathbf{0} & \mathbf{0}\\ \mathbf{C}_{21}^{trn} & \mathbf{0} & \mathbf{0}\\ \mathbf{0} & \mathbf{0} & \mathbf{0}\end{pmatrix}\begin{pmatrix}\dot{\boldsymbol{\phi}}\,\dot{\boldsymbol{\theta}}\\ \dot{\boldsymbol{\phi}}\,\dot{\boldsymbol{\psi}}\\ \dot{\boldsymbol{\theta}}\,\dot{\boldsymbol{\psi}}\end{pmatrix} = \begin{pmatrix}\mathbf{Q}_{\phi}\\ \mathbf{Q}_{\theta}\\ \mathbf{0}\end{pmatrix}\end{aligned} \tag{46}$$

Defining

$$M_{ij} = \sum_{k=max(i,j)}^{n+1} m_k \tag{47}$$

The coefficients of the submatrices are:

$$
\begin{aligned}
\left[A_{11}^{trn}\right]_{i,j} &= M_{ij} l_i l_j \big(\mathrm{c}_{\vartheta_\mathrm{i}}\, \mathrm{c}_{\vartheta_\mathrm{j}}\, \mathrm{c}_{\phi_\mathrm{ji}} \big)\\
\left[A_{12}^{trn}\right]_{i,j} &= M_{ij} l_i l_j \big(-\mathrm{c}_{\vartheta_\mathrm{i}}\, \mathrm{s}_{\vartheta_\mathrm{j}}\, \mathrm{s}_{\phi_\mathrm{ji}} \big)\\
\left[A_{21}^{trn}\right]_{i,j} &= M_{ij} l_i l_j \big(\mathrm{s}_{\vartheta_\mathrm{i}}\, \mathrm{c}_{\vartheta_\mathrm{j}}\, \mathrm{s}_{\phi_\mathrm{ji}} \big)\\
\left[A_{22}^{trn}\right]_{i,j} &= M_{ij} l_i l_j \big(\mathrm{s}_{\vartheta_\mathrm{i}}\, \mathrm{s}_{\vartheta_\mathrm{j}}\, \mathrm{c}_{\phi_\mathrm{ji}} + \mathrm{c}_{\vartheta_\mathrm{i}}\, \mathrm{c}_{\vartheta_\mathrm{j}} \big)\\
\\
\left[B_{11}^{trn}\right]_{i,j} &= M_{ij} l_i l_j \big(-\mathrm{c}_{\vartheta_\mathrm{i}}\, \mathrm{c}_{\vartheta_\mathrm{j}}\, \mathrm{s}_{\phi_\mathrm{ji}} \big)\\
\left[B_{12}^{trn}\right]_{i,j} &= M_{ij} l_i l_j \big(-\mathrm{c}_{\vartheta_\mathrm{i}}\, \mathrm{c}_{\vartheta_\mathrm{j}}\, \mathrm{s}_{\phi_\mathrm{ji}} \big) = \left[B_{11}\right]_{i,j}\\
\left[B_{21}^{trn}\right]_{i,j} &= M_{ij} l_i l_j \big(\mathrm{s}_{\vartheta_\mathrm{i}}\, \mathrm{c}_{\vartheta_\mathrm{j}}\, \mathrm{c}_{\phi_\mathrm{ji}} \big)\\
\left[B_{22}^{trn}\right]_{i,j} &= M_{ij} l_i l_j \big(\mathrm{s}_{\vartheta_\mathrm{i}}\, \mathrm{c}_{\vartheta_\mathrm{j}}\, \mathrm{c}_{\phi_\mathrm{ji}} - \mathrm{c}_{\vartheta_\mathrm{i}}\, \mathrm{s}_{\vartheta_\mathrm{j}} \big)\\
\\
\left[C_{11}^{trn}\right]_{i,j} &= M_{ij} l_i l_j \big(-2\, \mathrm{c}_{\vartheta_\mathrm{i}}\, \mathrm{s}_{\vartheta_\mathrm{j}}\, \mathrm{c}_{\phi_\mathrm{ji}} \big)\\
\left[C_{21}^{trn}\right]_{i,j} &= M_{ij} l_i l_j \big(-2\, \mathrm{s}_{\vartheta_\mathrm{i}}\, \mathrm{s}_{\vartheta_\mathrm{j}}\, \mathrm{s}_{\phi_\mathrm{ji}} \big)
\end{aligned}
\tag{48}
$$

where $i = 1, \ldots, n+1$ and $j = 1, \ldots, n+1$

3.2.2 Lagrange's equations of rotational kinetic energy

To derive the Lagrange's equations terms of the rotational kinetic energy we follow the same path of the above section 3.2.1. First of all let's write the expression of the energy.

Assuming the cross inertia moments null, the inertia moment tensor of the j^{th} segment relative to the local RF is a diagonal matrix:

$$
\mathbf{I}_j = \begin{pmatrix} I_{xj} & 0 & 0 \\ 0 & I_{yj} & 0 \\ 0 & 0 & I_{zj} \end{pmatrix}
$$

The rotational kinetic energy can be written as

$$
E_{rot} = \frac{1}{2} \sum_{j=1}^{n+1} \vec{\omega}'_j \mathbf{I}_j \vec{\omega}_j = \frac{1}{2} \sum_{j=1}^{n+1} (I_{xj}\omega_{xj}^2 + I_{yj}\omega_{yj}^2 + I_{zj}\omega_{zj}^2) \tag{49}
$$

where $\vec{\omega}_j$ is the angular velocity of the j^{th} segment in the local reference frame. Observe that it is different from the angles' velocity $\dot{\phi}$, $\dot{\vartheta}$ and $\dot{\psi}$. It can be calculated using the rotational matrix (1), (2) and (3). As described in section 2.2 the local RF is obtained from successive rotation of angles ϕ , θ and ψ of inertial RF. Each elementary rotation must be projected in the j^{th} local RF.

$$\vec{\omega}_j = R_{\psi_{\mathrm{j}}} \begin{pmatrix} 0 \\ 0 \\ \dot{\psi}_{\mathrm{j}} \end{pmatrix} + R_{\psi_{\mathrm{j}}} R_{\vartheta_{\mathrm{j}}} \begin{pmatrix} 0 \\ \dot{\vartheta}_{\mathrm{j}} \\ 0 \end{pmatrix} + R_{\psi_{\mathrm{j}}} R_{\vartheta_{\mathrm{j}}} R_{\phi_{\mathrm{j}}} \begin{pmatrix} \dot{\phi}_{\mathrm{j}} \\ 0 \\ 0 \end{pmatrix} =$$
$$\begin{pmatrix} 0 \\ 0 \\ \dot{\psi}_{\mathrm{j}} \end{pmatrix} + R_{\psi_{\mathrm{j}}} \begin{pmatrix} 0 \\ \dot{\vartheta}_{\mathrm{j}} \\ 0 \end{pmatrix} + R_{\psi_{\mathrm{j}}} R_{\vartheta_{\mathrm{j}}} \begin{pmatrix} \dot{\phi}_{\mathrm{j}} \\ 0 \\ 0 \end{pmatrix}$$

From that

$$\vec{\omega}_j = \begin{pmatrix} \dot{\vartheta}_{\mathrm{j}}\, \mathrm{s}_{\psi_{\mathrm{j}}} + \dot{\phi}_{\mathrm{j}}\, \mathrm{c}_{\psi_{\mathrm{j}}}\, \mathrm{c}_{\vartheta_{\mathrm{j}}} \\ \dot{\vartheta}_{\mathrm{j}}\, \mathrm{c}_{\psi_{\mathrm{j}}} - \dot{\phi}_{\mathrm{j}}\, \mathrm{c}_{\vartheta_{\mathrm{j}}}\, \mathrm{s}_{\psi_{\mathrm{j}}} \\ \dot{\psi}_{\mathrm{j}} - \dot{\phi}_{\mathrm{j}}\, \mathrm{s}_{\vartheta_{\mathrm{j}}} \end{pmatrix} \tag{50}$$

Substituting the angular velocity Equation (50) in the rotational kinetic energy expression, Equation (49), results:

$$\begin{aligned} E_{rot} = \frac{1}{2} \sum_{j=1}^{n+1} \Big\{ & \mathrm{I}_{\mathrm{xj}} \left(\dot{\vartheta}_{\mathrm{j}}^{\,2}\, \mathrm{s}_{\psi_{\mathrm{j}}}^{\;2} + \dot{\phi}_{\mathrm{j}}^{\,2}\, \mathrm{c}_{\vartheta_{\mathrm{j}}}^{\;2}\, \mathrm{c}_{\psi_{\mathrm{j}}}^{\;2} + 2\, \dot{\vartheta}_{\mathrm{j}}\, \dot{\phi}_{\mathrm{j}}\, \mathrm{c}_{\vartheta_{\mathrm{j}}}\, \mathrm{s}_{\psi_{\mathrm{j}}}\, \mathrm{c}_{\psi_{\mathrm{j}}} \right) \\ & + \mathrm{I}_{\mathrm{yj}} \left(\dot{\vartheta}_{\mathrm{j}}^{\,2}\, \mathrm{c}_{\psi_{\mathrm{j}}}^{\;2} + \dot{\phi}_{\mathrm{j}}^{\,2}\, \mathrm{c}_{\vartheta_{\mathrm{j}}}^{\;2}\, \mathrm{s}_{\psi_{\mathrm{j}}}^{\;2} - 2\, \dot{\vartheta}_{\mathrm{j}}\, \dot{\phi}_{\mathrm{j}}\, \mathrm{c}_{\vartheta_{\mathrm{j}}}\, \mathrm{s}_{\psi_{\mathrm{j}}}\, \mathrm{c}_{\psi_{\mathrm{j}}} \right) \\ & + \mathrm{I}_{\mathrm{zj}} \left(\dot{\psi}_{\mathrm{j}}^{\,2} + \dot{\phi}_{\mathrm{j}}^{\,2}\, \mathrm{s}_{\vartheta_{\mathrm{j}}}^{\;2} - 2\, \dot{\phi}_{\mathrm{j}}\, \dot{\psi}_{\mathrm{j}}\, \mathrm{s}_{\vartheta_{\mathrm{j}}} \right) \Big\} \end{aligned} \tag{51}$$

Differentiating respect the generalized coordinates q_i the sum is reduce to a one term for $j = i$.

For the generalized coordinates ϕ_{i} :

$$\frac{\partial E_{rot}}{\partial\, \phi_{\mathrm{i}}} = 0 \tag{52}$$

$$
\begin{aligned}
\frac{\partial E_{rot}}{\partial\,\dot{\phi}_{\rm i}} &= \mathrm{I_{xi}}\left(\,\dot{\phi}_{\rm i}\,\mathrm{c}_{\vartheta_{\rm i}}{}^{2}\,\mathrm{c}_{\psi_{\rm i}}{}^{2} + \dot{\vartheta}_{\rm i}\,\mathrm{c}_{\vartheta_{\rm i}}\,\mathrm{s}_{\psi_{\rm i}}\,\mathrm{c}_{\psi_{\rm i}}\,\right)\\
&\quad + \mathrm{I_{yi}}\left(\,\dot{\phi}_{\rm i}\,\mathrm{c}_{\vartheta_{\rm i}}{}^{2}\,\mathrm{s}_{\psi_{\rm i}}{}^{2} - \dot{\vartheta}_{\rm i}\,\mathrm{c}_{\vartheta_{\rm i}}\,\mathrm{s}_{\psi_{\rm i}}\,\mathrm{c}_{\psi_{\rm i}}\,\right) + \mathrm{I_{zi}}\left(\,\dot{\phi}_{\rm i}\,\mathrm{s}_{\vartheta_{\rm i}}{}^{2} - \dot{\psi}_{\rm i}\,\mathrm{s}_{\vartheta_{\rm i}}\,\right) =\\
&\qquad \left(\,\mathrm{I_{xi}} - \mathrm{I_{yi}}\,\right)\dot{\vartheta}_{\rm i}\,\mathrm{c}_{\vartheta_{\rm i}}\,\mathrm{s}_{\psi_{\rm i}}\,\mathrm{c}_{\psi_{\rm i}}\\
&\qquad + \mathrm{I_{xi}}\,\dot{\phi}_{\rm i}\,\mathrm{c}_{\vartheta_{\rm j}}{}^{2}\,\mathrm{c}_{\psi_{\rm i}}{}^{2} + \mathrm{I_{yi}}\,\dot{\phi}_{\rm i}\,\mathrm{c}_{\vartheta_{\rm i}}{}^{2}\,\mathrm{s}_{\psi_{\rm i}}{}^{2} + \mathrm{I_{zi}}\left(\,\dot{\phi}_{\rm i}\,\mathrm{s}_{\vartheta_{\rm i}}{}^{2} - \dot{\psi}_{\rm i}\,\mathrm{s}_{\vartheta_{\rm i}}\,\right)
\end{aligned}
\tag{53}
$$

Deriving the Equation (53) respect the time, results:

$$
\begin{aligned}
\frac{d}{dt}\Big(\frac{\partial E_{rot}}{\partial\,\dot{\phi}_{\rm i}}\Big) &= \left(\,\mathrm{I_{xi}} - \mathrm{I_{yi}}\,\right)\left(\,\ddot{\vartheta}_{\rm i}\,\mathrm{c}_{\vartheta_{\rm i}}\,\mathrm{s}_{\psi_{\rm i}}\,\mathrm{c}_{\psi_{\rm i}} + \dot{\vartheta}_{\rm i}\,\dot{\psi}_{\rm i}\,\mathrm{c}_{2\,\psi_{\rm i}}\,\mathrm{c}_{\vartheta_{\rm i}} - \dot{\vartheta}_{\rm i}{}^{2}\,\mathrm{s}_{\vartheta_{\rm i}}\,\mathrm{s}_{\psi_{\rm i}}\,\mathrm{c}_{\psi_{\rm i}}\,\right)\\
&\quad + \mathrm{I_{xi}}\left(\,\ddot{\phi}_{\rm i}\,\mathrm{c}_{\vartheta_{\rm i}}{}^{2}\,\mathrm{c}_{\psi_{\rm i}}{}^{2} - \dot{\phi}_{\rm i}\,\dot{\vartheta}_{\rm i}\,2\,\mathrm{s}_{\vartheta_{\rm i}}\,\mathrm{c}_{\vartheta_{\rm i}}\,\mathrm{c}_{\psi_{\rm i}}{}^{2} - \dot{\phi}_{\rm i}\,\dot{\psi}_{\rm i}\,2\,\mathrm{c}_{\vartheta_{\rm i}}{}^{2}\,\mathrm{s}_{\psi_{\rm i}}\,\mathrm{c}_{\psi_{\rm i}}\,\right)\\
&\quad + \mathrm{I_{yi}}\left(\,\ddot{\phi}_{\rm i}\,\mathrm{c}_{\vartheta_{\rm i}}{}^{2}\,\mathrm{s}_{\psi_{\rm i}}{}^{2} - \dot{\phi}_{\rm i}\,\dot{\vartheta}_{\rm i}\,2\,\mathrm{s}_{\vartheta_{\rm i}}\,\mathrm{c}_{\vartheta_{\rm i}}\,\mathrm{s}_{\psi_{\rm i}}{}^{2} + \dot{\phi}_{\rm i}\,\dot{\psi}_{\rm i}\,2\,\mathrm{c}_{\vartheta_{\rm i}}{}^{2}\,\mathrm{s}_{\psi_{\rm i}}\,\mathrm{c}_{\psi_{\rm i}}\,\right)\\
&\quad + \mathrm{I_{zi}}\left(\,\ddot{\phi}_{\rm i}\,\mathrm{s}_{\vartheta_{\rm i}}{}^{2} - \ddot{\psi}_{\rm i}\,\mathrm{s}_{\vartheta_{\rm i}} + \dot{\phi}_{\rm i}\,\dot{\vartheta}_{\rm i}\,2\,\mathrm{s}_{\vartheta_{\rm i}}\,\mathrm{c}_{\vartheta_{\rm i}} - \dot{\vartheta}_{\rm i}\,\dot{\psi}_{\rm i}\,\mathrm{c}_{\vartheta_{\rm i}}\,\right)
\end{aligned}
\tag{54}
$$

Assembling the derivatives just calculate Equation (52) and Equation (54) in the Lagrange's equation Equation (19) we obtain $n+1$ equations equal to Equation (54):

$$
\frac{d}{dt}\Big(\frac{\partial E_{trans}}{\partial\,\dot{\phi}_{\rm i}}\Big) - \frac{\partial E_{trans}}{\partial\,\phi_{\rm i}} = (54) \tag{55}
$$

Following a similar path, the Lagrange's equations of the rotational kinetic energy terms referred to the generalized coordinates $\vartheta_{\rm i}$ are calculated.

$$
\begin{aligned}
\frac{\partial E_{rot}}{\partial\,\vartheta_{\rm i}} &= \left(\,\mathrm{I_{xi}} - \mathrm{I_{yi}}\,\right)\left(\,-\,\dot{\phi}_{\rm i}\,\dot{\vartheta}_{\rm i}\,\mathrm{s}_{\vartheta_{\rm i}}\,\mathrm{s}_{\psi_{\rm i}}\,\mathrm{c}_{\psi_{\rm i}}\,\right) + \mathrm{I_{xi}}\left(\,-\,\dot{\phi}_{\rm i}{}^{2}\,\mathrm{s}_{\vartheta_{\rm i}}\,\mathrm{c}_{\vartheta_{\rm i}}\,\mathrm{c}_{\psi_{\rm i}}{}^{2}\,\right)\\
&\quad + \mathrm{I_{yi}}\left(\,-\,\dot{\phi}_{\rm i}{}^{2}\,\mathrm{s}_{\vartheta_{\rm i}}\,\mathrm{c}_{\vartheta_{\rm i}}\,\mathrm{s}_{\psi_{\rm i}}{}^{2}\,\right) + \mathrm{I_{zi}}\left(\,\dot{\phi}_{\rm i}{}^{2}\,\mathrm{s}_{\vartheta_{\rm i}}\,\mathrm{c}_{\vartheta_{\rm i}} - \dot{\vartheta}_{\rm i}\,\dot{\psi}_{\rm i}\,\mathrm{c}_{\vartheta_{\rm i}}\,\right)
\end{aligned}
\tag{56}
$$

$$
\begin{aligned}
\frac{\partial E_{rot}}{\partial\,\dot{\vartheta}_{\rm i}} &= \mathrm{I_{xi}}\left(\,\dot{\phi}_{\rm i}\,\mathrm{c}_{\vartheta_{\rm i}}\,\mathrm{s}_{\psi_{\rm i}}\,\mathrm{c}_{\psi_{\rm i}} + \dot{\vartheta}_{\rm i}\,\mathrm{s}_{\psi_{\rm i}}{}^{2}\,\right)\\
&\quad + \mathrm{I_{yi}}\left(\,-\,\dot{\phi}_{\rm i}\,\mathrm{c}_{\vartheta_{\rm i}}\,\mathrm{s}_{\psi_{\rm i}}\,\mathrm{c}_{\psi_{\rm i}} + \dot{\vartheta}_{\rm i}\,\mathrm{c}_{\psi_{\rm i}}{}^{2}\,\right)
\end{aligned}
\tag{57}
$$

Deriving the Equation (57) respect the time, results:

$$\frac{d}{dt}\Big(\frac{\partial E_{rot}}{\partial\,\dot{\vartheta}_{\mathrm{i}}}\Big) = \mathrm{I}_{\mathrm{xi}}\,\ddot{\vartheta}_{\mathrm{i}}\,{\mathrm{s}_{\psi_{\mathrm{i}}}}^2 + \mathrm{I}_{\mathrm{yi}}\,\ddot{\vartheta}_{\mathrm{i}}\,{\mathrm{c}_{\psi_{\mathrm{i}}}}^2$$
$$+ \big(\,\mathrm{I}_{\mathrm{xi}} - \mathrm{I}_{\mathrm{yi}}\,\big)\big(\,\ddot{\phi}_{\mathrm{i}}\,\mathrm{c}_{\vartheta_{\mathrm{i}}}\,\mathrm{s}_{\psi_{\mathrm{i}}}\,\mathrm{c}_{\psi_{\mathrm{i}}} - \dot{\phi}_{\mathrm{i}}\,\dot{\vartheta}_{\mathrm{i}}\,\mathrm{s}_{\vartheta_{\mathrm{i}}}\,\mathrm{s}_{\psi_{\mathrm{i}}}\,\mathrm{c}_{\psi_{\mathrm{i}}}$$
$$+ \dot{\phi}_{\mathrm{i}}\,\dot{\psi}_{\mathrm{i}}\,\mathrm{c}_{\vartheta_{\mathrm{i}}}\,\mathrm{c}_{2\,\psi_{\mathrm{i}}} + \dot{\vartheta}_{\mathrm{i}}\,\dot{\psi}_{\mathrm{i}}\,2\,\mathrm{s}_{\psi_{\mathrm{i}}}\,\mathrm{c}_{\psi_{\mathrm{i}}}\,\big) \quad (58)$$

Assembling the derivatives just calculate Equation (56) and Equation (58) in the Lagrange's equation Equation (19) we obtain $n+1$ equations of the type:

$$\frac{d}{dt}\Big(\frac{\partial E_{trans}}{\partial\,\dot{\vartheta}_{\mathrm{i}}}\Big) - \frac{\partial E_{trans}}{\partial\,\vartheta_{\mathrm{i}}} = \mathrm{I}_{\mathrm{xi}}\,\big(\,\ddot{\vartheta}_{\mathrm{i}}\,{\mathrm{s}_{\psi_{\mathrm{i}}}}^2 + {\dot{\phi}_{\mathrm{i}}}^2\,\mathrm{s}_{\vartheta_{\mathrm{i}}}\,\mathrm{c}_{\vartheta_{\mathrm{i}}}\,{\mathrm{c}_{\psi_{\mathrm{i}}}}^2\,\big)$$
$$+ \mathrm{I}_{\mathrm{yi}}\,\big(\,\ddot{\vartheta}_{\mathrm{i}}\,{\mathrm{c}_{\psi_{\mathrm{i}}}}^2 + {\dot{\phi}_{\mathrm{i}}}^2\,\mathrm{s}_{\vartheta_{\mathrm{i}}}\,\mathrm{c}_{\vartheta_{\mathrm{i}}}\,{\mathrm{s}_{\psi_{\mathrm{i}}}}^2\,\big)$$
$$\big(\,\mathrm{I}_{\mathrm{xi}} - \mathrm{I}_{\mathrm{yi}}\,\big)\big(\,\ddot{\phi}_{\mathrm{i}}\,\mathrm{c}_{\vartheta_{\mathrm{i}}}\,\mathrm{s}_{\psi_{\mathrm{i}}}\,\mathrm{c}_{\psi_{\mathrm{i}}} + \dot{\phi}_{\mathrm{i}}\,\dot{\psi}_{\mathrm{i}}\,\mathrm{c}_{\vartheta_{\mathrm{i}}}\,\mathrm{c}_{2\,\psi_{\mathrm{i}}} + \dot{\vartheta}_{\mathrm{i}}\,\dot{\psi}_{\mathrm{i}}\,2\,\mathrm{s}_{\psi_{\mathrm{i}}}\,\mathrm{c}_{\psi_{\mathrm{i}}}\,\big)$$
$$+ \mathrm{I}_{\mathrm{zi}}\,\big(\,-\,{\dot{\phi}_{\mathrm{i}}}^2\,\mathrm{s}_{\vartheta_{\mathrm{i}}}\,\mathrm{c}_{\vartheta_{\mathrm{i}}} + \dot{\vartheta}_{\mathrm{i}}\,\dot{\psi}_{\mathrm{i}}\,\mathrm{c}_{\vartheta_{\mathrm{i}}}\,\big) \quad (59)$$

Finally, observe that, different from the transitional kinetic energy case, Equation (51) is a function of ψ and $\dot{\psi}$ so the Lagrange's equations can be derived for the generalized coordinates ψ_{i} for $i = 1, \ldots, n$.

$$\frac{\partial E_{rot}}{\partial\,\psi_{\mathrm{i}}} = \big(\,\mathrm{I}_{\mathrm{xi}} - \mathrm{I}_{\mathrm{yi}}\,\big)\big(\,-\,{\dot{\phi}_{\mathrm{i}}}^2\,{\mathrm{c}_{\vartheta_{\mathrm{i}}}}^2\,\mathrm{s}_{\psi_{\mathrm{i}}}\,\mathrm{c}_{\psi_{\mathrm{i}}} + {\dot{\vartheta}_{\mathrm{i}}}^2\,\mathrm{s}_{\psi_{\mathrm{i}}}\,\mathrm{c}_{\psi_{\mathrm{i}}} + \dot{\phi}_{\mathrm{i}}\,\dot{\vartheta}_{\mathrm{i}}\,\mathrm{c}_{\vartheta_{\mathrm{i}}}\,\mathrm{c}_{2\,\psi_{\mathrm{i}}}\,\big) \quad (60)$$

$$\frac{\partial E_{rot}}{\partial\,\dot{\psi}_{\mathrm{i}}} = \mathrm{I}_{\mathrm{zi}}\,\big(\,-\,\dot{\phi}_{\mathrm{i}}\,\mathrm{s}_{\vartheta_{\mathrm{i}}} + \dot{\psi}_{\mathrm{i}}\,\big) \quad (61)$$

Deriving the Equation (61) respect the time, results:

$$\frac{d}{dt}\Big(\frac{\partial E_{rot}}{\partial\,\dot{\psi}_{\mathrm{i}}}\Big) = \mathrm{I}_{\mathrm{zi}}\,\big(\,-\,\ddot{\phi}_{\mathrm{i}}\,\mathrm{s}_{\vartheta_{\mathrm{i}}} + \ddot{\psi}_{\mathrm{i}} - \dot{\phi}_{\mathrm{i}}\,\dot{\vartheta}_{\mathrm{i}}\,\mathrm{c}_{\vartheta_{\mathrm{i}}}\,\big) \quad (62)$$

Assembling the derivatives just calculate Equation (60) and Equation (62) in the Lagrange's equation Equation (19) we obtain $n+1$ equations of the type:

$$
\begin{aligned}
\frac{d}{dt}\Big(\frac{\partial E_{trans}}{\partial\,\dot{\psi}_{\mathrm{i}}}\Big) - \frac{\partial E_{trans}}{\partial\,\psi_{\mathrm{i}}} &= \mathrm{I_{zi}}\,\big(-\ddot{\phi}_{\mathrm{i}}\,\mathrm{s}_{\vartheta_{\mathrm{i}}} + \ddot{\psi}_{\mathrm{i}} - \dot{\phi}_{\mathrm{i}}\,\dot{\vartheta}_{\mathrm{i}}\,\mathrm{c}_{\vartheta_{\mathrm{i}}}\big) \\
&+ \big(\mathrm{I_{xi}} - \mathrm{I_{yi}}\big)\big(\dot{\phi}_{\mathrm{i}}{}^{2}\,\mathrm{c}_{\vartheta_{\mathrm{i}}}{}^{2}\,\mathrm{s}_{\psi_{\mathrm{i}}}\,\mathrm{c}_{\psi_{\mathrm{i}}} - \dot{\vartheta}_{\mathrm{i}}{}^{2}\,\mathrm{s}_{\psi_{\mathrm{i}}}\,\mathrm{c}_{\psi_{\mathrm{i}}} - \dot{\phi}_{\mathrm{i}}\,\dot{\vartheta}_{\mathrm{i}}\,\mathrm{c}_{\vartheta_{\mathrm{i}}}\,\mathrm{c}_{2\,\psi_{\mathrm{i}}}\big) \quad (63)
\end{aligned}
$$

Assembling in matrix form

As the above section 3.2.1 the derived $3(n+1)$ equations are rewritten in a matrix form.

$$
\begin{aligned}
&\begin{pmatrix} \mathbf{A}_{11}^{rot} & \mathbf{A}_{12}^{rot} & \mathbf{A}_{13}^{rot} \\ \mathbf{A}_{21}^{rot} & \mathbf{A}_{22}^{rot} & \mathbf{0} \\ \mathbf{A}_{31}^{rot} & \mathbf{0} & \mathbf{A}_{33}^{rot} \end{pmatrix} \begin{pmatrix} \ddot{\boldsymbol{\phi}} \\ \ddot{\boldsymbol{\theta}} \\ \ddot{\boldsymbol{\psi}} \end{pmatrix} + \begin{pmatrix} \mathbf{0} & \mathbf{B}_{12}^{rot} & \mathbf{0} \\ \mathbf{B}_{21}^{rot} & \mathbf{0} & \mathbf{0} \\ \mathbf{B}_{31}^{rot} & \mathbf{B}_{32}^{rot} & \mathbf{0} \end{pmatrix} \; diag \begin{pmatrix} \dot{\boldsymbol{\phi}} \\ \dot{\boldsymbol{\theta}} \\ \dot{\boldsymbol{\psi}} \end{pmatrix} \begin{pmatrix} \dot{\boldsymbol{\phi}} \\ \dot{\boldsymbol{\theta}} \\ \dot{\boldsymbol{\psi}} \end{pmatrix} \\
&\qquad + \begin{pmatrix} \mathbf{C}_{11}^{rot} & \mathbf{C}_{12}^{rot} & \mathbf{C}_{13}^{rot} \\ \mathbf{0} & \mathbf{C}_{22}^{rot} & \mathbf{C}_{23}^{rot} \\ \mathbf{C}_{31}^{rot} & \mathbf{0} & \mathbf{0} \end{pmatrix} \begin{pmatrix} \dot{\boldsymbol{\phi}}\,\dot{\boldsymbol{\theta}} \\ \dot{\boldsymbol{\phi}}\,\dot{\boldsymbol{\psi}} \\ \dot{\boldsymbol{\theta}}\,\dot{\boldsymbol{\psi}} \end{pmatrix} = \begin{pmatrix} \mathbf{0} \\ \mathbf{0} \\ \mathbf{Q}_{\boldsymbol{\psi}} \end{pmatrix} \quad (64)
\end{aligned}
$$

The coefficients of the submatrices are null out of the diagonal. In other word they exist only for $i = j$ with $i = 1, \ldots, n+1$. Results:

$$
\begin{aligned}
\left[A_{11}^{rot}\right]_{i,i} &= \mathrm{I_{xi}}\,\mathrm{c}_{\vartheta_\mathrm{i}}{}^2\,\mathrm{c}_{\psi_\mathrm{i}}{}^2 + \mathrm{I_{yi}}\,\mathrm{c}_{\vartheta_\mathrm{i}}{}^2\,\mathrm{s}_{\psi_\mathrm{i}}{}^2 + \mathrm{I_{zi}}\,\mathrm{s}_{\vartheta_\mathrm{i}}{}^2 \\
\left[A_{12}^{rot}\right]_{i,i} &= \left(\mathrm{I_{xi}} - \mathrm{I_{yi}}\right)\mathrm{c}_{\vartheta_\mathrm{i}}\,\mathrm{s}_{\psi_\mathrm{i}}\,\mathrm{c}_{\psi_\mathrm{i}} \\
\left[A_{13}^{rot}\right]_{i,i} &= -\,\mathrm{I_{zi}}\,\mathrm{s}_{\vartheta_\mathrm{i}} \\
\left[A_{21}^{rot}\right]_{i,i} &= \left(\mathrm{I_{xi}} - \mathrm{I_{yi}}\right)\mathrm{c}_{\vartheta_\mathrm{i}}\,\mathrm{s}_{\psi_\mathrm{i}}\,\mathrm{c}_{\psi_\mathrm{i}} \\
\left[A_{22}^{rot}\right]_{i,i} &= \mathrm{I_{xi}}\,\mathrm{s}_{\psi_\mathrm{i}}{}^2 + \mathrm{I_{yi}}\,\mathrm{c}_{\psi_\mathrm{i}}{}^2 \\
\left[A_{31}^{rot}\right]_{i,i} &= -\,\mathrm{I_{zi}}\,\mathrm{s}_{\vartheta_\mathrm{i}} \\
\left[A_{33}^{rot}\right]_{i,i} &= \mathrm{I_{zi}} \\
\\
\left[B_{12}^{rot}\right]_{i,i} &= \left(\mathrm{I_{xi}} - \mathrm{I_{yi}}\right)\left(-\,\mathrm{s}_{\vartheta_\mathrm{i}}\,\mathrm{s}_{\psi_\mathrm{i}}\,\mathrm{c}_{\psi_\mathrm{i}}\right) \\
\left[B_{21}^{rot}\right]_{i,i} &= \left(\mathrm{I_{xi}}\,\mathrm{c}_{\psi_\mathrm{i}}{}^2 + \mathrm{I_{yi}}\,\mathrm{s}_{\psi_\mathrm{i}}{}^2 - \mathrm{I_{zi}}\right)\mathrm{s}_{\vartheta_\mathrm{i}}\,\mathrm{c}_{\vartheta_\mathrm{j}} \\
\left[B_{31}^{rot}\right]_{i,i} &= \left(\mathrm{I_{xi}} - \mathrm{I_{yi}}\right)\mathrm{c}_{\vartheta_\mathrm{i}}{}^2\,\mathrm{s}_{\psi_\mathrm{i}}\,\mathrm{c}_{\psi_\mathrm{i}} \\
\left[B_{32}^{rot}\right]_{i,i} &= \left(\mathrm{I_{xi}} - \mathrm{I_{yi}}\right)\left(-\,\mathrm{s}_{\psi_\mathrm{i}}\,\mathrm{c}_{\psi_\mathrm{i}}\right) \\
\\
\left[C_{11}^{rot}\right]_{i,i} &= \left(-\,\mathrm{I_{xi}}\,\mathrm{c}_{\psi_\mathrm{i}}{}^2 - \mathrm{I_{yi}}\,\mathrm{s}_{\psi_\mathrm{i}}{}^2 + \mathrm{I_{zi}}\right)2\,\mathrm{s}_{\vartheta_\mathrm{i}}\,\mathrm{c}_{\vartheta_\mathrm{i}} \\
\left[C_{12}^{rot}\right]_{i,i} &= \left(\mathrm{I_{xi}} - \mathrm{I_{yi}}\right)\left(-\,2\,\mathrm{c}_{\vartheta_\mathrm{i}}{}^2\,\mathrm{s}_{\psi_\mathrm{i}}\,\mathrm{c}_{\psi_\mathrm{i}}\right) \\
\left[C_{13}^{rot}\right]_{i,i} &= \left(\mathrm{I_{xi}} - \mathrm{I_{yi}}\right)\mathrm{c}_{\vartheta_\mathrm{i}}\,\mathrm{c}_{2\,\psi_\mathrm{i}} - \mathrm{I_{zi}}\,\mathrm{c}_{\vartheta_\mathrm{i}} \\
\left[C_{22}^{rot}\right]_{i,i} &= \left(\mathrm{I_{xi}} - \mathrm{I_{yi}}\right)\mathrm{c}_{\vartheta_\mathrm{i}}\,\mathrm{c}_{2\,\psi_\mathrm{i}} \\
\left[C_{23}^{rot}\right]_{i,i} &= \left(\mathrm{I_{xi}} - \mathrm{I_{yi}}\right)2\,\mathrm{s}_{\psi_\mathrm{i}}\,\mathrm{c}_{\psi_\mathrm{i}} + \mathrm{I_{zi}}\,\mathrm{c}_{\vartheta_\mathrm{i}} \\
\left[C_{31}^{rot}\right]_{i,i} &= \left(\mathrm{I_{xi}} - \mathrm{I_{yi}}\right)\left(-\,\mathrm{c}_{\vartheta_\mathrm{i}}\,\mathrm{c}_{2\,\psi_\mathrm{i}}\right) - \mathrm{I_{zi}}\,\mathrm{c}_{\vartheta_\mathrm{i}}
\end{aligned}
\tag{65}
$$

for $i = 1, \dots, n+1$

As already said in section 2.1 a cable's segment is modeled as a weightless rod and lumped mass. His inertia moment relative to the z axis $\mathrm{I_{zi}}$ can be neglected ($\mathrm{I_{zi}} = 0$). This is not true for the virtual segment corresponding to the UAS, where the inertia moments of the vehicle are imposed. For the cable the lumped mass has a distance from the i^{th} local RF equal to the segment length and it is located on his z axis. Therefore, the segment moment of inertia relative to the axis x and y can be calculated with the Huygens-Steiner theorem:

$$\begin{cases} \mathrm{I_{xi}} = \mathrm{I_{yi}} = m_i l_i^2 = I_i \\ \mathrm{I_{zi}} = 0 \end{cases} \qquad i = 1, \ldots, n \tag{66}$$

The difference $\mathrm{I_{xi}} - \mathrm{I_{yi}} = 0$ is null. Under these hypotheses the Equation (63) is reduced to zero for the cable segment. As a consequence, the Lagrange's Equations are not used to compute the ψ angle. The submatrices (65) are reduced to, for $i = 1, \ldots, n$:

$$\begin{aligned}
&\left[A_{11}^{rot}\right]_{i,i} = \mathrm{I_i}\,\mathrm{c}_{\vartheta_\mathrm{i}}{}^2 \\
&\left[A_{22}^{rot}\right]_{i,i} = \mathrm{I_i} \\
&\left[A_{12}^{rot}\right]_{i,i} = \left[A_{13}^{rot}\right]_{i,i} = \left[A_{21}^{rot}\right]_{i,i} = \left[A_{31}^{rot}\right]_{i,i} = \left[A_{33}^{rot}\right]_{i,i} = 0 \\
\\
&\left[B_{21}^{rot}\right]_{i,i} = \mathrm{I_i}\,\mathrm{s}_{\vartheta_\mathrm{i}}\,\mathrm{c}_{\vartheta_\mathrm{j}} \\
&\left[B_{12}^{rot}\right]_{i,i} = \left[B_{31}^{rot}\right]_{i,i} = \left[B_{32}^{rot}\right]_{i,i} = 0 \\
\\
&\left[C_{11}^{rot}\right]_{i,i} = -\,\mathrm{I_i}\,2\,\mathrm{s}_{\vartheta_\mathrm{i}}\,\mathrm{c}_{\vartheta_\mathrm{i}} \\
&\left[C_{12}^{rot}\right]_{i,i} = \left[C_{13}^{rot}\right]_{i,i} = \left[C_{22}^{rot}\right]_{i,i} = \left[C_{23}^{rot}\right]_{i,i} = \left[C_{31}^{rot}\right]_{i,i} = 0
\end{aligned} \tag{67}$$

3.2.3 Total Lagrange's equations with fixed cable length

The total Lagrange's equations are obtained summing the two matrices equations Equation (46) and Equation (64), in other word summing the matrices:

$$\begin{aligned}
\mathbf{A} &= \mathbf{A}^{trn} + \mathbf{A}^{rot} \\
\mathbf{B} &= \mathbf{B}^{trn} + \mathbf{B}^{rot} \\
\mathbf{C} &= \mathbf{C}^{trn} + \mathbf{C}^{rot}
\end{aligned} \tag{68}$$

Finally, the total Lagrange's equations in matrix form results:

$$
\begin{pmatrix} \mathbf{A}_{11} & \mathbf{A}_{12} & \mathbf{A}_{13} \\ \mathbf{A}_{21} & \mathbf{A}_{22} & \mathbf{A}_{23} \\ \mathbf{A}_{31} & \mathbf{A}_{32} & \mathbf{A}_{33} \end{pmatrix} \begin{pmatrix} \ddot{\boldsymbol{\phi}} \\ \ddot{\boldsymbol{\theta}} \\ \ddot{\boldsymbol{\psi}} \end{pmatrix} + \begin{pmatrix} \mathbf{B}_{11} & \mathbf{B}_{12} & \mathbf{B}_{13} \\ \mathbf{B}_{21} & \mathbf{B}_{22} & \mathbf{B}_{23} \\ \mathbf{B}_{31} & \mathbf{B}_{32} & \mathbf{B}_{33} \end{pmatrix} \; diag \begin{pmatrix} \dot{\boldsymbol{\phi}} \\ \dot{\boldsymbol{\theta}} \\ \dot{\boldsymbol{\psi}} \end{pmatrix} \begin{pmatrix} \dot{\boldsymbol{\phi}} \\ \dot{\boldsymbol{\theta}} \\ \dot{\boldsymbol{\psi}} \end{pmatrix}
$$

$$
+ \begin{pmatrix} \mathbf{C}_{11} & \mathbf{C}_{12} & \mathbf{C}_{13} \\ \mathbf{C}_{21} & \mathbf{C}_{22} & \mathbf{C}_{23} \\ \mathbf{C}_{31} & \mathbf{C}_{32} & \mathbf{C}_{33} \end{pmatrix} \begin{pmatrix} \dot{\boldsymbol{\phi}}\,\dot{\boldsymbol{\theta}} \\ \dot{\boldsymbol{\phi}}\,\dot{\boldsymbol{\psi}} \\ \dot{\boldsymbol{\theta}}\,\dot{\boldsymbol{\psi}} \end{pmatrix} = \begin{pmatrix} \mathbf{Q}_{\phi} \\ \mathbf{Q}_{\theta} \\ \mathbf{Q}_{\psi} \end{pmatrix} \tag{69}
$$

Some consideration should be done about this matrices form. The cable's segments, except the virtual one (label $n+1$ element), are independent from the angles ψ_{i} for $i = 1, \ldots, n$, as reckon in section 3.2.1 and 3.2.2. Moreover, the Lagrange's equations are not used to compute the ψ angle. In other words, the angle ψ is fixed and set equal to zero, reducing of one the DOFs of each element of the cable. This is equivalent to substituting the spherical joint with a universal one. The DOFs of the overall system became $3(n+1) - n = 2n + 3$.

3.3 Lagrange's equation with cable variable length

The system since here is modelled with a fixed length cable. In order to model a variable length cable, the length of the first segment is a function of time, $l_1 = l_1(t)$. When it reaches a maximum value a new element is added. Associate with him two generalized coordinates and Lagrange's equations are jointed to the system model equations. Vice versa when the cable is winded up the first element's length reduces up to an arbitrary small value. It will eliminate together with him variables and Lagrange's equations.

In order to create a more versatile UAS model the cable length, roll up velocity and acceleration are supposed known. They are calculated by an external winch model with a force feedback acting by the cable to the ground station.

The 1^{th} cable's segment length changes over time. For this reason, his time derivative is not null, therefore let's define

$$
\dot{l}_1 = \frac{dl_1}{dt} \neq 0 \tag{70}
$$

$$
\ddot{l}_1 = \frac{d^2 l_1}{dt^2} \neq 0 \tag{71}
$$

Observe that the only cable segment varying his length is always the closest to the winch. For all others the time derivatives are unchanged equal to zero. Furthermore, also the 1^{th} element lumped mass and moment of inertia are functions of the segment length. Theme time derivatives are not null:

$$\frac{dm_1}{dt} = \frac{d}{dt}(\mu l_1) = \mu\, \dot{l}_1 \tag{72}$$

$$\frac{dI_1}{dt} = \frac{d}{dt}(m_1 l_1^2) = \frac{d}{dt}(\mu l_1^3) = 3\mu l_1^2\, \dot{l}_1 = 3 m_1 l_1\, \dot{l}_1 \tag{73}$$

Following the same path of section 3.2 the Lagrange's equations are calculated decomposing the kinetic energy in two components: transitional and rotational.

3.3.1 Lagrange's equations of transitional kinetic energy

The formulation of the segments velocity in the inertial reference frame calculated in section 2.2 must be corrected taking into account Equation (70). Deriving relative to the time the Cartesian nodes position, Equation (8):

$$\begin{cases} \dot{X}_k = -\,\dot{l}_1\, \mathrm{s}_{\vartheta_1} + \sum_{j=1}^{k} -l_j(\dot{\vartheta}_\mathrm{j}\, \mathrm{c}_{\vartheta_\mathrm{j}}) \\ \dot{Y}_k = -\,\dot{l}_1\, \mathrm{s}_{\phi_1}\, \mathrm{c}_{\vartheta_1} + \sum_{j=1}^{k} l_j(-\,\dot{\phi}_\mathrm{j}\, \mathrm{c}_{\phi_\mathrm{j}}\, \mathrm{c}_{\vartheta_\mathrm{j}} + \dot{\vartheta}_\mathrm{j}\, \mathrm{s}_{\phi_\mathrm{j}}\, \mathrm{s}_{\vartheta_\mathrm{j}}) \qquad k = 1, \ldots, n+1 \\ \dot{Z}_k = \dot{l}_1\, \mathrm{c}_{\phi_1}\, \mathrm{c}_{\vartheta_1} + \sum_{j=1}^{k} l_j(-\,\dot{\phi}_\mathrm{j}\, \mathrm{s}_{\phi_\mathrm{j}}\, \mathrm{c}_{\vartheta_\mathrm{j}} - \dot{\vartheta}_\mathrm{j}\, \mathrm{c}_{\phi_\mathrm{j}}\, \mathrm{s}_{\vartheta_\mathrm{j}}) \end{cases} \tag{74}$$

$$\begin{cases} \dot{X}_k^2 = \sum_{i=1}^{k} \sum_{j=1}^{k} \left\{ l_i l_j (\dot{\vartheta}_\mathrm{i}\, \mathrm{c}_{\vartheta_\mathrm{i}})(\dot{\vartheta}_\mathrm{j}\, \mathrm{c}_{\vartheta_\mathrm{j}}) \right\} \\ \qquad\qquad + \dot{l}_1^{\,2}\, \mathrm{s}_{\vartheta_1}{}^2 + 2\, \dot{l}_1\, \mathrm{s}_{\vartheta_1} \sum_{j=1}^{k} \left(l_j\, \dot{\vartheta}_\mathrm{j}\, \mathrm{c}_{\vartheta_\mathrm{j}} \right) \\ \dot{Y}_k^2 = \sum_{i=1}^{k} \sum_{j=1}^{k} \left\{ l_i l_j (-\,\dot{\phi}_\mathrm{i}\, \mathrm{c}_{\phi_\mathrm{i}}\, \mathrm{c}_{\vartheta_\mathrm{i}} + \dot{\vartheta}_\mathrm{i}\, \mathrm{s}_{\phi_\mathrm{i}}\, \mathrm{s}_{\vartheta_\mathrm{i}})(-\,\dot{\phi}_\mathrm{j}\, \mathrm{c}_{\phi_\mathrm{j}}\, \mathrm{c}_{\vartheta_\mathrm{j}} + \dot{\vartheta}_\mathrm{j}\, \mathrm{s}_{\phi_\mathrm{j}}\, \mathrm{s}_{\vartheta_\mathrm{j}}) \right\} \\ \qquad\qquad + \dot{l}_1^{\,2}\, \mathrm{s}_{\phi_1}{}^2\, \mathrm{c}_{\vartheta_1}{}^2 + 2\, \dot{l}_1\, \mathrm{s}_{\phi_1}\, \mathrm{c}_{\vartheta_1} \sum_{j=1}^{k} \left(-\,\dot{\phi}_\mathrm{j}\, \mathrm{c}_{\phi_\mathrm{j}}\, \mathrm{c}_{\vartheta_\mathrm{j}} + \dot{\vartheta}_\mathrm{j}\, \mathrm{s}_{\phi_\mathrm{j}}\, \mathrm{s}_{\vartheta_\mathrm{j}} \right) \\ \dot{Z}_k^2 = \sum_{i=1}^{k} \sum_{j=1}^{k} \left\{ l_i l_j (-\,\dot{\phi}_\mathrm{i}\, \mathrm{s}_{\phi_\mathrm{i}}\, \mathrm{c}_{\vartheta_\mathrm{i}} - \dot{\vartheta}_\mathrm{i}\, \mathrm{c}_{\phi_\mathrm{i}}\, \mathrm{s}_{\vartheta_\mathrm{i}})(-\,\dot{\phi}_\mathrm{j}\, \mathrm{s}_{\phi_\mathrm{j}}\, \mathrm{c}_{\vartheta_\mathrm{j}} - \dot{\vartheta}_\mathrm{j}\, \mathrm{c}_{\phi_\mathrm{j}}\, \mathrm{s}_{\vartheta_\mathrm{j}}) \right\} \\ \qquad\qquad + \dot{l}_1^{\,2}\, \mathrm{c}_{\phi_1}{}^2\, \mathrm{c}_{\vartheta_1}{}^2 + 2\, \dot{l}_1\, \mathrm{c}_{\phi_1}\, \mathrm{c}_{\vartheta_1} \sum_{j=1}^{k} \left(-\,\dot{\phi}_\mathrm{j}\, \mathrm{s}_{\phi_\mathrm{j}}\, \mathrm{c}_{\vartheta_\mathrm{j}} - \dot{\vartheta}_\mathrm{j}\, \mathrm{c}_{\phi_\mathrm{j}}\, \mathrm{s}_{\vartheta_\mathrm{j}} \right) \end{cases} \tag{75}$$

for $k = 1, \ldots, n+1$

Assembling Equation (75) into the total square velocity

$$\left|\vec{V}_k\right|^2 = \sum_{i=1}^{k}\sum_{j=1}^{k}\Big\{l_i l_j \big[\, \dot{\phi}_{\mathrm{i}}\, \dot{\phi}_{\mathrm{j}}\, \mathrm{c}_{\vartheta_{\mathrm{i}}}\, \mathrm{c}_{\vartheta_{\mathrm{j}}}\, \mathrm{c}_{\phi_{\mathrm{ji}}} + \dot{\vartheta}_{\mathrm{i}}\, \dot{\vartheta}_{\mathrm{j}} \left(\mathrm{s}_{\vartheta_{\mathrm{i}}}\, \mathrm{s}_{\vartheta_{\mathrm{j}}}\, \mathrm{c}_{\phi_{\mathrm{ji}}} + \mathrm{c}_{\vartheta_{\mathrm{i}}}\, \mathrm{c}_{\vartheta_{\mathrm{j}}} \right) + 2\ \dot{\vartheta}_{\mathrm{i}}\, \dot{\phi}_{\mathrm{j}}\, \mathrm{s}_{\vartheta_{\mathrm{i}}}\, \mathrm{c}_{\vartheta_{\mathrm{j}}}\, \mathrm{s}_{\phi_{\mathrm{ji}}} \,\big]\Big\} + \dot{l}_1^{\,2} + 2\,\dot{l}_1 \sum_{j=1}^{k}\Big\{l_j \big[\, \dot{\phi}_{\mathrm{j}}\, \mathrm{c}_{\vartheta_{\mathrm{j}}}\, \mathrm{c}_{\vartheta_1}\, \mathrm{s}_{\phi_{1\mathrm{j}}} + \dot{\vartheta}_{\mathrm{j}} \left(\mathrm{c}_{\vartheta_{\mathrm{j}}}\, \mathrm{s}_{\vartheta_1} - \mathrm{s}_{\vartheta_{\mathrm{j}}}\, \mathrm{c}_{\vartheta_1}\, \mathrm{c}_{\phi_{1\mathrm{j}}} \right)\big]\Big\} \quad (76)$$

It's now possible explicit the transitional kinetic energy with the cable's segments velocity calculated in Equation (76). Observe that for $j = 1$ the term inside the last sum is null

$$\big[\, \dot{\phi}_1\, \mathrm{c}_{\vartheta_1}\, \mathrm{c}_{\vartheta_1}\, \mathrm{s}_{\phi_{11}} + \dot{\vartheta}_1 \left(\mathrm{c}_{\vartheta_1}\, \mathrm{s}_{\vartheta_1} - \mathrm{s}_{\vartheta_1}\, \mathrm{c}_{\vartheta_1}\, \mathrm{c}_{\phi_{11}} \right)\big] = 0$$

results:

$$E_{trans} = \frac{1}{2}\sum_{k=1}^{n+1}\sum_{i=1}^{k}\sum_{j=1}^{k}\Big\{m_k l_i l_j \Big[\dot{\phi}_{\mathrm{i}} \left(\dot{\phi}_{\mathrm{j}}\, \mathrm{c}_{\vartheta_{\mathrm{i}}}\, \mathrm{c}_{\vartheta_{\mathrm{j}}}\, \mathrm{c}_{\phi_{\mathrm{ji}}} - \dot{\vartheta}_{\mathrm{j}}\, \mathrm{c}_{\vartheta_{\mathrm{i}}}\, \mathrm{s}_{\vartheta_{\mathrm{j}}}\, \mathrm{s}_{\phi_{\mathrm{ji}}} \right) + \dot{\vartheta}_{\mathrm{i}} \left(\dot{\phi}_{\mathrm{j}}\, \mathrm{s}_{\vartheta_{\mathrm{i}}}\, \mathrm{c}_{\vartheta_{\mathrm{j}}}\, \mathrm{s}_{\phi_{\mathrm{ji}}} + \dot{\vartheta}_{\mathrm{j}} \left(\mathrm{s}_{\vartheta_{\mathrm{i}}}\, \mathrm{s}_{\vartheta_{\mathrm{j}}}\, \mathrm{c}_{\phi_{\mathrm{ji}}} + \mathrm{c}_{\vartheta_{\mathrm{i}}}\, \mathrm{c}_{\vartheta_{\mathrm{j}}} \right)\right)\Big]\Big\} + \frac{1}{2}\,\dot{l}_1^{\,2} \sum_{k=1}^{n+1}(m_k) + \sum_{k=2}^{n+1}\sum_{j=2}^{k}\Big\{m_k\, \dot{l}_1\, l_j \big[\, \dot{\phi}_{\mathrm{j}}\, \mathrm{c}_{\vartheta_{\mathrm{j}}}\, \mathrm{c}_{\vartheta_1}\, \mathrm{s}_{\phi_{1\mathrm{j}}} + \dot{\vartheta}_{\mathrm{j}} \left(\mathrm{c}_{\vartheta_{\mathrm{j}}}\, \mathrm{s}_{\vartheta_1} - \mathrm{s}_{\vartheta_{\mathrm{j}}}\, \mathrm{c}_{\vartheta_1}\, \mathrm{c}_{\phi_{1\mathrm{j}}} \right)\big]\Big\} \quad (77)$$

Observe that the Equation (77) is equal to the transitional kinetic energy calculated in section 3.2.1 (Equation (37)) summed to other two terms proportional to $\dot{l}_1$. In order to simplify the notation all the below equations are written as a sum of the equations calculated into section 3.2 plus some terms proportional to $\dot{l}_1$ and $\ddot{l}_1$.

Recalling the Equation (47):

$$
\begin{aligned}
E_{trans} = (37) + \frac{1}{2}\,\dot{l}_1^{\,2}\, M_{1,1} \\
+ \sum_{k=2}^{n+1}\sum_{j=2}^{k}\Big\{ m_k\,\dot{l}_1\, l_j \big[\,\dot{\phi}_{\mathrm{j}}\,\mathrm{c}_{\vartheta_{\mathrm{j}}}\,\mathrm{c}_{\vartheta_1}\,\mathrm{s}_{\phi_{1\mathrm{j}}} + \dot{\vartheta}_{\mathrm{j}}\,\big(\,\mathrm{c}_{\vartheta_{\mathrm{j}}}\,\mathrm{s}_{\vartheta_1} - \mathrm{s}_{\vartheta_{\mathrm{j}}}\,\mathrm{c}_{\vartheta_1}\,\mathrm{c}_{\phi_{1\mathrm{j}}}\,\big)\big]\Big\}
\end{aligned}
\tag{78}
$$

Observe that the generalized coordinates of the 1^{th} cable element (ϕ_1,ϑ_1) appear inside the sum. The derivative must be evaluated separately according the index i of the q_i. In particular for $i = 2, \ldots, n+1$ are calculated the Lagrange's equations referred to the generalize coordinates ϕ_{i} and ϑ_{i} different from the ones calculated for $i = 1$.

$i = 2, \ldots, n+1$

Differentiating the kinetic energy relative to the angle ϕ_{i} and its time derivative $\dot{\phi}_{\mathrm{i}}$.

$$
\frac{\partial E_{trans}}{\partial\,\phi_{\mathrm{i}}} = (38) + M_{i,2} l_i\,\dot{l}_1\,\big[- \dot{\phi}_{\mathrm{i}}\,\mathrm{c}_{\vartheta_{\mathrm{i}}}\,\mathrm{c}_{\vartheta_1}\,\mathrm{c}_{\phi_{1\mathrm{i}}} - \dot{\vartheta}_{\mathrm{i}}\,\mathrm{s}_{\vartheta_{\mathrm{i}}}\,\mathrm{c}_{\vartheta_1}\,\mathrm{s}_{\phi_{1\mathrm{i}}}\,\big] \tag{79}
$$

$$
\frac{\partial E_{trans}}{\partial\,\dot{\phi}_{\mathrm{i}}} = (39) + M_{i,2} l_i\,\dot{l}_1\,\mathrm{c}_{\vartheta_{\mathrm{i}}}\,\mathrm{c}_{\vartheta_1}\,\mathrm{s}_{\phi_{1\mathrm{i}}} \tag{80}
$$

Deriving the Equation (80) relative to the time, observing that

$$
\frac{d(39)}{dt} = (40) + M_{i,2} l_i\,\dot{l}_1\,\big[\,\dot{\phi}_1\,\mathrm{c}_{\vartheta_{\mathrm{i}}}\,\mathrm{c}_{\vartheta_1}\,\mathrm{c}_{\phi_{1\mathrm{i}}} - \dot{\vartheta}_1\,\mathrm{c}_{\vartheta_{\mathrm{i}}}\,\mathrm{s}_{\vartheta_1}\,\mathrm{s}_{\phi_{1\mathrm{i}}}\,\big]
$$

results:

$$
\begin{aligned}
\frac{d}{dt}\Big(\frac{\partial E_{trans}}{\partial\,\dot{\phi}_{\mathrm{i}}}\Big) = (40) + M_{i,2} l_i\,\ddot{l}_1\,\mathrm{c}_{\vartheta_{\mathrm{i}}}\,\mathrm{c}_{\vartheta_1}\,\mathrm{s}_{\phi_{1\mathrm{i}}} \\
M_{i,2} l_i\,\dot{l}_1\,\big[- \dot{\phi}_{\mathrm{i}}\,\mathrm{c}_{\vartheta_{\mathrm{i}}}\,\mathrm{c}_{\vartheta_1}\,\mathrm{c}_{\phi_{1\mathrm{i}}} - \dot{\vartheta}_{\mathrm{i}}\,\mathrm{s}_{\vartheta_{\mathrm{i}}}\,\mathrm{c}_{\vartheta_1}\,\mathrm{s}_{\phi_{1\mathrm{i}}} \\
+ 2\,\dot{\phi}_1\,\mathrm{c}_{\vartheta_{\mathrm{i}}}\,\mathrm{c}_{\vartheta_1}\,\mathrm{c}_{\phi_{1\mathrm{i}}} - 2\,\dot{\vartheta}_1\,\mathrm{c}_{\vartheta_{\mathrm{i}}}\,\mathrm{s}_{\vartheta_1}\,\mathrm{s}_{\phi_{1\mathrm{i}}}\,\big]
\end{aligned}
\tag{81}
$$

Assembling the derivatives just calculate Equation (79) and Equation (81) into the Lagrange's equation Equation (19) we obtain n equations of the type:

$$\frac{d}{dt}\Big(\frac{\partial E_{trans}}{\partial\,\dot{\phi}_{\mathrm{i}}}\Big) - \frac{\partial E_{kinetic}}{\partial\,\phi_{\mathrm{i}}} = (41) + 2M_{i,2}l_i\,\dot{l}_1\,\big[\,\dot{\phi}_1\,\mathrm{c}_{\vartheta_{\mathrm{i}}}\,\mathrm{c}_{\vartheta_1}\,\mathrm{c}_{\phi_{1\mathrm{i}}}$$

$$-\,\dot{\vartheta}_1\,\mathrm{c}_{\vartheta_{\mathrm{i}}}\,\mathrm{s}_{\vartheta_1}\,\mathrm{s}_{\phi_{1\mathrm{i}}}\,\big] = Q_{\phi_{\mathrm{i}}} - M_{i,2}l_i\,\ddot{l}_1\,\mathrm{c}_{\vartheta_{\mathrm{i}}}\,\mathrm{c}_{\vartheta_1}\,\mathrm{s}_{\phi_{1\mathrm{i}}} \quad (82)$$

Following a similar path, the Lagrange's equations referred to the generalized coordinates ϑ_{i} are evaluated.

$$\frac{\partial E_{trans}}{\partial\,\vartheta_{\mathrm{i}}} = (42) + M_{i,2}l_i\,\dot{l}_1\,\big[-\,\dot{\phi}_{\mathrm{i}}\,\mathrm{s}_{\vartheta_{\mathrm{i}}}\,\mathrm{c}_{\vartheta_1}\,\mathrm{s}_{\phi_{1\mathrm{i}}}$$

$$+\,\dot{\vartheta}_{\mathrm{i}}\,\big(-\,\mathrm{s}_{\vartheta_{\mathrm{i}}}\,\mathrm{s}_{\vartheta_1} - \mathrm{c}_{\vartheta_{\mathrm{i}}}\,\mathrm{c}_{\vartheta_1}\,\mathrm{c}_{\phi_{1\mathrm{i}}}\,\big)\big] \quad (83)$$

$$\frac{\partial E_{trans}}{\partial\,\dot{\vartheta}_{\mathrm{i}}} = (43) + M_{i,2}l_i\,\dot{l}_1\,\big(\,\mathrm{c}_{\vartheta_{\mathrm{i}}}\,\mathrm{s}_{\vartheta_1} - \mathrm{s}_{\vartheta_{\mathrm{i}}}\,\mathrm{c}_{\vartheta_1}\,\mathrm{c}_{\phi_{1\mathrm{i}}}\,\big) \quad (84)$$

Deriving the Equation (84) relative to the time, observing that

$$\frac{d(43)}{dt} = (44) + M_{i,2}l_i\,\dot{l}_1\,\big[\,\dot{\phi}_1\,\mathrm{s}_{\vartheta_{\mathrm{i}}}\,\mathrm{c}_{\vartheta_1}\,\mathrm{s}_{\phi_{1\mathrm{i}}} + \dot{\vartheta}_1\,\big(\,\mathrm{c}_{\vartheta_{\mathrm{i}}}\,\mathrm{c}_{\vartheta_1} + \mathrm{s}_{\vartheta_{\mathrm{i}}}\,\mathrm{s}_{\vartheta_1}\,\mathrm{c}_{\phi_{1\mathrm{i}}}\,\big)\big]$$

results:

$$\frac{d}{dt}\Big(\frac{\partial E_{trans}}{\partial\,\dot{\vartheta}_{\mathrm{i}}}\Big) = (44) + M_{i,2}l_i\,\ddot{l}_1\,\big(\,\mathrm{c}_{\vartheta_{\mathrm{i}}}\,\mathrm{s}_{\vartheta_1} - \mathrm{s}_{\vartheta_{\mathrm{i}}}\,\mathrm{c}_{\vartheta_1}\,\mathrm{c}_{\phi_{1\mathrm{i}}}\,\big)$$

$$+\,M_{i,2}l_i\,\dot{l}_1\,\big[-\,\dot{\phi}_{\mathrm{i}}\,\mathrm{s}_{\vartheta_{\mathrm{i}}}\,\mathrm{c}_{\vartheta_1}\,\mathrm{s}_{\phi_{1\mathrm{i}}} + \dot{\vartheta}_{\mathrm{i}}\,\big(-\,\mathrm{s}_{\vartheta_{\mathrm{i}}}\,\mathrm{s}_{\vartheta_1} - \mathrm{c}_{\vartheta_{\mathrm{i}}}\,\mathrm{c}_{\vartheta_1}\,\mathrm{c}_{\phi_{1\mathrm{i}}}\,\big)$$

$$+\,2\,\dot{\phi}_1\,\mathrm{s}_{\vartheta_{\mathrm{i}}}\,\mathrm{c}_{\vartheta_1}\,\mathrm{s}_{\phi_{1\mathrm{i}}} + 2\,\dot{\vartheta}_{\mathrm{i}}\,\big(\,\mathrm{c}_{\vartheta_{\mathrm{i}}}\,\mathrm{c}_{\vartheta_1} + \mathrm{s}_{\vartheta_{\mathrm{i}}}\,\mathrm{s}_{\vartheta_1}\,\mathrm{c}_{\phi_{1\mathrm{i}}}\,\big)\big] \quad (85)$$

Assembling the derivatives just calculate Equation (83) and Equation (85) into the Lagrange's equation Equation (19) we obtain n equations of the type:

$$\frac{d}{dt}\Big(\frac{\partial E_{trans}}{\partial\,\dot{\vartheta}_{\mathrm{i}}}\Big) - \frac{\partial E_{trans}}{\partial\,\vartheta_{\mathrm{i}}} = (45) + 2M_{i,2}l_i\,\dot{l}_1\,\big[\,\dot{\phi}_1\,\mathrm{s}_{\vartheta_{\mathrm{i}}}\,\mathrm{c}_{\vartheta_1}\,\mathrm{s}_{\phi_{1\mathrm{i}}}$$

$$+\,\dot{\vartheta}_1\,\big(\,\mathrm{c}_{\vartheta_{\mathrm{i}}}\,\mathrm{c}_{\vartheta_1} + \mathrm{s}_{\vartheta_{\mathrm{i}}}\,\mathrm{s}_{\vartheta_1}\,\mathrm{c}_{\phi_{1\mathrm{i}}}\,\big)\big]$$

$$= Q_{\vartheta_{\mathrm{i}}} - M_{i,2}l_i\,\ddot{l}_1\,\big(\,\mathrm{c}_{\vartheta_{\mathrm{i}}}\,\mathrm{s}_{\vartheta_1} - \mathrm{s}_{\vartheta_{\mathrm{i}}}\,\mathrm{c}_{\vartheta_1}\,\mathrm{c}_{\phi_{1\mathrm{i}}}\,\big) \quad (86)$$

$i = 1$

Differentiating the kinetic energy respect the angle ϕ_1 and its time derivative $\dot{\phi}_1$.

$$\frac{\partial E_{trans}}{\partial \phi_1} = (38) + \sum_{k=2}^{n+1} \sum_{j=2}^{k} \Big\{ m_k \, \dot{l}_1 \, l_j \big[\, \dot{\phi}_{\mathrm{j}} \, \mathrm{c}_{\vartheta_{\mathrm{j}}} \, \mathrm{c}_{\vartheta_1} \, \mathrm{c}_{\phi_{1\mathrm{j}}} + \dot{\vartheta}_{\mathrm{j}} \, \mathrm{s}_{\vartheta_{\mathrm{j}}} \, \mathrm{c}_{\vartheta_1} \, \mathrm{s}_{\phi_{1\mathrm{j}}} \, \big] \Big\} \tag{87}$$

$$\frac{\partial E_{trans}}{\partial \dot{\phi}_1} = \Big[(39) \Big]_{i=1} = \sum_{k=1}^{n+1} \sum_{j=1}^{k} \Big\{ m_k l_1 l_j \big[\, \dot{\phi}_{\mathrm{j}} \, \mathrm{c}_{\vartheta_1} \, \mathrm{c}_{\vartheta_{\mathrm{j}}} \, \mathrm{c}_{\phi_{\mathrm{j}1}} - \dot{\vartheta}_{\mathrm{j}} \, \mathrm{c}_{\vartheta_1} \, \mathrm{s}_{\vartheta_{\mathrm{j}}} \, \mathrm{s}_{\phi_{\mathrm{j}1}} \, \big] \Big\} \tag{88}$$

Observe that for $j = 1$:

$$\big[\, \dot{\phi}_1 \, \mathrm{c}_{\vartheta_1} \, \mathrm{c}_{\vartheta_1} \, \mathrm{c}_{\phi_{11}} - \dot{\vartheta}_1 \, \mathrm{c}_{\vartheta_1} \, \mathrm{s}_{\vartheta_1} \, \mathrm{s}_{\phi_{11}} \, \big] = \dot{\phi}_1 \, {\mathrm{c}_{\vartheta_1}}^2$$

$$\frac{\partial E_{trans}}{\partial \dot{\phi}_1} = \sum_{k=2}^{n+1} \sum_{j=2}^{k} \Big\{ m_k l_1 l_j \big[\, \dot{\phi}_{\mathrm{j}} \, \mathrm{c}_{\vartheta_1} \, \mathrm{c}_{\vartheta_{\mathrm{j}}} \, \mathrm{c}_{\phi_{\mathrm{j}1}} - \dot{\vartheta}_{\mathrm{j}} \, \mathrm{c}_{\vartheta_1} \, \mathrm{s}_{\vartheta_{\mathrm{j}}} \, \mathrm{s}_{\phi_{\mathrm{j}1}} \, \big] \Big\} \\ + M_{1,1} l_1^2 \, \dot{\phi}_1 \, {\mathrm{c}_{\phi_1}}^2 \tag{89}$$

Recalling the Equation (47) and Equation (72)

$$\frac{d}{dt} \Big(\frac{\partial E_{trans}}{\partial \dot{\phi}_1} \Big) = (40) + M_{1,1} 2 l_1 \, \dot{l}_1 \, \dot{\phi}_1 \, {\mathrm{c}_{\vartheta_1}}^2 + \mu l_1^2 \, \dot{l}_1 \, \dot{\phi}_1 \, {\mathrm{c}_{\vartheta_1}}^2 \\ + \sum_{k=2}^{n+1} \sum_{j=2}^{k} \Big\{ m_k \, \dot{l}_1 \, l_j \big[\, \dot{\phi}_{\mathrm{j}} \, \mathrm{c}_{\vartheta_1} \, \mathrm{c}_{\vartheta_{\mathrm{j}}} \, \mathrm{c}_{\phi_{\mathrm{j}1}} - \dot{\vartheta}_{\mathrm{j}} \, \mathrm{c}_{\vartheta_1} \, \mathrm{s}_{\vartheta_{\mathrm{j}}} \, \mathrm{s}_{\phi_{\mathrm{j}1}} \, \big] \Big\} \tag{90}$$

Assembling the derivatives just calculate Equation (87) and Equation (90) into the Lagrange's equation Equation (19), observe that $\mathrm{c}_{\phi_{\mathrm{j}1}} = \mathrm{c}_{\phi_{1\mathrm{j}}}$ and $\mathrm{s}_{\phi_{\mathrm{j}1}} = -\,\mathrm{s}_{\phi_{1\mathrm{j}}}$, we obtain an equation of the type:

$$\frac{d}{dt} \Big(\frac{\partial E_{trans}}{\partial \dot{\phi}_1} \Big) - \frac{\partial E_{kinetic}}{\partial \phi_1} = (41) + \dot{\phi}_1 \, {\mathrm{c}_{\vartheta_1}}^2 \, \dot{l}_1 \, l_1 \big(2 M_{1,1} + m_1 \big) = Q_{\phi_1} \tag{91}$$

Following a similar path the Lagrange's equations referred to the generalized coordinates ϑ_1 are evaluated.

$$\frac{\partial E_{trans}}{\partial \vartheta_1} = (42) + \sum_{k=2}^{n+1}\sum_{j=2}^{k}\Big\{ m_k\, \dot{l}_1\, l_j \big[-\dot{\phi}_{\mathrm{j}}\, \mathrm{c}_{\vartheta_{\mathrm{j}}}\, \mathrm{s}_{\vartheta_1}\, \mathrm{s}_{\phi_{1\mathrm{j}}} + \dot{\vartheta}_{\mathrm{j}} \left(\mathrm{c}_{\vartheta_{\mathrm{j}}}\, \mathrm{c}_{\vartheta_1} + \mathrm{s}_{\vartheta_{\mathrm{j}}}\, \mathrm{c}_{\vartheta_1}\, \mathrm{s}_{\phi_{1\mathrm{j}}} \right)\big]\Big\} \quad (92)$$

$$\frac{\partial E_{trans}}{\partial \dot{\vartheta}_1} = \Big[(43)\Big]_{i=1} = \sum_{k=1}^{n+1}\sum_{j=1}^{k}\Big\{ m_k l_1 l_j \big[\dot{\phi}_{\mathrm{j}}\, \mathrm{s}_{\vartheta_1}\, \mathrm{c}_{\vartheta_{\mathrm{j}}}\, \mathrm{s}_{\phi_{\mathrm{j}1}} + \dot{\vartheta}_{\mathrm{j}} \left(\mathrm{c}_{\vartheta_{\mathrm{j}}}\, \mathrm{c}_{\vartheta_1} + \mathrm{s}_{\vartheta_{\mathrm{j}}}\, \mathrm{s}_{\vartheta_1}\, \mathrm{c}_{\phi_{\mathrm{j}1}} \right)\big]\Big\} \quad (93)$$

Observe that for $j = 1$:

$$\big[\dot{\phi}_1\, \mathrm{s}_{\vartheta_1}\, \mathrm{c}_{\vartheta_1}\, \mathrm{s}_{\phi_{11}} + \dot{\vartheta}_1 \left(\mathrm{c}_{\vartheta_1}\, \mathrm{c}_{\vartheta_1} + \mathrm{s}_{\vartheta_1}\, \mathrm{s}_{\vartheta_1}\, \mathrm{c}_{\phi_{11}} \right)\big] = \dot{\vartheta}_1$$

$$\frac{\partial E_{trans}}{\partial \dot{\vartheta}_1} = \sum_{k=2}^{n+1}\sum_{j=2}^{k}\Big\{ m_k l_1 l_j \big[\dot{\phi}_{\mathrm{j}}\, \mathrm{s}_{\vartheta_1}\, \mathrm{c}_{\vartheta_{\mathrm{j}}}\, \mathrm{s}_{\phi_{\mathrm{j}1}} + \dot{\vartheta}_{\mathrm{j}} \left(\mathrm{c}_{\vartheta_{\mathrm{j}}}\, \mathrm{c}_{\vartheta_1} + \mathrm{s}_{\vartheta_{\mathrm{j}}}\, \mathrm{s}_{\vartheta_1}\, \mathrm{c}_{\phi_{\mathrm{j}1}} \right)\big]\Big\} + M_{1,1} l_1^2\, \dot{\vartheta}_1 \quad (94)$$

Recalling the Equation (47) and Equation (72)

$$\frac{d}{dt}\Big(\frac{\partial E_{trans}}{\partial \dot{\vartheta}_1}\Big) = (44) + M_{1,1} 2 l_1\, \dot{l}_1\, \dot{\vartheta}_1 + \mu l_1^2\, \dot{l}_1\, \dot{\vartheta}_1 + \sum_{k=2}^{n+1}\sum_{j=2}^{k}\Big\{ m_k\, \dot{l}_1\, l_j \big[\dot{\phi}_{\mathrm{j}}\, \mathrm{s}_{\vartheta_1}\, \mathrm{c}_{\vartheta_{\mathrm{j}}}\, \mathrm{s}_{\phi_{\mathrm{j}1}} + \dot{\vartheta}_{\mathrm{j}} \left(\mathrm{c}_{\vartheta_{\mathrm{j}}}\, \mathrm{c}_{\vartheta_1} + \mathrm{s}_{\vartheta_{\mathrm{j}}}\, \mathrm{s}_{\vartheta_1}\, \mathrm{c}_{\phi_{\mathrm{j}1}} \right)\big]\Big\} \quad (95)$$

Assembling the derivatives just calculate Equation (92) and Equation (95) into the Lagrange's equation Equation (19), observe that $\mathrm{c}_{\phi_{\mathrm{j}1}} = \mathrm{c}_{\phi_{1\mathrm{j}}}$ and $\mathrm{s}_{\phi_{\mathrm{j}1}} = -\,\mathrm{s}_{\phi_{1\mathrm{j}}}$, we obtain an equation of the type:

$$\frac{d}{dt}\Big(\frac{\partial E_{trans}}{\partial \dot{\vartheta}_1}\Big) - \frac{\partial E_{kinetic}}{\partial \vartheta_1} = (45) + \dot{\vartheta}_1\, \dot{l}_1\, l_1 \big(2M_{1,1} + m_1\big) = Q_{\vartheta_1} \quad (96)$$

3.3.2 Lagrange's equations of rotational kinetic energy

Different from the transitional kinetic energy for variable length cable studied in section 3.2.1, the rotational kinetic energy is independent from the segment length. So, the expression of rotational kinetic energy is equal to the Equation (51) and also the partial derivative equations are the same. Anyway, the cable segments moment of inertia is a function of their length. The 1^{th} element length is the only one function of time (Equation (72)). As consequence for $i = 2, \ldots, n+1$ the Lagrange's equations of the rotational kinetic energy are the same derived in section 3.2.2. The only case that should be studied is for $i = 1$.

$$\frac{\partial E_{rot}}{\partial \phi_1} = \Big[(52)\Big]_{i=1} = 0 \tag{97}$$

$$\frac{\partial E_{rot}}{\partial \dot{\phi}_1} = \Big[(53)\Big]_{i=1} = I_1 \, \dot{\phi}_1 \, \mathrm{c}_{\vartheta_1}{}^2 \tag{98}$$

Recalling the time derivative of I_1, describe in Equation (72)

$$\frac{d}{dt}\Big(\frac{\partial E_{rot}}{\partial \dot{\phi}_1}\Big) = \Big[(54)\Big]_{i=1} + \dot{\phi}_1 \, 3 m_1 l_1 \, \dot{l}_1 \, \mathrm{c}_{\vartheta_1}{}^2 \tag{99}$$

$$\frac{d}{dt}\Big(\frac{\partial E_{rot}}{\partial \dot{\phi}_1}\Big) - \frac{\partial E_{rot}}{\partial \phi_1} = \Big[(55)\Big]_{i=1} + \dot{\phi}_1 \, 3 m_1 l_1 \, \dot{l}_1 \, \mathrm{c}_{\vartheta_1}{}^2 \tag{100}$$

For the generalized coordinates ϑ_1:

$$\frac{\partial E_{rot}}{\partial \vartheta_1} = \Big[(56)\Big]_{i=1} = - \, \dot{\phi}_1 \, I_1 \, \mathrm{c}_{\vartheta_1} \, \mathrm{s}_{\vartheta_1} \tag{101}$$

Recalling that for cable's elements the moment of inertia are Equation (66)

$$\frac{\partial E_{rot}}{\partial \dot{\vartheta}_1} = \Big[(57)\Big]_{i=1} = I_1 \, \dot{\vartheta}_1 \tag{102}$$

and the time derivative of I_1 describe into Equation (72)

$$\frac{d}{dt}\Big(\frac{\partial E_{rot}}{\partial \dot{\vartheta}_1}\Big) = \Big[(58)\Big]_{i=1} + \dot{\vartheta}_1 \, 3 m_1 l_1 \, \dot{l}_1 \tag{103}$$

$$\frac{d}{dt}\Big(\frac{\partial E_{rot}}{\partial \dot{\vartheta}_1}\Big) - \frac{\partial E_{rot}}{\partial \vartheta_1} = \Big[(59)\Big]_{i=1} + \dot{\vartheta}_1 \, 3 m_1 l_1 \, \dot{l}_1 \tag{104}$$

No such equations about the angle ψ_1 are calculated since, just like written above, They aren't generalized coordinates for the cable's segments. In fact from the Equation (67) the matrix elements refer to the Lagrange's equations are null.

3.4 Total Lagrange's equations

The total Lagrange's equations in matrix form are:

$$\mathbf{A}^{tot}\begin{pmatrix}\ddot{\boldsymbol{\phi}}\\ \ddot{\boldsymbol{\theta}}\\ \ddot{\boldsymbol{\psi}}\end{pmatrix}+\Big[\mathbf{B}^{tot}\cdot\ diag\begin{pmatrix}\dot{\boldsymbol{\phi}}\\ \dot{\boldsymbol{\theta}}\\ \dot{\boldsymbol{\psi}}\end{pmatrix}+\mathbf{D}\Big]\begin{pmatrix}\dot{\boldsymbol{\phi}}\\ \dot{\boldsymbol{\theta}}\\ \dot{\boldsymbol{\psi}}\end{pmatrix}+\mathbf{C}^{tot}\begin{pmatrix}\dot{\boldsymbol{\phi}}\,\dot{\boldsymbol{\theta}}\\ \dot{\boldsymbol{\phi}}\,\dot{\boldsymbol{\psi}}\\ \dot{\boldsymbol{\theta}}\,\dot{\boldsymbol{\psi}}\end{pmatrix}=\begin{pmatrix}\mathbf{Q}_{\phi}^{tot}\\ \mathbf{Q}_{\theta}^{tot}\\ \mathbf{Q}_{\psi}\end{pmatrix} \quad (105)$$

where **A**, **B** and **C** are the matrices (68) calculate in section 3.2 and

$$\begin{aligned}\mathbf{Q}_{\phi}^{tot}&=\mathbf{Q}_{\phi}+\mathbf{Q}_{\phi}''\\ \mathbf{Q}_{\theta}^{tot}&=\mathbf{Q}_{\theta}+\mathbf{Q}_{\theta}''\end{aligned} \quad (106)$$

where $\mathbf{Q}_{\phi}$, $\mathbf{Q}_{\theta}$ and $\mathbf{Q}_{\psi}$ are the generalized forces calculated in section 3.1 and $\mathbf{Q}_{\phi}''$, $\mathbf{Q}_{\theta}''$ contain the terms calculated in section 3.3.1 due to the cable variable length proportional to $\ddot{l}_1$.

Remembering from section 3.3.1 that the equations must be distinct for $i=2,\dots,n+1$ and $i=1$.

$$\begin{aligned}\big[D_{11}\big]_{i,1}&=2M_{i,2}l_1\,\dot{l}_1\,\mathrm{c}_{\vartheta_\mathrm{i}}\,\mathrm{c}_{\vartheta_1}\,\mathrm{c}_{\phi_{1\mathrm{i}}}\\ \big[D_{12}\big]_{i,1}&=2M_{i,2}l_1\,\dot{l}_1\,\mathrm{c}_{\vartheta_1}\,\mathrm{s}_{\vartheta_1}\,\mathrm{s}_{\phi_{1\mathrm{i}}}\\ \big[D_{21}\big]_{i,1}&=2M_{i,2}l_1\,\dot{l}_1\,\mathrm{s}_{\vartheta_\mathrm{i}}\,\mathrm{s}_{\phi_{1\mathrm{i}}}\\ \big[D_{22}\big]_{i,1}&=2M_{i,2}l_1\,\dot{l}_1\,\big(\,\mathrm{c}_{\vartheta_\mathrm{i}}\,\mathrm{c}_{\vartheta_1}+\mathrm{s}_{\vartheta_\mathrm{i}}\,\mathrm{s}_{\vartheta_1}\,\mathrm{c}_{\phi_{1\mathrm{i}}}\,\big)\\ Q''_{\phi_\mathrm{i}}&=-M_{i,2}l_1\,\ddot{l}_1\,\mathrm{c}_{\vartheta_\mathrm{i}}\,\mathrm{s}_{\vartheta_1}\,\mathrm{s}_{\phi_{1\mathrm{i}}}\\ Q''_{\vartheta_\mathrm{i}}&=-M_{i,2}l_1\,\ddot{l}_1\,\big(\,\mathrm{c}_{\vartheta_\mathrm{i}}\,\mathrm{s}_{\vartheta_1}-\mathrm{s}_{\vartheta_\mathrm{i}}\,\mathrm{c}_{\vartheta_1}\,\mathrm{c}_{\phi_{1\mathrm{i}}}\,\big)\end{aligned}\qquad i=2,\dots,n+1 \quad (107)$$

$$\begin{aligned}\big[D_{11}\big]_{1,1}&=\big(2M_{1,1}+4m_1\big)l_1\,\dot{l}_1\,{\mathrm{c}_{\vartheta_1}}^2\\ \big[D_{22}\big]_{1,1}&=\big(2M_{1,1}+4m_1\big)l_1\,\dot{l}_1\end{aligned}\qquad i=1 \quad (108)$$

The just above Equation (108) are the sum of the terms due to transitional kinetic energy (Equation (91) and (96)) and potential one (Equation (100) and (104)).

3.5 Estimation of cable's Tension

The system's internal force, as the cable tension, are not explicit. In order to estimate them, the free body diagram of a generic j^{th} cable's element is drawn in Figure 3.1, where $\vec{F}_{ext_j}$ is the external force acting on the element, $\vec{F}_{j+1}$ is the force applied by the successive element, $\vec{a_j}$ is the linear acceleration of the element in the inertial RF, $\vec{F}_{weightj}$ is the weight force $[0; 0; -m_j g]$, and $\vec{F_j}$ is the force applied by the previous cable's element.

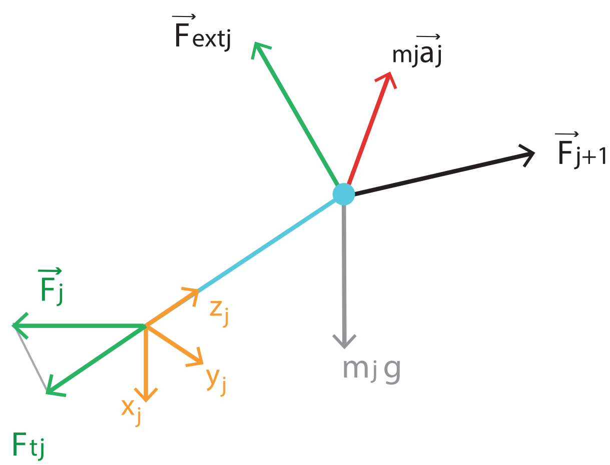

Figure 3.1: j^{th} cable's element free body diagram.

For the dynamics equilibrium of the force:

$$\sum \vec{F} = \vec{F}_{ext_j} + \vec{F}_{j+1} + m_j \vec{a_j} + \vec{F}_{weightj} + \vec{F_j} = \vec{0} \tag{109}$$

The cable tension F_{t_j} of the considered segment will be equal to the component along the local RF z axis of $\vec{F_j}$. Remembering the rotational matrix (4) F_{t_j} is:

$$F_{t_j} = -F_{jx}\,\mathrm{s}_{\vartheta_j} - F_{jy}\,\mathrm{s}_{\phi_j}\,\mathrm{c}_{\vartheta_j} + F_{jz}\,\mathrm{c}_{\phi_j}\,\mathrm{c}_{\vartheta_j} \tag{110}$$

The linear acceleration $\vec{a_j}$ is obtained deriving relative to the time the linear velocity, Equation (74).

$$
\begin{cases}
\ddot{X}_k = -\ddot{l}_1\,\mathrm{s}_{\vartheta_1} - \dot{l}_1\,\dot{\vartheta}_1\,\mathrm{c}_{\vartheta_1} + \sum_{j=1}^{k} l_j(-\ddot{\vartheta}_{\mathrm{j}}\,\mathrm{c}_{\vartheta_{\mathrm{j}}} + \dot{\vartheta}_{\mathrm{j}}{}^2\,\mathrm{s}_{\vartheta_{\mathrm{j}}}) \\
\ddot{Y}_k = -\ddot{l}_1\,\mathrm{s}_{\phi_1}\,\mathrm{c}_{\vartheta_1} - \dot{l}_1\,\dot{\phi}_1\,\mathrm{c}_{\phi_1}\,\mathrm{c}_{\vartheta_1} + \dot{l}_1\,\dot{\vartheta}_1\,\mathrm{s}_{\phi_1}\,\mathrm{s}_{\vartheta_1} \\
\quad + \sum_{j=1}^{k} l_j(-\ddot{\phi}_{\mathrm{j}}\,\mathrm{c}_{\phi_{\mathrm{j}}}\,\mathrm{c}_{\vartheta_{\mathrm{j}}} + \ddot{\vartheta}_{\mathrm{j}}\,\mathrm{s}_{\phi_{\mathrm{j}}}\,\mathrm{s}_{\vartheta_{\mathrm{j}}} + \dot{\phi}_{\mathrm{j}}{}^2\,\mathrm{s}_{\phi_{\mathrm{j}}}\,\mathrm{c}_{\vartheta_{\mathrm{j}}} + \dot{\vartheta}_{\mathrm{j}}{}^2\,\mathrm{s}_{\phi_{\mathrm{j}}}\,\mathrm{c}_{\vartheta_{\mathrm{j}}} + 2\,\dot{\phi}_{\mathrm{j}}\,\dot{\vartheta}_{\mathrm{j}}\,\mathrm{c}_{\phi_{\mathrm{j}}}\,\mathrm{s}_{\vartheta_{\mathrm{j}}}) \qquad k = 1, \ldots, n{+}1 \\
\ddot{Z}_k = -\ddot{l}_1\,\mathrm{c}_{\phi_1}\,\mathrm{c}_{\vartheta_1} - \dot{l}_1\,\dot{\phi}_1\,\mathrm{s}_{\phi_1}\,\mathrm{c}_{\vartheta_1} - \dot{l}_1\,\dot{\vartheta}_1\,\mathrm{c}_{\phi_1}\,\mathrm{s}_{\vartheta_1} \\
\quad + \sum_{j=1}^{k} l_j(-\ddot{\phi}_{\mathrm{j}}\,\mathrm{s}_{\phi_{\mathrm{j}}}\,\mathrm{c}_{\vartheta_{\mathrm{j}}} - \ddot{\vartheta}_{\mathrm{j}}\,\mathrm{c}_{\phi_{\mathrm{j}}}\,\mathrm{s}_{\vartheta_{\mathrm{j}}} - \dot{\phi}_{\mathrm{j}}{}^2\,\mathrm{c}_{\phi_{\mathrm{j}}}\,\mathrm{c}_{\vartheta_{\mathrm{j}}} - \dot{\vartheta}_{\mathrm{j}}{}^2\,\mathrm{c}_{\phi_{\mathrm{j}}}\,\mathrm{c}_{\vartheta_{\mathrm{j}}} + 2\,\dot{\phi}_{\mathrm{j}}\,\dot{\vartheta}_{\mathrm{j}}\,\mathrm{s}_{\phi_{\mathrm{j}}}\,\mathrm{s}_{\vartheta_{\mathrm{j}}})
\end{cases}
\tag{111}
$$

4 Numerical Implementation

In order to implement the dynamics of the system numerically the acceleration terms should be isolated. To do this the matrix $\mathbf{A}$ must be inverted. The matrix $\mathbf{A}$, how it's written since now, is not invertible: his rank is not maximum. In fact, as already write in section 3.2.3, the cable's segments are independent from the angle ψ_i, except for the virtual element associate to the UAV label as $n+1$ element. The associate equation to the ψ_i angles for $i = 1, \dots, n$ not exist for the cable element and they are not generalized coordinates of the system. This rows can be simply eliminated from the matrix for $i = 1, \dots, n$.

Calling $\boldsymbol{\zeta}$ the column vector

$$\boldsymbol{\zeta}_{2n+3\times 1} = \begin{pmatrix} \phi_1 \\ \vartheta_1 \\ \vdots \\ \phi_{n+1} \\ \vartheta_{n+1} \\ \psi_{n+1} \end{pmatrix} \rightarrow \dot{\boldsymbol{\zeta}} = \begin{pmatrix} \dot\phi_1 \\ \dot\vartheta_1 \\ \vdots \\ \dot\phi_{n+1} \\ \dot\vartheta_{n+1} \\ \dot\psi_{n+1} \end{pmatrix} \rightarrow \ddot{\boldsymbol{\zeta}} = \begin{pmatrix} \ddot\phi_1 \\ \ddot\vartheta_1 \\ \vdots \\ \ddot\phi_{n+1} \\ \ddot\vartheta_{n+1} \\ \ddot\psi_{n+1} \end{pmatrix}$$

and the Euler's angles time derivatives mix product the vector $\boldsymbol{\sigma}$

$$\boldsymbol{\sigma} = \begin{pmatrix} \dot\phi_1\,\dot\vartheta_1 \\ \vdots \\ \dot\phi_n\,\dot\vartheta_n \\ 0_{n\times 1} \\ \dot\phi_{n+1}\,\dot\vartheta_{n+1} \\ \dot\phi_{n+1}\,\dot\psi_{n+1} \\ \dot\vartheta_{n+1}\,\dot\psi_{n+1} \end{pmatrix}$$

$$\mathbf{A}_{fin}^{2n+3\times 2n+3} = \left(\begin{array}{c|c} \begin{bmatrix}[A_{11} \quad A_{12}]_{j=1}\dots[A_{11} \quad A_{12}]_{j=n+1} \\ [A_{21} \quad A_{22}]_{j=1}\dots[A_{21} \quad A_{22}]_{j=n+1}\end{bmatrix}_{i=1} & \mathbf{0}_{n+1\times 1} \\ \vdots & \\ \begin{bmatrix}[A_{11} \quad A_{12}]_{j=1}\dots[A_{11} \quad A_{12}]_{j=n+1} \\ [A_{21} \quad A_{22}]_{j=1}\dots[A_{21} \quad A_{22}]_{j=n+1}\end{bmatrix}_{i=n+1} & \mathbf{0}_{n+1\times 1} \\ [A_{31} \quad A_{32}]_{i=n+1,j=1}\dots[A_{31} \quad A_{32}]_{i=n+1,j=n+1} & [A_{33}]_{i=n+1,j=n+1} \end{array}\right)$$

$$\mathbf{B}_{fin}^{2n+3\times 2n+3} = \left(\begin{array}{c|c} \begin{bmatrix}[B_{11} \quad B_{12}]_{j=1}\dots[B_{11} \quad B_{12}]_{j=n+1} \\ [B_{21} \quad B_{22}]_{j=1}\dots[B_{21} \quad B_{22}]_{j=n+1}\end{bmatrix}_{i=1} & \mathbf{0}_{n+1\times 1} \\ \vdots & \\ \begin{bmatrix}[B_{11} \quad B_{12}]_{j=1}\dots[B_{11} \quad B_{12}]_{j=n+1} \\ [B_{21} \quad B_{22}]_{j=1}\dots[B_{21} \quad B_{22}]_{j=n+1}\end{bmatrix}_{i=n+1} & \mathbf{0}_{n+1\times 1} \\ [B_{31} \quad B_{32}]_{i=n+1,j=1}\dots[B_{31} \quad B_{32}]_{i=n+1,j=n+1} & [B_{33}]_{i=n+1,j=n+1} \end{array}\right)$$

$$\mathbf{D}_{fin}^{2n+3\times 2n+3} = \left(\begin{array}{c|c} \begin{bmatrix}[D_{11} \quad D_{12}]_{j=1}\dots[D_{11} \quad D_{12}]_{j=n+1} \\ [D_{21} \quad D_{22}]_{j=1}\dots[D_{21} \quad D_{22}]_{j=n+1}\end{bmatrix}_{i=1} & \mathbf{0}_{n+1\times 1} \\ \vdots & \\ \begin{bmatrix}[D_{11} \quad D_{12}]_{j=1}\dots[D_{11} \quad D_{12}]_{j=n+1} \\ [D_{21} \quad D_{22}]_{j=1}\dots[D_{21} \quad D_{22}]_{j=n+1}\end{bmatrix}_{i=n+1} & \mathbf{0}_{n+1\times 1} \\ [D_{31} \quad D_{32}]_{i=n+1,j=1}\dots[D_{31} \quad D_{32}]_{i=n+1,j=n+1} & [D_{33}]_{i=n+1,j=n+1} \end{array}\right)$$

$$\mathbf{C}_{fin}^{2n+3\times 2n+3} = \left(\begin{array}{c|c} \begin{bmatrix}[C_{11} \quad C_{12}]_{j=1}\dots[C_{11} \quad C_{12}]_{j=n+1} \\ [C_{21} \quad C_{22}]_{j=1}\dots[C_{21} \quad C_{22}]_{j=n+1}\end{bmatrix}_{i=1} & \mathbf{0}_{n+1\times 1} \\ \vdots & \\ \begin{bmatrix}[C_{11} \quad C_{12}]_{j=1}\dots[C_{11} \quad C_{12}]_{j=n+1} \\ [C_{21} \quad C_{22}]_{j=1}\dots[C_{21} \quad C_{22}]_{j=n+1}\end{bmatrix}_{i=n+1} & \mathbf{0}_{n+1\times 1} \\ [C_{31} \quad C_{32}]_{i=n+1,j=1}\dots[C_{31} \quad C_{32}]_{i=n+1,j=n+1} & [C_{33}]_{i=n+1,j=n+1} \end{array}\right) \tag{112}$$

$$\mathbf{A}_{fin}\,\ddot{\boldsymbol{\zeta}} + \Big[\mathbf{B}_{fin}\cdot\ diag(\dot{\boldsymbol{\zeta}}) + \mathbf{D}_{fin}\Big]\,\dot{\boldsymbol{\zeta}} + \mathbf{C}_{fin}\,\boldsymbol{\sigma} = \begin{pmatrix} \mathbf{Q}_{\phi}^{tot} \\ \mathbf{Q}_{\theta}^{tot} \\ \mathbf{Q}_{\psi} \end{pmatrix} \tag{113}$$

Premultiply the Equation (113) for the inverse of matrix $\mathbf{A}_{fin}$ and isolating $\ddot{\boldsymbol{\zeta}}$, results:

$$\ddot{\boldsymbol{\zeta}} = -\mathbf{A}_{fin}^{-1}\Big[\mathbf{B}_{fin}\cdot\ diag(\dot{\boldsymbol{\zeta}}) + \mathbf{D}_{fin}\Big]\,\dot{\boldsymbol{\zeta}} - \mathbf{A}_{fin}^{-1}\mathbf{C}_{fin}\,\boldsymbol{\sigma} + \mathbf{A}_{fin}^{-1}\begin{pmatrix} \mathbf{Q}_{\phi}^{tot} \\ \mathbf{Q}_{\theta}^{tot} \\ \mathbf{Q}_{\psi} \end{pmatrix} \tag{114}$$

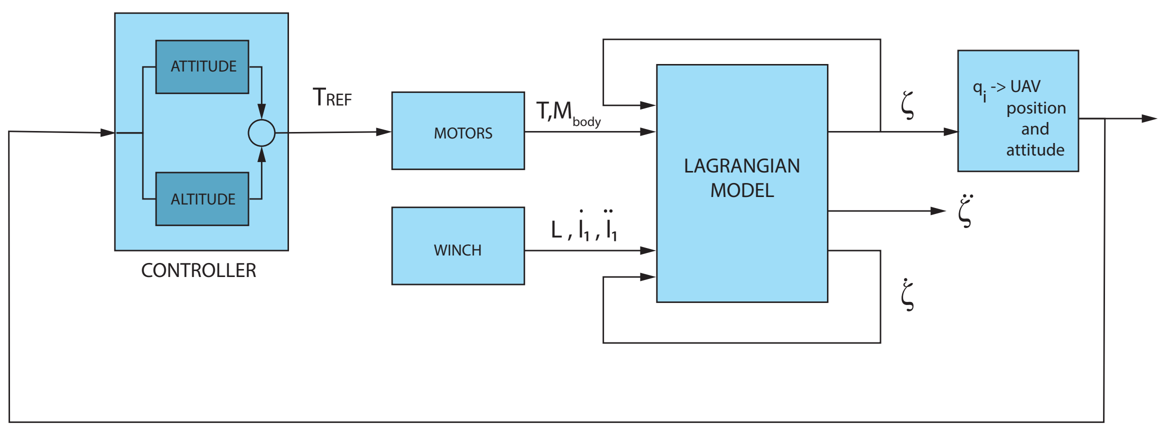

Figure 4.1: Block diagram numerical simulation flow.

5 Simulations and results

The described model is implemented in Matlab/Simulink 2018b. Five simulations with different operational conditions are investigated and summarized in Table 5.1. The parameters of the model and controller are reported in appendix A. The UAV total mass is $25kg$ with a pay load around $7.6kg$. The simulation time step is $0.001s$ and the length of each cable's element is $1.5m$.

Sim #	Z_{ref} [m]	$Z_{initial}$ [m]	Wind Speed $[V_x^w, V_y^w, V_z^w]$
1	20	0.1	[0, 0, 0]
2	20	0.1	[5, 0, 0]
3	20	20	[5, 0, 0]
4	20	20	[25, 0, 0]
5	20	20	[5, 5, 0]

Table 5.1: Simulations profile

5.1 Take-off without wind

The simulation starts with the vehicle on the ground and no wind. The Z coordinate of the UAV is the position of his center of mass. Initially it is equal to $0.1m$, distance between the UAV's mass center and the connection point with the cable. The unwinding velocity of the cable is constant and equal to $\dot{l}_1 = 1m/s$. As described above, $\dot{l}_1$ is imposed from the outside of the Lagrangian model therefore the UAV rate of climb is limited by this value. The altitude increases linearly and reaches the reference value of $20m$ after $19.9s$, Figure 5.1a. At this time $\dot{l}_1$ is instantaneously set to zero. As mentioned in section 2.1, the cable is supposed inextensible, consequently, the UAV rate of climb becomes immediately zero without overshot or transient. This is an unrealistic behaviour. In order to avoid it a possible solution can be to add an elastic element to the model. Two solutions are suggested by the writer as further work: concentrate the cable elasticity at the winch or adding an elastic element between the vehicle and the cable. Figure 5.1b shows the cable at different simulation times. The circles represent the junction points between two consecutive cable segments; the last element is the UAS virtual element. The total number of elements involved in the cable is reported to show that the system can manage a variable cable length. Figure 5.1c presents the force acting to the ground station by the cable. At the time 19.9s the UAV quote reach the reference value, the altitude error results zero as his controller proportional term. The UAV thrust falls to the steady state value.

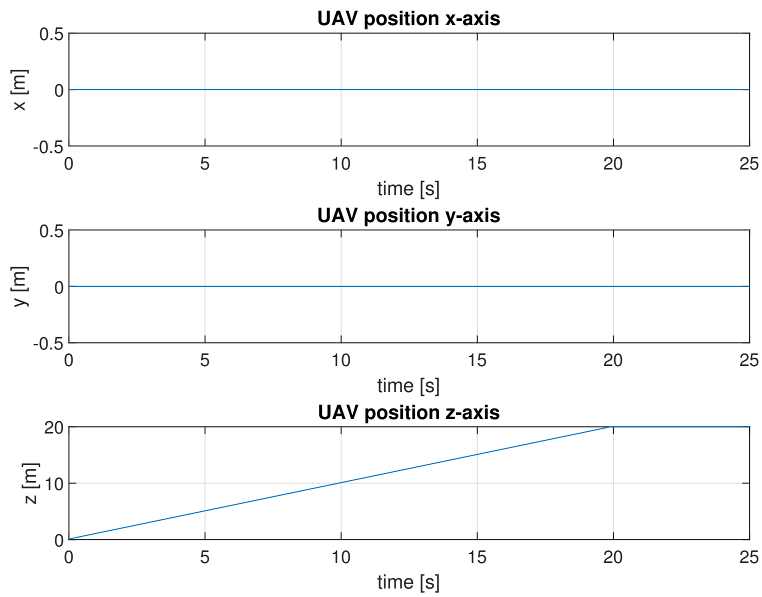

Figure 5.1a: Vehicle position - Simulations 1: UAS take-off in no wind conditions.

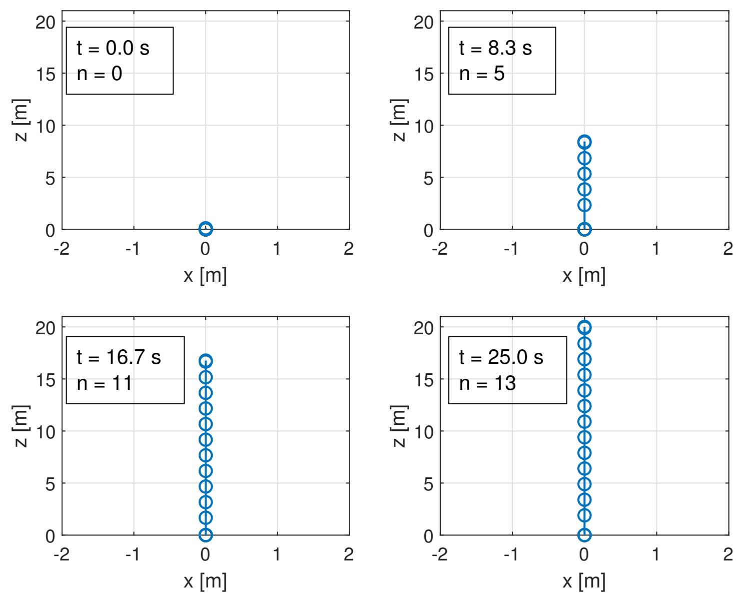

Figure 5.1b: Cable unwinding - Simulations 1: UAS take-off in no wind conditions.

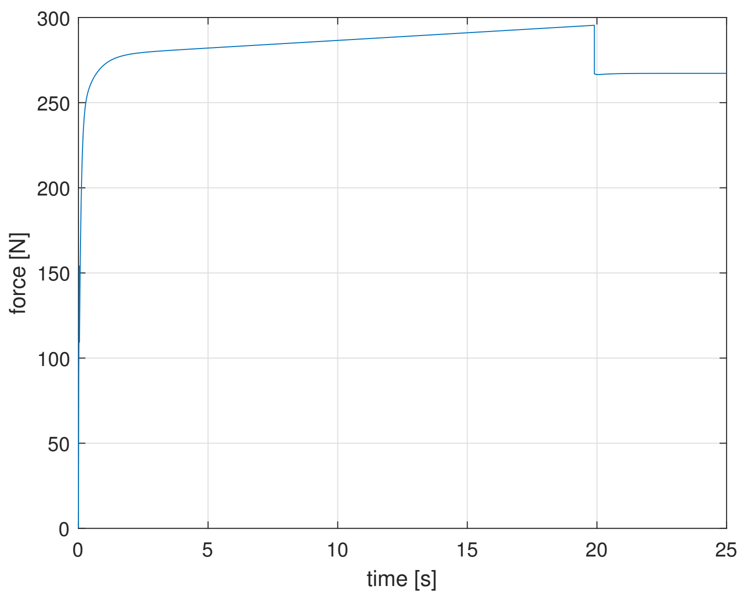

Figure 5.1c: Force acting to the winch by the cable - Simulations 1: UAS take-off in no wind conditions.

5.2 Take-off with wind of $5m/s$

The initial conditions of this simulation are the same of the previous one, section 5.1, except for a wind of $5m/s$ along the X axis of the inertial RF. As consequence the UAS moves to positive X under the effect of the wind, Figure 5.2c, since no such position controller is implemented. Due to the wind the UAV is not able to reach the command altitude $Z_{ref} = 20m$. At the end of the transient a new balance between the UAS and the wind is found, Figure 5.2a.

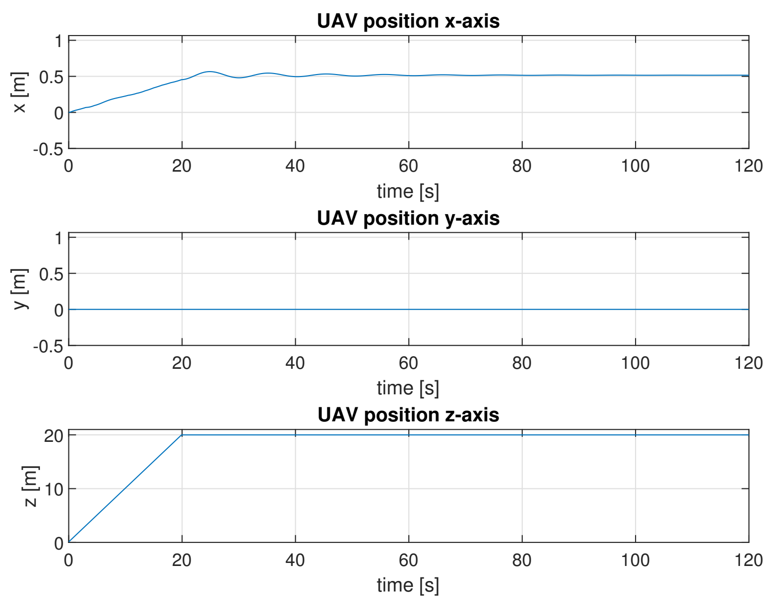

Figure 5.2a: Vehicle position - Simulation 2: UAS take-off with wind of $5m/s$ along X axis.

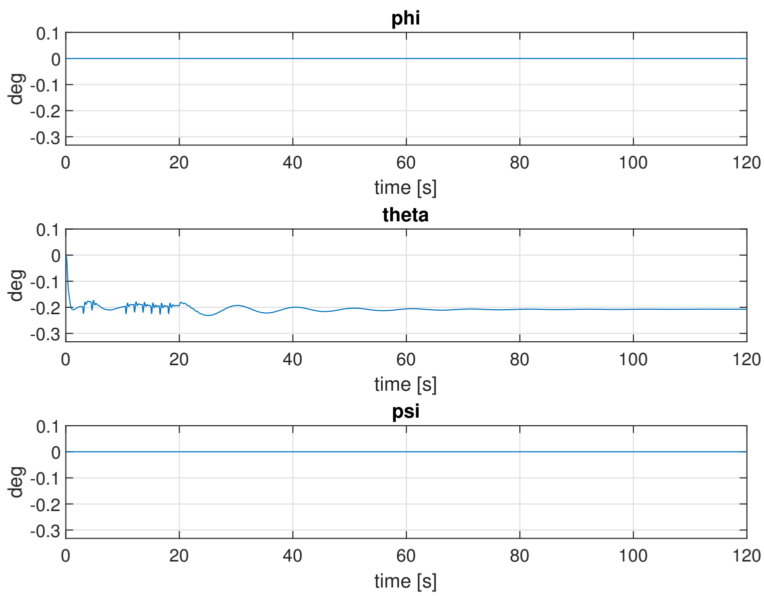

Figure 5.2b: Vehicle attitude - Simulation 2: UAS take-off with wind of $5m/s$ along X axis.

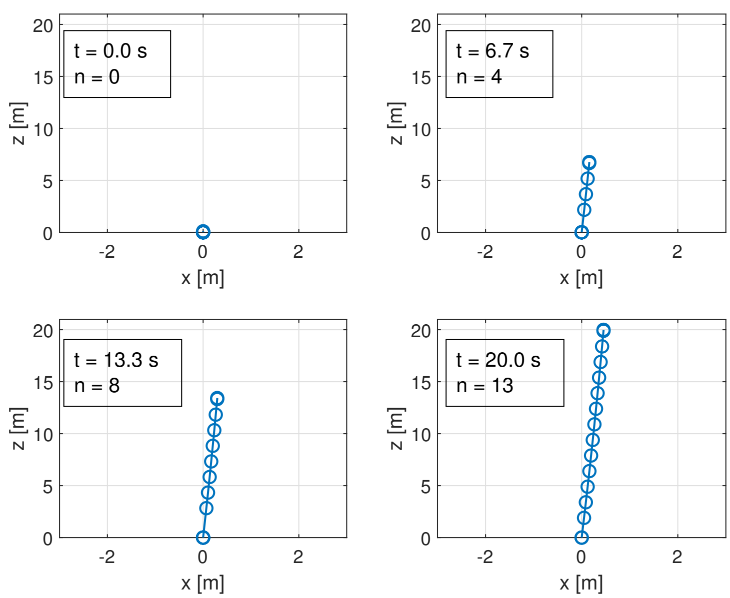

Figure 5.2c: Cable unwinding - Simulation 2: UAS take-off with wind of $5m/s$ along X axis.

5.3 Hovering with wind of $5m/s$

The simulation starts with the UAS hovering at 20 m above ground. Moreover, a constant wind speed (5 m/s along the IRF X axis) is introduced. The aerodynamics forces acting on the cable are responsible for a variation of the pitch angle ϑ, as in Figure 5.3b. Moreover, due to the wind the UAS is not able to keep a constant position and it moves toward the wind's direction (Figure 5.3a). Finally, the cable dynamic behaviour is in Figure 5.3c. It is important to recall that the cable is assumed inextensible. As a consequence of the wind speed, the cable bends and the vehicle altitude decreases during the transient. Then, a new equilibrium point is reached by the system with a steady state altitude and pitch errors. Figure 5.3d reports the force acting by the cable to the ground station. Observe that it keeps increasing after the transient end. The altitude controller is the responsible: the integrative term continues to rise until the reference altitude is reached and this is not possible due to the wind effect. It is clear that the cable tension should be a controlled parameter.

The model is able to simulate the system up to a wind intensity of $20m/s$. Higher wind speeds result in unstable system behaviour and cannot be simulated. For example, with $25m/s$ wind the controller is not able to compensate the wind effects. The UAV moves to positive X and his altitude is forced to decrease almost to the ground, Figure 5.4. At this time, the Euler Angles reach the singularity condition $\vartheta = \frac{\pi}{2}$ for a cable element. The simulation stops at the following step since the matrix A_{fin} is no more invertible.

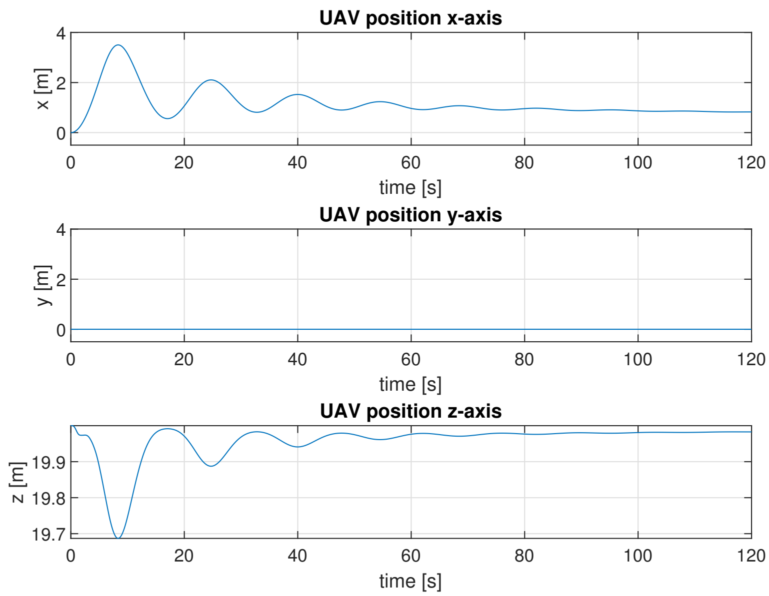

Figure 5.3a: Vehicle position - Simulation 3: UAS hovering in wind conditions of $5m/s$

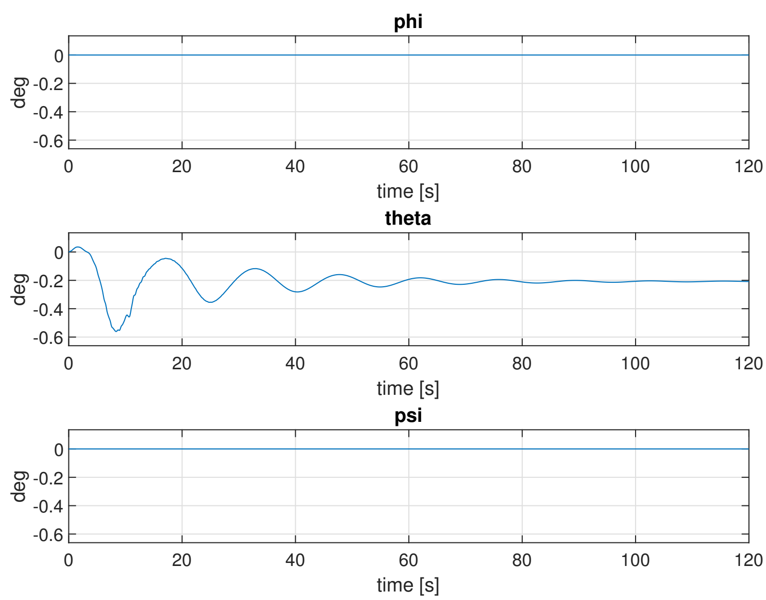

Figure 5.3b: Vehicle attitude - Simulation 3: UAS hovering in wind conditions of $5m/s$

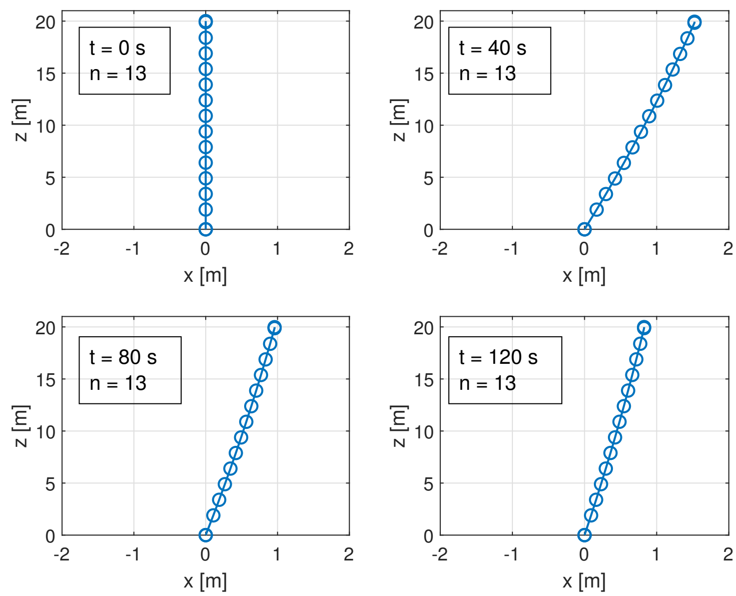

Figure 5.3c: Cable unwinding - Simulation 3: UAS hovering in wind conditions of $5m/s$

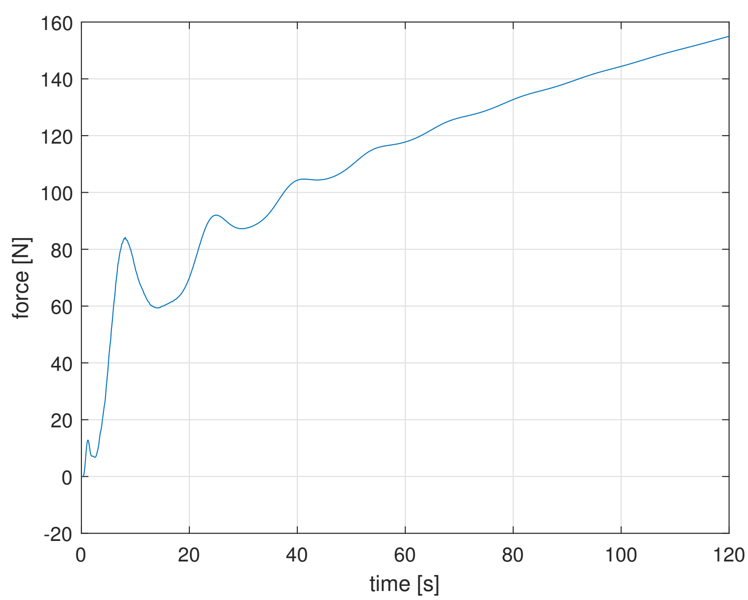

Figure 5.3d: Force acting to the ground station by the cable - Simulation 3: UAS hovering in wind conditions of $5m/s$

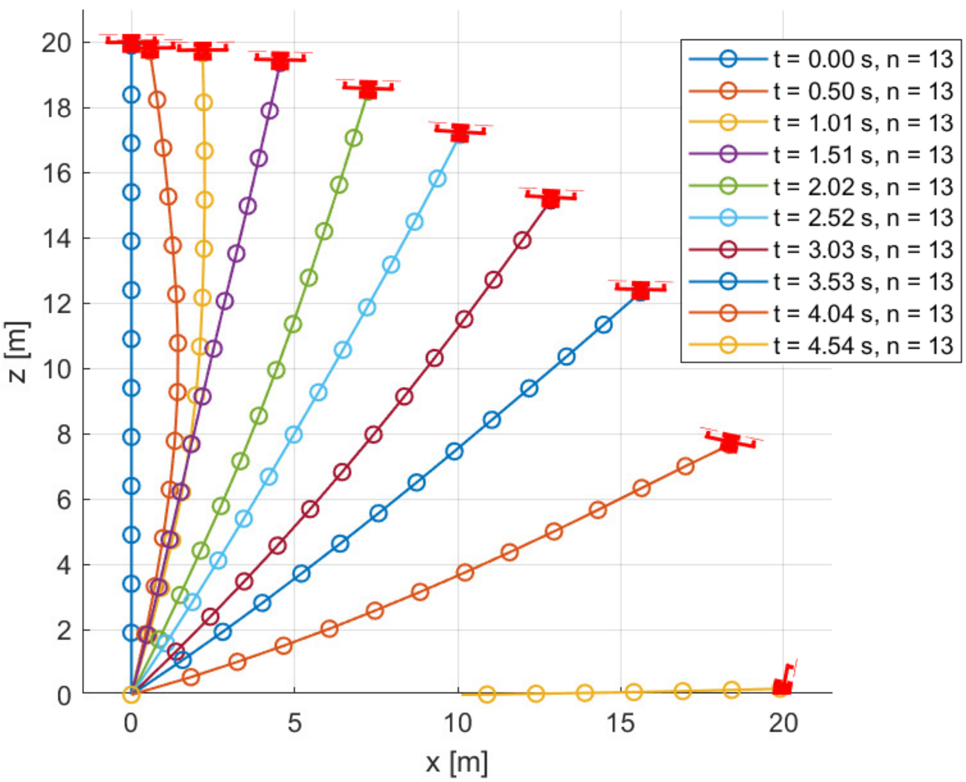

Figure 5.4: UAS position in wind conditions of $25m/s$ - Simulation 4.

5.4 Hovering with wind in X and Y directions

In the following simulation, the UAS is hovering while a constant wind speed is acting along IRF X and Y axes. As shown in Figure 5.5b, the attitude of the vehicle is affected by the wind. When the transient ends, a new equilibrium is found with limited ϕ and θ angle errors. At the same time, a constant position error is shown in Figure 5.5a as the autopilot is not able to compensate the effect of the wind.

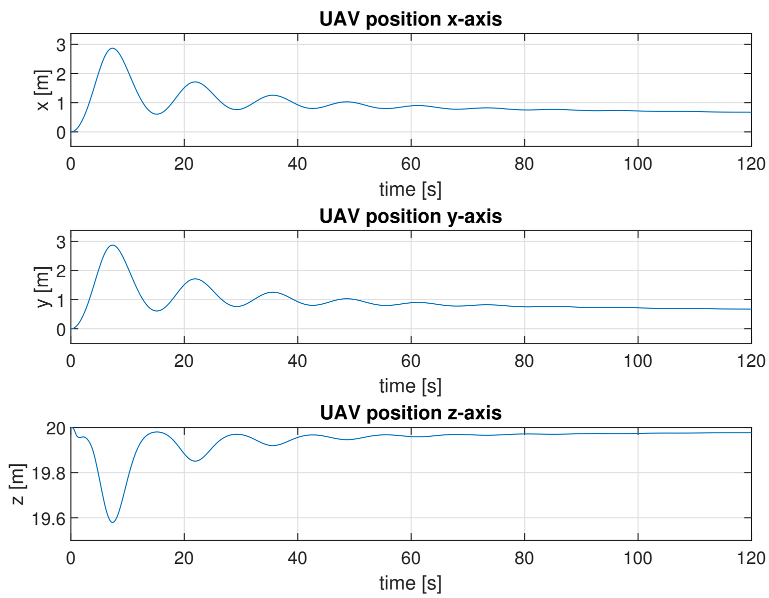

Figure 5.5a: Vehicle position - Simulation 5: UAS hovering with constant wind in both X and Y directions.

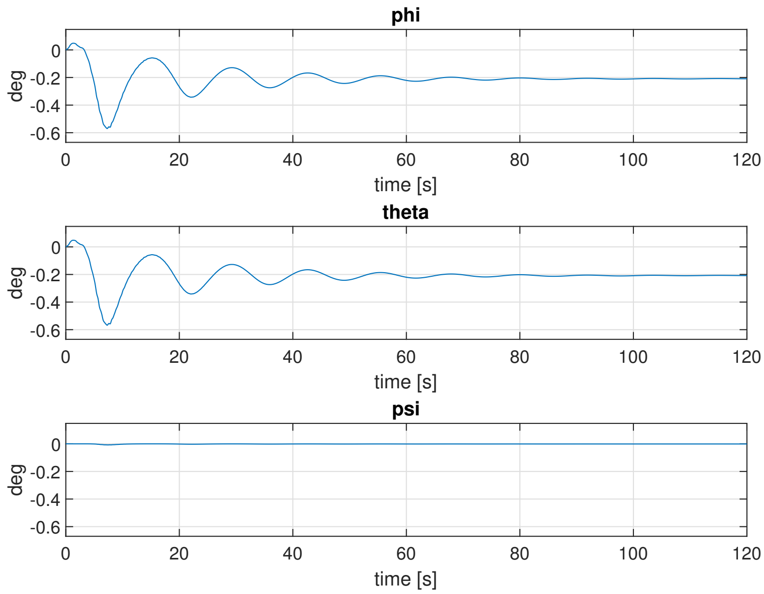

Figure 5.5b: Vehicle attitude - Simulation 5: UAS hovering with constant wind in both X and Y directions.

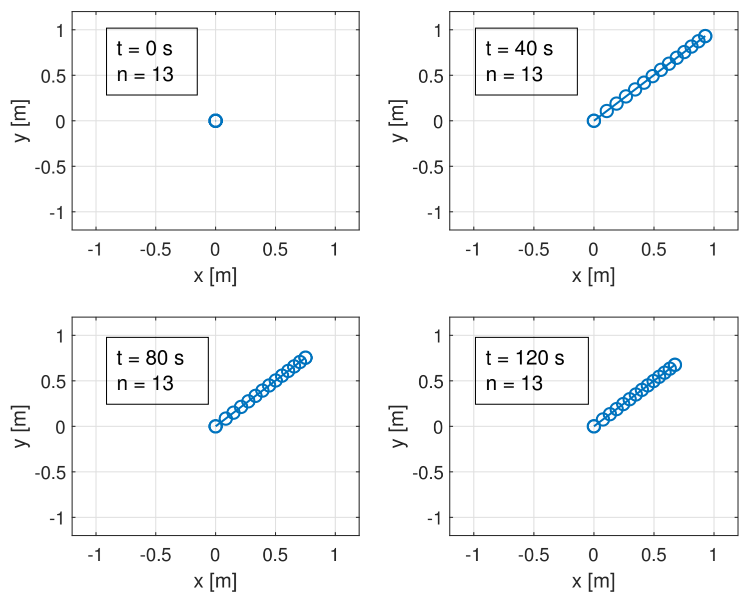

Figure 5.5c: Cable unwinding - Simulation 5: UAS hovering with constant wind in both X and Y directions.

6 Conclusions

A tethered UAS simulation model is presented and discussed. The Finite Elements Method (FEM) is used to evaluate the dynamic behavior of the system. The cable consists of n segments linked end to end by a spherical joint. The length of the first segment is not constant in order to model a variable cable length to simulate UAS take-off or landing operations. An additional virtual element is used to simulate the unmanned vehicle. The Lagrange's Equations are derived to describe the dynamics of the complete system. Thrust and torque generated by the propellers are computed using the Blade Element Theory. Moreover, aerodynamic forces due to wind are introduced as external disturbances acting on the cable and UAV. Simulation results corroborate the proposed model. It is able to simulate the system in both wind and still air conditions. The main limitation of the model is given by the representation of the cable segment orientations based on the Euler's angles. Gimbal lock occurs when the cable is placed on the ground or the UAS propeller plane is perpendicular to ground ($\theta = \pm\pi/2$). This condition can occur in different situations. As presented in section 5.3 the incapacity of the controller to stabilize the UAS disturbed by wind involves the singularity condition. Moreover, during the ordinary operation the first cable segment, due to vehicle altitude loss, can reach the Gimbal lock. Future works include decoupling the dynamics of the UAS from the cable making it even more versatile. This allows to attach in easily way the cable to an existing UAV model. A suitable solution is adding a viscoelastic connection between the vehicle and the cable, [30]. Furthermore, this will permit to concentrate the cable elasticity, supposed inextensible, in this connection. A detailed mathematical model for the UAV will be introduced, in addition to the implementation of a position controller for the aerial vehicle. Moreover, a simplified winch model will be proposed to control the tension and unwinding velocity of the cable as a function of the UAS operations.

A Simulation Parameters

```
%% cable paramiters
cableMu = 85e-3;                        % [kg/m] cable ...
    linear density

Cd = 0.8;                               % cable drag coeficent
Cf = 0.01;                              % cable ...
    aerodynamics frictioncoeficient
cableDiameter = 5.8e-3;                 % [m] cable diameter
Lmax = 22;                              % [m] Cable ...
    maximum length
segmentLengthMax = 1.5;                 % [m] Cable ...
    element maximum length
segmentLengthMin = 1e-4;                % [m] Cable ...
    element minimum length

nMax = ceil(Lmax/segmentLengthMax);     % Maximum number ...
    of cable segment -> 15
fristSegmentAddictionalLength = 1.5; % [m] Addoctional ...
    length of the first element
fristSegmentMin = 1;                    % [m] First ...
    element minimum length

%% UAV paramiters
UAVConnectionPointBody = [0;0;-0.1]; % [m] Connection ...
    point coordinates in UAV body Reference Frame
UAVmass = 25;                           % [kg] UAV total mass

propeller_arm = 1500e-3;                % [m] Distance ...
    between motor axis
alpha = deg2rad(45);                    % [rad] Angle ...
    between x axis and the arm of the frame on the first ...
    quadrant
momentPropArmx = propeller_arm/2*sin(alpha); % [m] ...
    Distance of the motors from x axis in UAV body RF
momentPropArmy = propeller_arm/2*cos(alpha); % [m] ...
    Distance of the motors from y axis in UAV body RF
```

```
CdUAV = [0.85; 0.85; 0.85];          % Axial force Cdx, ...
    side force Cdy, normal force Cdz
MdUAV = [0;0;0];                     % rolling moment ...
    Cl, pitching moment Cm, yawing moment Cn
%% Main Box
c = 370e-3;   % [m] Main Box dimension along x-axis
a = 370e-3;   % [m] Main Box dimension along y-axis
b = 300e-3;   % [m] Main Box dimension along z-axis
z(1) = 0;     % [m] RF centered in the main box (RF_main)
m(1) = 2;     % [kg]

%% Battery
c = 210e-3;      % [m] Battery dimension along x-axis
a = 140e-3;      % [m] Battery dimension along y-axis
b = 7.8e-3;      % [m] Battery dimension along z-axis
z(2) = b/2;     % [m] Battery distance form XY plane in ...
    RF_main
m(2) = 0.395*14; % [kg] 14 cell for 0.395 kg/cell

%% Motors
rm = 147.5e-3/2;       % [m] Motors external radius
hm = 55e-3;            % [m] Motors height
zm = propeller_arm/2;  % [m] Distance of motor from z-axis
xm = momentPropArmy;   % [m] distance of motor from y axis
ym = momentPropArmx;   % [m] distance of motor from x axis
z(3) = 70e-3;          % [m] Motors distance form XY ...
    plane in RF_main
m(3) = 1.740;          % [kg] Single motor mass
m(3) = 4*m(3);         % [kg] All motors mass

%% Propellers
rp = 919.5e-3/2;        % [m] Propellers radius
zp = zm;                % [m] Distance of propeller ...
    from z-axis
xp = xm;                % [m] Distance of propeller ...
    from y axis
yp = ym;                % [m] Distance of propeller ...
    from x axis
```

```
z(4) = z(3) + 15.5e-3;  % [m] Propellers distance form ...
    XY plane in RF_main
m(4) = 230e-3;          % [kg] Single propeller mass
m(4) = 4*m(4);          % [kg] All propellers mass

%% Frame
rf = 40e-3;                       % [m] Frame rod radius
lf = propeller_arm - 2*rm;        % [m] Frame rod length
sf = 3e-3;                        % [m] Frame rod thickness
z(5) = z(3);                      % [m] Frame rod ...
    longitudinal axis distance form XY plane in RF_main
m(5) = 2e3*pi*sf*(2*rf - sf)*lf; % [kg] carbon fiber ~ ...
    2000 kg/m^3*(pi*(rf^2-rfint) = 10 kg/m -> 1.9630 kg

%% Pay Load
mtot = sum(m(1:end-1));          % [kg] UAV mass without ...
    pay load

c = 200e-3;                      % [m] Pay Load ...
    dimension along x-axis
a = 200e-3;                      % [m] Pay Load ...
    dimension along y-axis
b = 200e-3;                      % [m] Pay Load ...
    dimension along z-axis
z(end) = z(1) - zb/2 +(-b/2);    % [m] Pay Load distance ...
    form XY plane in RF_main
m(end) = UAVmass - mtot;         % [kg] Pay Load mass = ...
    7.6270 kg

%% Center of Mass along z (Suppose to be symmetric ...
    along x and y axis)
z_centralMass = sum(m.*z)/UAVmass; % [m] z coordinate ...
    of the bdy RF origin in RF_main
z = z + z_centralMass;             % [m] z coordinates ...
    of UAV bodis in UAV body RF

%% Total inertia moment
I_xx = 3.3473; % [Kg*m^2] Inertia moment respect the ...
    x-axis in UAV body RF
```

```
I_yy = 3.3586; % [Kg*m^2] Inertia moment respect the ...
    y-axis in UAV body RF
I_zz = 5.2730; % [Kg*m^2] Inertia moment respect the ...
    z-axis in UAV body RF

UAVConnectionPointLength = ...
    norm(UAVConnectionPointBody); % [m] distance from ...
    the UAV mass center to the cable connection point
I_UAV = [Ixx+UAVmass*UAVConnectionPointLength^2; ...
    Iyy+UAVmass*UAVConnectionPointLength^2; Izz]; % ...
    [Kg*m^2] UAV inertia moments respect the n+1 local RF

%% UAV Propeller Motor
prop.Kt = 0.1639;          % [Nm/A] Gain from armature ...
    currents to motor torque
prop.J = 0.00212 + 0.013; % [kg*m^2] Motor and ...
    propeller inertia =1/12*ML^2
prop.f = 0;                % [Nms] motor viscous factor
prop.maxCurrent = 110.4;   % [A] Motor armature maximum ...
    currents
prop.maxOmega = 330;       % [rad/s] Motor maximum ...
    angular velocity

%% Air condition
rho = 1.225;    % [kg/m^3] air density

%% Gravity acceleration
g = 9.80665;    % [m/s^2]

%% Attitude Control Parameters
phiControl.P = 40;                        % [1/s] ...
    Proportional Gain, error to acceleration
phiControl.I = 0.004;                     % [1/s^2] ...
    Integral Gain, error to acceleration
phiControl.D = 18;                        % [s] Derivative ...
    Gain, error to acceleration
phiControl.maxAngularMoment = 0.75;    % [rad/s^2] ...
    Maximum reference angular moment

```

```
thetaControl.P = 40;                        % [1/s] ...
    Proportional Gain, error to acceleration
thetaControl.I = 0.004;                     % [1/s^2] ...
    Integral Gain, error to acceleration
thetaControl.D = 18;                        % [s] Derivative ...
    Gain, error to acceleration
thetaControl.maxAngularMoment = 0.75; % [rad/s^2] ...
    Maximum reference angular moment

psiControl.P = 40;                          % [1/s] ...
    Proportional Gain, error to acceleration
psiControl.I = 0.004;                       % [1/s^2] ...
    Integral Gain, error to acceleration
psiControl.D = 14;                          % [s] Derivative ...
    Gain, error to acceleration
psiControl.maxAngularMoment = 0.05;   % [rad/s^2] ...
    Maximum reference angular moment

%% Altitude Control
altitudeControl.P = 100;  % [1/s] Proportional Gain, ...
    error to acceleration
altitudeControl.I = 3.5;  % [1/s^2] Integral Gain, ...
    error to acceleration
altitudeControl.D = 0;    % [s] Derivative Gain, error ...
    to acceleration
altitudeControl.maxAcecelerarion = 1.5*g; % [m/s^2] ...
    Maximum reference Z linear aceleration in inertial RF

%% Propeller Motor Control
propControl.P = 1.16;     % [1/s] Proportional Gain, ...
    error to acceleration
propControl.I = 2.69;     % [1/s^2] Integral Gain, ...
    error to acceleration
```

References

[1] H. Shakhatreh, A. H. Sawalmeh, A. Al-Fuqaha, Z. Dou, E. Almaita, I. Khalil, N. S. Othman, A. Khreishah, and M. Guizani, "Unmanned Aerial Vehicles (UAVs): A Survey on Civil Applications and Key Research Challenges," *IEEE Access*, vol. 7, pp. 48 572–48 634, 2019, ISSN: 2169-3536. DOI: `10.1109/ACCESS.2019.2909530`.

[2] O. Alvear, N. R. Zema, E. Natalizio, and C. T. Calafate, "Using UAV-Based Systems to Monitor Air Pollution in Areas with Poor Accessibility," en, *Journal of Advanced Transportation*, 2017. DOI: `https://doi.org/10.1155/2017/8204353`.

[3] N. Samir Labib, G. Danoy, J. Musial, M. R. Brust, and P. Bouvry, "Internet of Unmanned Aerial Vehicles—A Multilayer Low-Altitude Airspace Model for Distributed UAV Traffic Management," en, *Sensors*, vol. 19, no. 21, Jan. 2019. DOI: `10.3390/s19214779`.

[4] R. B. Anette Eltner Hannes Sardemann, "Unmanned aerial and water vehicle data for hydro-morphological," *Geophysical Research Abstracts*, no. 21, Jan. 2019.

[5] A. Eltner, H. Sardemann, and R. Blaskow, "Unmanned aerial and water vehicle data for hydro-morphological river monitoring.," in *Geophysical Research Abstracts*, vol. 21, 2019, EGU2019–14 517.

[6] M. E. Lussier, J. M. Bradley, and C. Detweiler, "Extending Endurance of Multicopters: The Current State-of-the-Art," en, in *AIAA Scitech 2019 Forum*, San Diego, California: American Institute of Aeronautics and Astronautics, Jan. 2019, ISBN: 978-1-62410-578-4. DOI: `10.2514/6.2019-1790`.

[7] K. R. B. Sri, P. Aneesh, K. Bhanu, and M. Natarajan, "Design Analysis of Solar-Powered Unmanned Aerial Vehicle," en, *Journal of Aerospace Technology and Management*, vol. 8, no. 4, pp. 397–407, Dec. 2016, ISSN: 2175-9146. DOI: `10.5028/jatm.v8i4.666`.

[8] K. Swider-Lyons, R. Stroman, B. Gould, J. Rodgers, J. Mackrell, M. Schuette, and G. Page, "Hydrogen Fuel Cells for Small Unmanned Air Vehicles," *ECS Transactions*, vol. 64, pp. 963–972, Aug. 2014. DOI: `10.1149/06403.0963ecst`.

[9] E. Mercatali, “Tethered UAV Feasibility study for the propulsion of a tethered UAV,” Politecnico di Torino, 2018.

[10] Young-il Choo and Mario J. Casarella, “A Survey of Analytical Methods for Dynamic Simulation of Cable-Body Systems.,” *Journal of Hydronautics*, vol. 7, no. 4, pp. 137–144, 1973, ISSN: 0022-1716. DOI: 10.2514/3.62948.

[11] J. W. Kamman and R. L. Huston, “Modeling of Variable Length Towed and Tethered Cable System,” *Journal of Guidance, Control, and Dynamics*, vol. 22, no. 4, Aug. 1999.

[12] Taeyoung Lee, “Geometric Controls for a Tethered Quadrotor UAV,” vol. 15, December 15-18, 2015. Osaka, Japan, pp. 2749–2754, ISBN: 978-1-4799-7886-1.

[13] Sina Doroudgar, “Static and Dynamic Modeling and Simulation of the Umbilical Cable in A Tethered Unmanned Aerial System,” en, PhD thesis, SIMON FRASER UNIVERSITY, Jun. 2016.

[14] C. Ablow and S. Schechter, “Numerical simulation of undersea cable dynamics,” en, *Ocean Engineering*, vol. 10, no. 6, pp. 443–457, Jan. 1983, ISSN: 00298018. DOI: 10.1016/0029-8018(83)90046-X.

[15] O. O. Ajayi and O. O. Aribike, “MODELLING AND SIMULATION OF SUBSEA UMBILICAL DYNAMICS: A NUMERICAL APPROACH,” en, *International Journal of Computer Thechniques*, vol. 2, no. 1, p. 12, 2015.

[16] V. K. Srivastava, Y. Sanyasiraju, and M. Tamsir, “Dynamic Behavior of Underwater Towed-cable in Linear Profile,” en, *International Journl of Scientific & Engineering Researh*, vol. 2, no. 7, p. 10, ISSN: 2229-5518.

[17] T.-V. Mai, H.-S. Choi, J.-Y. Kim, D.-H. Ji, H.-J. Son, and N.-H. Tran, “A Study on the Dynamics of Marine Umbilical Cable for Underwater Vehicle,” in *AETA 2015: Recent Advances in Electrical Engineering and Related Sciences*, vol. 371, Springer International Publishing, 2016, pp. 575–588, ISBN: 978-3-319-27245-0 978-3-319-27247-4. DOI: 10.1007/978-3-319-27247-4_49.

[18] Kurt A. Talke, Mauricio de Oliveira, and Thomas Bewley, “Catenary Tether Shape Analysis for a UAV - USV Team,” Madrid, Spain, October 1-5, 2018, pp. 7803–7809, ISBN: 978-1-5386-8094-0.

[19] Piero Graziano Ioppo, "The Design, Modelling and Control of an Autonomous Tethered Multirotor UAV," en, PhD thesis, University of Stellenbosch, Mar. 2017.

[20] D. Ferreira de Castro, J. S. Santos, M. Batista, D. Antônio dos Santos, and L. C. Góes, "Modeling and Control of Tethered Unmanned Multicopters in Hovering Flight," en, in *AIAA Modeling and Simulation Technologies Conference*, Dallas, TX: American Institute of Aeronautics and Astronautics, Jun. 2015, ISBN: 978-1-62410-355-1. DOI: `10.2514/6.2015-2333`.

[21] Marco Tognon, "Attitude and Tension Control of a Tethered Formation of Aerial Vehicles," PhD thesis, University of Pauda, Mar. 2014.

[22] Frédéric Muttin, "Umbilical deployment modeling for tethered UAV detecting oil pollution from ship," *Applied Ocean Research*, vol. 33, pp. 332–343, 2011. DOI: `10.1016/j.apor.2011.06.004`.

[23] S. Puneet, D. Mortari, and J. Junkins, "How to avoid singularity when using Euler angles?" *Advances in the Astronautical Sciences*, vol. 119, pp. 1409–1426, Jan. 2005.

[24] M. Krznar, D. Kotarski, P. Piljek, and D. Pavkovic, "On-line Inertia Measurement of Unmanned Aerial Vehicles using on board Sensors and Bifilar Pendulum," *Interdisciplinary Description of Complex Systems*, vol. 16, pp. 149–161, 2018. DOI: `10.7906/indecs.16.1.12`.

[25] M. Drela. (Nov. 30, 2001). Xfoil documentation, [Online]. Available: `https://web.mit.edu/drela/Public/web/xfoil/xfoil_doc.txt` (visited on 11/28/2019).

[26] AirfoilTools. (). Lift & drag polars, [Online]. Available: `http://airfoiltools.com/airfoil/details?r=polar` (visited on 11/28/2019).

[27] Sighard F. Hoerner, *Fluid-Dynamic Drag: Practical Information on Aerodynamic Drag and Hydrodynamic Resistance*, 1965.

[28] Laura Novaro Mascarello, "Analysis and development of harmless sUAS (small Unmanned Aerial Systems)," PhD thesis, Politecnico di Torino, 2018.

[29] A. A. Shabana, *Dynamics of multibody systems*, 4th ed. Cambridge: Cambridge University Press, 2013, ISBN: 978-1-107-33721-3. DOI: `10.1017/CBO9781107337213`.

[30] N. Slegers, “Modeling and Control of a Tethered Rotorcraft,” en, p. 25,